Synthetic lethal treatment strategies for tumor cell senescence
(German: Synthetisch-letale Therapiestrategien für Tumorzellseneszenz)

Dissertation

zur Erlangung des akademischen Grades

doctor rerum naturalium (Dr. rer. nat.)

im Promotionsfach Biologie

eingereicht an der Lebenswissenschaftlichen Fakultät
der Humboldt-Universität zu Berlin

angefertigt von Jan Rafael Dörr, M.Bioc.

Präsidentin der Humboldt-Universität zu Berlin
Prof. Dr.-Ing. Dr. Sabine Kunst

Dekan des Lebenswissenschaftlichen Fakultät
Prof. Dr. Bernhard Grimm

Gutachter: 1. Prof. Dr. Thomas Sommer

2. Prof. Dr. Clemens A. Schmitt

3. Prof. Dr. Simone Fulda

Tag der mündlichen Prüfung: 22.06.2017

Meiner Familie

Table of contents

1. Preface

The results of this thesis have been presented in the following publication:

Jan R. Dörr[1], Yong Yu[2], Maja Milanovic[1], Gregor Beuster[2], Christin Zasada[3], J. Henry M. Däbritz[1], Jan Lisec[1,4], Dido Lenze[5], Anne Gerhardt[1], Katharina Schleicher[1], Susanne Kratzat[6], Bettina Purfürst[2], Stefan Walenta[7], Wolfgang Mueller-Klieser[7], Markus Gräler[8], Michael Hummel[5], Ulrich Keller[6], Andreas K. Buck[9], Bernd Dörken[1,2], Lothar Willmitzer[10], Maurice Reimann[1], Stefan Kempa[3], Soyoung Lee[1,2] & Clemens A. Schmitt[1,2]

"Synthetic lethal metabolic targeting of cellular senescence in cancer therapy"

Nature, 19 September 2013; Volume 501: 421-425

1) Charité-Universitätsmedizin Berlin, Molekulares Krebsforschungszentrum (MKFZ), Augustenburger Platz 1, 13353 Berlin, Germany
2) Max-Delbrück-Center for Molecular Medicine (MDC), Robert-Rössle-Straße 10, 13125 Berlin, Germany
3) Integrative Metabolomics and Proteomics, Berlin Institute of Medical Systems Biology, Max-Delbrück-Center for Molecular Medicine, Robert-Rössle-Straße 10, 13125 Berlin, Germany
4) German Cancer Consortium, Deutsches Krebsforschungzentrum (DKFZ), Im Neuenheimer Feld 280, 69120 Heidelberg, Germany.
5) Charité-Universitätsmedizin Berlin, Department of Pathology, Charitéplatz 1, 10117 Berlin, Germany
6) Technische Universität München, III Medical Department, Ismaninger Straße 22, 81675 Munich, Germany
7) Universitätsmedizin der Johannes Gutenberg-Universität, Institute of Physiology and Pathophysiology, Duesbergweg 6, 55128 Mainz, Germany
8) Universitätsklinikum Jena, Department of Anesthesiology and Intensive Care Medicine & Center for Sepsis Control and Care (CSCC), Erlanger Allee 1, 07747 Jena, Germany
9) Universitätsklinikum Würzburg, Department of Nuclear Medicine, Oberdürrbacher Straße 6, 97080 Würzburg, Germany
10) Max Planck Institute of Molecular Plant Physiology, Am Mühlenberg 1, 14476 Potsdam, Germany

The respective experimental contributions of the co-authors are indicated in the methods section.

2. Summary (German)

In Krebszellen induzieren Onkogene und Chemotherapie zelluläre Seneszenz. Dabei handelt es sich um einen terminalen Wachstumsarrest, bei dem durch Trimethylierung der Aminosäure Lysin an Position 9 (K9) des Histons H3 (H3K9me3) die Aktivierung S-Phase-relevanter Gene epigenetisch blockiert ist. Obwohl Therapie-induzierte Seneszenz (TIS) das Gesamtüberleben von Mäusen mit einer Lymphomerkrankung verbessert, stellt eine Elimination seneszenter Zellen aufgrund weiterhin bestehender und neu erworbener tumorigener Eigenschaften ein wichtiges therapeutisches Ziel dar. Die Arbeit zeigt anhand des transgenen Eμ-*myc* Mausmodells, in dem TIS in Abhängigkeit von der H3K9-Histonmethyltransferase Suv39h1 durch Chemotherapie induziert wird, dass TIS-Zellen *in vitro* und *in vivo* einer metabolischen Reprogrammierung unterliegen, die therapeutisch genutzt werden kann. TIS-kompetente Lymphome erhöhen im Gegensatz zu TIS-kompromittierten, Suv39h1-defizienten Lymphomen den Glukoseumsatz und die Produktion von ATP. Diese Umstellung des Stoffwechsels erfolgt als Antwort auf eine erhöhte Proteotoxizität, die durch Bestandteile des Seneszenz-assoziierten sekretorischen Phänotyps (SASP) hervorgerufen wird. SASP-Faktoren lösen in TIS-Zellen erhöhten Stress im endoplasmischen Retikulum (ER) aus und forcieren die Fehlfaltung von Proteinen, die nach vermehrter Ubiquitinierung durch Autophagie unter Energieverbrauch abgebaut werden. Deshalb sind stark SASP-exprimierende TIS-Lymphome im Vergleich zu genetisch durch die Inhibition des Transkriptionsfaktors NfκB veränderten und dadurch SASP-supprimierten TIS-Lymphomen empfindlich gegenüber der Inhibition des Glukosestoffwechsels oder der Blockade von Autophagie. Beides führt zur Elimination von TIS Zellen durch Caspase-12- und Caspase-3-abhängige, ER-initiierte Apoptose. Folglich erwirkt die pharmokologische Inhibition dieser veränderten Stoffwechselbedürfnisse nach TIS Induktion eine Tumorregression und ein verbessertes Gesamtüberleben *in vivo*. Zusammenfassend zeigen diese Ergebnisse eine katabole Stoffwechsellage seneszenter Zellen, die therapeutisch durch konzeptionell neue „synthetisch-letale“, metabolische Therapien eliminiert werden können. Damit wird erstmals in der Krebstherapie ein Tumor-selektives Seneszenzprogramm zusammen mit der Blockade von Stoffwechselwegen genutzt.

3. Summary (English)

Cellular senescence is a terminal growth arrest of viable cells characterized by S-phase entry-blocking histone 3 lysine 9 trimethylation (H3K9me3) in response to oncogene activation and anticancer chemotherapy. Although therapy-induced senescence (TIS) improves long-term outcome, senescent tumor cells acquire potentially harmful characteristics. Therefore, their quantitative elimination presents a therapeutic opportunity. In this thesis the Eμ-*myc* transgenic mouse lymphoma model, in which TIS depends on the H3K9 histone methyltransferase Suv39h1, is used to show mechanism and therapeutic exploitation of senescence-related metabolic reprogramming *in vitro* and *in vivo*. After senescence-inducing chemotherapy, TIS-competent lymphomas but not TIS-incompetent *Suv39h1*$^{-}$ lymphomas displayed increased glucose turnover and higher ATP production. The thesis demonstrates that this was due to massive proteotoxic stress, which is a consequence of the enhanced production of secretory proteins - referred to as the senescence-associated secretory phenotype (SASP) - of senescent cells. Consequently, SASP-producing TIS cells exhibited endoplasmic reticulum stress, an unfolded protein response (UPR), and increased ubiquitination, thereby targeting toxic proteins for autophagy in an acutely energy-consuming fashion. Accordingly, TIS lymphomas, unlike senescence models that lack a strong SASP response, for example due to the inhibition of the transcription factor NfκB, were more sensitive to blocking glycolysis or autophagy, which lead to their selective elimination through caspase-12- and caspase-3-mediated endoplasmic reticulum-related apoptosis. Consequently, pharmacological targeting of these metabolic liabilities upon TIS induction *in vivo* prompted tumor regression and improved treatment outcome further. These findings unveil the hypercatabolic nature of TIS that is therapeutically exploitable by synthetic lethal metabolic targeting. Thus, this treatment approach for the first time combines the inhibition of a tumor-specific senescence program with the interference of a metabolic pathway.

4. Synopsis

Senescence is a complex cellular stress response. It permanently arrests the proliferation of cells subjected to acute or chronic insults in a process which is often associated with the accumulation of DNA damage.[1] While the senescent proliferation arrest was – like apoptotic cell death – originally viewed as the major purpose of this cellular failsafe program, it has become apparent that senescent cells modify their tissue environment long after senescence has been triggered with either beneficial or detrimental consequences.[2] An important component of senescence-induced tissue remodelling is the senescence-associated secretory phenotype (SASP).[3] It consists of a wide range of mostly pro-inflammatory cytokines and extracellular matrix proteins, which are continuously secreted from senescent cells.

While senescence has previously been described to frequently occur in ageing (chronic stress) and cancer (acute stress in response to oncogene activation or cancer therapy), it is now recognized to also actively contribute to tissue remodelling in many other physiological and pathophysiological processes during development from embryogenesis to degenerative diseases such as Alzheimer's disease.[4,5] In embryogenesis, senescence complements apoptosis in embryonic patterning and organ development by regulating the balance between different cell populations.[6] Senescent cells induce cell proliferation, differentiation or death in their environment before they get eliminated by macrophages.[7] Thereby, senescence shapes embyronic tissue and organ structures. Examples of senescence in embryonic development include the formation of the mesonephric tubules in the transitory embryonic kidney, the apical ectodermal ridge of the limbs and the closing neural tube.[8,9] Importantly, genetic disruption of senescence in embryogenesis is partially compensated by activation of apoptosis, but still produces morphological defects in a fraction of adult animals.

Senescence also maintains tissue integrity under physiological and pathophysiological conditions. In liver cirrhosis, which is typically triggered by chronic liver damage resulting from hepatitis virus infection or alcohol abuse[10], hepatic stellate cells (HSCs)

develop into senescent myofibroblasts and produce a stable fibrotic scar. The SASP elicited from senescent myofibroblasts attracts immune cells and initiates their clearance by the host immune system. This process partially resolves the fibrotic scar and thereby prohibits the development of hepatocellular carcinoma associated with progressive cirrhosis.[11]

Whereas senescence contributes to tissue development in embyrogenesis or tissue regeneration during fibrosis, senescence promotes tissue degeneration during ageing and in several pathophysiological contexts, for example obesity, by restraining the regenerative capacity of tissue stem cells or progenitor compartments, such as neuronal stem cells or pancreatic islet cells.[12] Dietary or genetic obesity promotes adipocyte senescence and induces an inflammatory response which supports the development of a metabolic syndrome, particularly insulin resistance.[13] This is accompanied by proliferative exhaustion and concomitant loss of pancreatic β-cells. Similarly, type 2 diabetes induced by genetic manipulations in β-cells of mice correlates with increased levels of DNA damage and senescence.[14] In mouse models of ageing tissue degeneration has been linked genetically to the accumulation of the cell-cycle inhibitor p16INK4a in senescence.[15] Consistently, genetic ablation of p16INK4a in a mouse model with accelerated ageing attenuates aging phenotypes in a subset of tissues, such as in adipose tissue or skeletal muscle. Importantly, selective clearance of p16INK4a-positive, i.e. senescent, cells in these mice also delays the onset of age-related pathologies in these tissues.[16] Hence, the removal of senescent cells can prevent or at least delay tissue dysfunction and prolong health during ageing.

Therefore, a central question in senescence research is under which circumstances senescence induction and maintenance or rather the elimination of senescent cells improves health and how these outcomes can be selectively accomplished. Moreover, the senescent phenotype is heterogeneous since it contains multiple features, for example DNA as well as chromatin modifications, autophagy and cytokine secretion, but their contribution to senescence varies depending on the cell type and the senescence trigger. Currently, the different features of senescence are added to define senescence with more or less confidence – i.e. simultaneous presence of many

or few senescence features. However, it remains to be determined which components or regulators of the senescence response are essential to maintain the phenotype, i.e. avoid its reversal or elimination, and which contribute positively or detrimentally to tissue integrity. Furthermore, strategies to seperate these layers in order to maintain favourable aspects of senescence and to remove the deleterious components await further investigation.

In light of the presented complexities the thesis discusses the role of senescence in tumor development and therapy with emphasis on the questions (1) how senescence contributes to treatment outcome and (2) whether strategies to selectively remove senescent cells following pro-senescent therapies improve survival. For this purpose the thesis demonstrates that senescent cells reprogram their metabolism and booster autophagy in a SASP-dependent manner. On this ground the thesis investigates potential synthetic lethal interactions of metabolic and autophagy inhibitors with premature senescence, illustrates their mechanistic principle and explores their relevance for cancer therapy.

5. Introduction

Senescence in cancer development and therapy

Cancer arises from cells which have escaped safeguard mechanisms that control cell replication, growth, mortality and dissemination. These mechanisms comprise cell-autonomous and non-cell-autonomous surveillance strategies which suppress or eliminate tumor cells and their pre-neoplastic precursors and thereby maintain tissue integrity. Similarly, cancer therapy tries to rejuvinate these failsafe programs to eliminate neoplastic cells and potentially to restore tissue integrity. In the past two decades senescence has been established as a powerful failsafe mechanism which counteracts excessive mitogenic signaling from activated oncogenes in preneoplastic cells and which controls tumor growth as part of cytotoxic treatment regiments *in vitro* and *in vivo* in both mice and men.[17–20] Melanocytic naevi are a paradigm example of the senescence failsafe response, since despite oncogene activation and enhanced mitogenic signals benign nevi eventually lose all proliferative activity, remain growth-arrested for decades and hence prevent melanoma formation.[21] Similarly, senescence occurs in benign tumors at risk of malignant transformation, for example in colon adenoma or intraepithelial neoplasia of the prostate, and in human breast cancer in response to neoadjuvant chemotherapy.[22,23]

Therefore, senescence stands alongside apopotosis as an important cellular failsafe program, which counteracts tumor formation, particularly in response to the activation of oncogenes, or which inhibits tumor progression as a result of cancer therapy. In contrast to apoptotic cells, whose desintegrated remainders are quickly removed from the tumor tissue by the innate immune system without a profound impact on the tumor environment, senescent cells remain viable components of the tumor with the potential to persistently alter the tumor environment, for example due to their immune-modulating function.[24]

Consequently, tumor cells must develop strategies to a priori bypass (apoptosis and senescence) or later escape (senescence) these safeguard mechanisms. Despite

open questions as to the interconnection between senescence and apoptosis, for example whether they are complementary or alternative failsafe programs, senescence has been established as a major antitumor response *in vivo*.[25] In fact, tumors which have acquired resistance to either apoptosis or senescence often remain sensitive to the other: Importantly, in apoptotically compromised tumors senescence is often engaged upon treatment.[26] This at least in part explains the poor correlation between sensivity for apoptosis and overall survival in cancer therapy.[27] While the proliferation arrest remains the dominant mechanism by which cellular senescence suppresses cancer, components of the SASP also reinforce senescence in an autocrine fashion and spread senescence by paracrine signals in different tissues and contexts.[28] Furthermore, immune clearance mechanisms for senescent cells exist, which contribute to a lasting tumor growth control.[24,29]

Nevertheless, senescence also entails features which promote tumorigenesis. Importantly, senescent cells remodel the tumor microenvironment by secretion of chemokines and cytokines, which can induce inflammation, angiogenesis and contribute to tumor dissemination.[30] Additionally, genetic models, in which tumor suppressors can be inactivated after senescence induction, suggest that senescent cells can escape the cell-cycle arrest and might later contribute to tumor outgrowth and treatment resistance.[31] Furthermore, senescent cells seem to acquire resistance to undergo apoptosis in response to conventional chemotherapy.[25] Senescent fibroblasts show reduced apoptotic sensitivity to DNA damaging treatments due to the upregulation of anti-apoptotic proteins, such as Bcl2, and reduced levels of p53.[32,33] However, therapeutic strategies which target anti-apoptotic proteins, such as the senolytic agent Navitoclax, or which induce apoptosis downstream of mitochondrial cell death effector proteins, for example small molecule caspase activators, effectively induce apoptosis in senescent cells.[2,34] Concomitantly, new anticancer compounds which specifically induce senescence or remove senescent cells are tested in clinical trials against a several different cancers.[35] However, their successful application will likely depend on a combination of factors, such as the tumor type, the senescence trigger and of course potential genetic defects in the apoptotic pathway acquired prior to senescence induction.

Types of senescence

As described above senescence is a failsafe mechanism which induces a permanent proliferation arrest in response to different cellular insults. These insults can be either acute or chronic, but almost invariably lead to an accumulation of DNA damage. Historically, replicative senescence, which describes the limited replicative capacity of normal human diploid fibroblasts (HDFs) in culture, was the first example of a senescence arrest program.[36] Replicative senescence occurs in the vast majority of normal cells after a finite number of cell divisions and has been tightly associated with cellular and organismal ageing.[37] It is triggered in response to irresolvable telomeric DNA damage which accumulates with each DNA replication and the associated shortening in telomere length.[38,39] Conversely, specific cell types, such as stem cells, activated lymphocytes, and, most prominently, cancer cells, which can synthezise telomeric DNA due to the expression of the enzyme telomerase or alternative mechanisms, postpone or even prevent the execution of replicative senescence. Furthermore, exogenous expression of telomerase in primary human cells delays replicative senescence and extends their lifespan.[40]

However, cellular senescence can also be induced independent of telemore length in normal or cancer cells. Since these senescence programs occur before cells have exceeded their replicative potential they are collectively referred to as premature senescence. Although premature senescence occurs in response to various internal and external stresses, such as viral infections or suboptimal nutrient supply, under both physiological and pathophysiological conditions two forms are of particular importance due to their clinical significance: oncogene-induced senescence (OIS) and therapy-induced senescence (TIS).

Oncogene-induced senescence (OIS)

OIS was first described in fibroblasts, in which overexpression of an oncogenic version of HRAS ($HRAS^{G12V}$) and hence activation of the MAPK (mitogen-activated protein kinase) signaling pathway unexpectedly leads to an acute proliferation arrest with

features reminiscent of replicative senescence.[20] On a molecular level, this is explained by accumulating DNA damage and the derepression of the *CDKN2A* locus in response to acute replication stress.[41] The *CDKN2A* locus encodes the tumor suppressor genes *p16INK4a* and *p14ARF* (*p19Arf* in the mouse).[42] p16 inhibits the cyclin dependent kinases 4 and 6 (CDK4 and CDK6) and activates the retinoblastoma (RB) family of proteins, which block G1-to-S phase transition by repression of growth-promoting E2F target genes.[43] The repression of E2F target genes is subsequently stabilized by the formation of heterochromatin marks, which requires the histone H3 lysine 9 (H3K9) trimethylation activity of the histone methyltransferase SUV39H1.[44] p14ARF induces the tumor suppressor p53, which is also activated by the DNA damage response via ataxia telangiectasia mutated (ATM) and ataxia telangiectasia and RAD3 related (ATR) kinases.[45,46] p53 promotes the cell-cycle arrest condition by activation of growth inhibitory genes. Furthermore, inhibition of CDK–cyclin complexes by the cyclin-dependent kinase (CDK) inhibitors p15INK4B (encoded by *CDKN2B*), p21WAF1 (encoded by *CDKN1A*) and p27KIP1 (encoded by *CDKN1B*) orchestrate the proliferation arrest, and, hence, may contribute to senescence.[47,48,49] Furthermore, OIS is epigenetically controlled: RB promotes the formation of heterochromatin around E2F target genes which contain repressive epigenetic marks, such as methylated H3K9, HP1, and macroH2A.[50] Of note, exogenous expression of telomerase, which is sufficient to delay or rescue replicative senescence, does not prevent OIS.[51] Therefore, it remains to be determined how signals which initiate and maintain a stable cell cycle arrest are qualitatively and quantitatively converted into pro-senescent signals, and whether or not the senescence condition requires the permanent presence of such upstream triggers.

Whereas the loss of either p53 or both p16 and ARF generally abrogates OIS, the contribution of other tumor suppressors depends on the cell type and the oncogene.[52] For instance, the ARF–p53 pathway is a crucial activator of OIS in mice, whereas the DDR–p53 pathway seems to be more important for OIS in human cells.[53,54] Furthermore, deletion of p16 abrogates senescence in many human cells whereas it is dispensible for OIS in mouse cells.[55] Also, RB-deficient cells arrest in response to oncogene activation, because they encounter a proliferation barrier imposed by p53

and p21 in response to DNA damaging replication stress, and because they maintain the transition checkpoint by compensatory activity of other RB family members.[56] However, the combined loss of both p21 and RB licences cells to aberrantly replicate DNA and hence circumvent OIS as a cellular failsafe mechanism.[57] Also, the acute inactivation of all three RB family members in senescent cells permits cell-cycle re-entry in mouse embryo fibroblasts.[58] Besides the oncogenic forms of RAS, which remain the the prototypic drivers of OIS, other MAPK signaling components, for example BRAF and MEK, as well as oncogenes such as MYC and ERBB2, elicit senescence.[59,60] Therefore, OIS is an important tumor failsafe mechanism in many cancers, particularly in RAS- or BRAF-driven tumors. In human nevi senescence is associated with the presence of oncogenic $NRAS^{Q61R/K}$ or $BRAF^{V600E}$ *in vivo.*[61] Similar marks of senescence are also found in human prostate intraepithelial neoplasia (PIN) lesions, which form premalignant conditions in prostate cancer.[62]

Of note, loss of tumor suppressors can also induce senescence, probably as a result of unrestricted mitogenic signaling. Interestingly, loss of the tumor suppressor PTEN in prostate cells, which prevents unchecked PI3K signaling, induces a phenotype resembling senescent PIN lesions, but occurs without an overt DNA damage response.[63] Similarly, loss-of-function mutations in the NF1 tumor suppressor trigger excessive RAS signaling and thereby drive the familial cancer syndrome neurofibromatosis type I, in which neoplastic lesions known as neurofibromas express markers of senescence.[64]

Therapy-induced senescence (TIS)

Besides OIS as a cellular failsafe mechanism for cells at risk of transformation, Figure 1 illustrates that senescence also occurs in cancer cells as an acute stress response to DNA damaging treatments, such as chemotherapy or γ-irradiation.[65,23] Therefore, therapy-induced senescence (TIS) should effectively and persistently inhibit cancer growth and complement apoptosis as antineoplastic treatment principle, particularly in tumors in which apoptotic pathways are compromised.[66] Tumor cell senescence in response to cytotoxic therapies almost unequivocally depends on the generation of

DNA damage by single- or double-strand breaks and the production of reactive oxygen species, which additionally cause lipid and protein damage.[67]

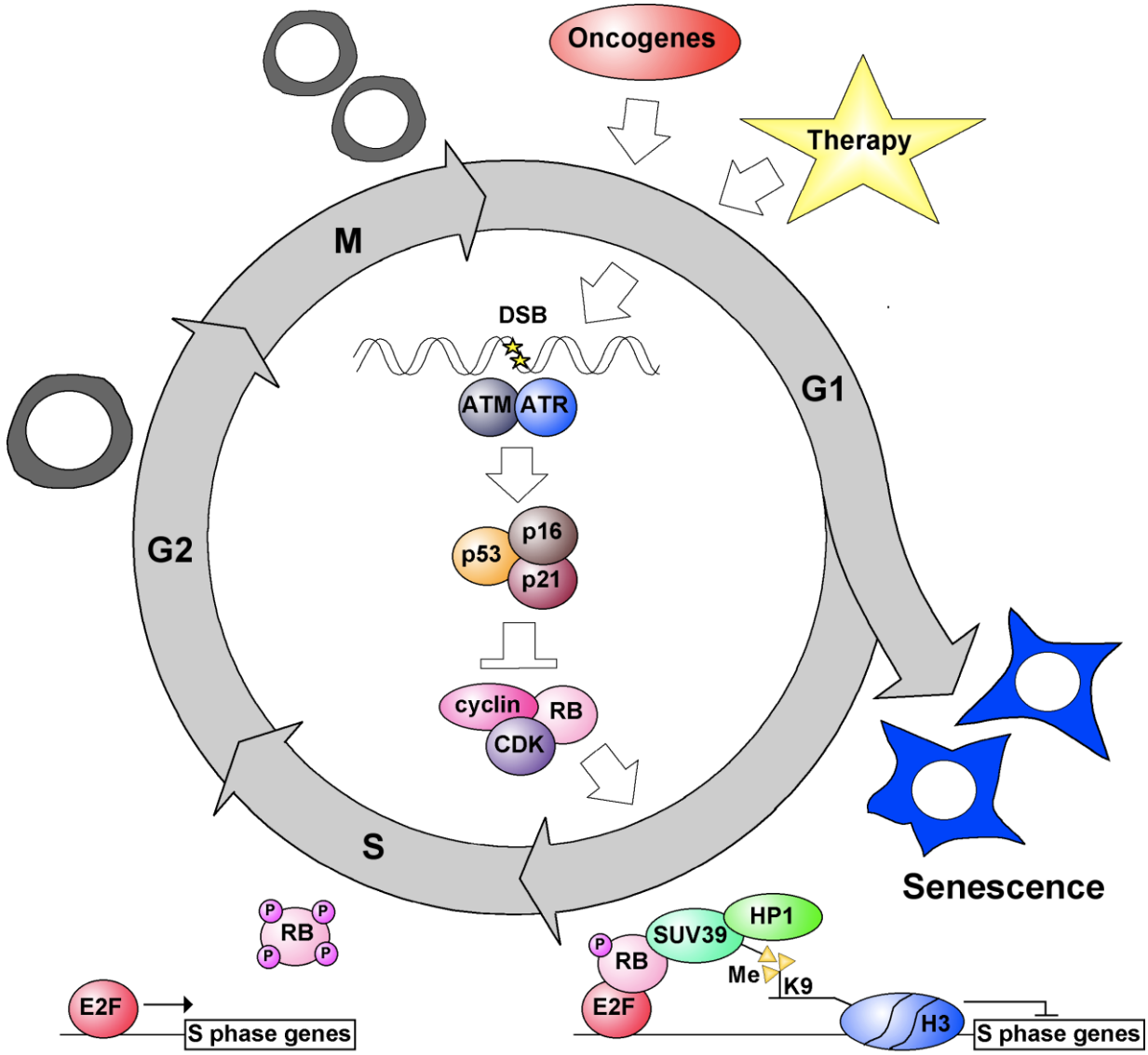

Figure 1. Signaling in OIS and TIS. Activation of oncogenes or application of chemotherapy induces DNA damage, for example double-strand breaks (DSB). This initiates a DNA damage response (DDR) which involves the recruitment and phosphorylation of protein kinases ATM and ATR and subsequently the activation of the tumor suppressors p53, p21, p16. Both p21 and p16 inhibit cyclin dependent kinases (CDK) and thereby prevent phosphorylation and inactivation of the tumor suppressor RB. Hypophosphorylated RB establishes a repressive chromatin structure around E2F target gene promoters by recruiting the methyltransferase SUV39 to histones and promoting trimethlyation of lysine 9 on histone H3 (H3K9me3). This blocks the transcription of E2F-responsive S-phase genes and triggers a senescent G1 cell cycle arrest. ATM = Ataxia telangiectasia mutated, ATR = Ataxia telangiectasia and RAD3 related, p21WAF1 = CDKN1A (cyclin-dependent kinase inhibitor 1a), p16INK4A = CDKN2A (cyclin dependent kinase inhibitor 2a), RB = Retinoblastoma protein, CDK = cyclin-dependent kinase, SUV39 = Suppressor of variegation 3-9, HP1 = heterochromatin protein 1, H3 = histone 3.

Persistent DNA damage and the concomitant DNA damage response (DDR) is associated with therapy-induced senescence primarily through p53 and p21 activation.[23,68] Other components of the DDR pathway also contribute to TIS, particularly the protein kinase ATM. ATM senses DNA double strand breaks and subsequently activates and stabilizes p53 both directly and indirectly through interference with the p53 inhibitor MDM2.[69] Whereas the loss of ATM compromises DDR-initiated replicative senescence and strongly affects TIS, other components of the DDR pathway, such as ATR, and checkpoint homologs 1 and 2 (CHK1 and CHK2), are less important in the execution of senescence.[70] For instance, loss of ATR is compensated by ATM but not vice versa.[71] Furthermore, inactivation of CHK1 rather stabilizes the senescence growth arrest, because it delays the resolution of DNA damage foci and hence maintains DDR signaling.[72]

However, different DNA-damaging compounds as compared to anti-microtubule drugs or irradiation seem to elicit senescence to varying degrees: Treatment of HT1080 fibrosarcoma cells with equitoxic (i.e. 85% growth inhibition after continuous exposure for four days) levels of different drugs *in vitro* revealed that the DNA-interactive agents adriamycin, also called doxorubicin, and cisplatin produce the strongtest TIS response (>50% senescence based on the measurement of senescence-associated β-galactosidase (SA-β-gal) activity and cell cycle analysis).[73] Furthermore, etoposide, 5-fluorouracil and irradiation also proved effective in eliciting TIS, whereas the microtubule-targeting drugs docetaxel and vincristine, which typically trigger a mitotic catastrophe, produce only low amounts of TIS. In fact, the topoisomerase inhibitor adriamycin induces senescence in numerous human cancer cell lines and mouse models of cancer.[74,75–77]

Notably, TIS occurs in human tumors *in vivo*, as demonstrated in response to genotoxic treatments as part of neoadjuvant chemotherapy. For instance, breast tumors show positive Sa-β-gal staining after treatment with cyclophosphamide, adriamycin, and 5-fluorouracil.[78] Similarly, TIS is present in lung tumors after treatment with carboplatin and docetaxel.[79] Also, senescence levels at diagnosis might serve as a predictor for treatment outcome as suggested for metastasized colorectal cancer.[80]

Besides classical chemotherapy novel anticancer drugs can also induce TIS. These pro-senescent therapies often either directly activate senescence pathways or re-install silenced components of the senescent program. For instance, modulation of the epigentic landscape by the DNA methyltransferase inhibitor 5-Azacytidine, which inhibits DNA methylation, or the histone DNA acetylase inhibitor sirtinol, which alters normal chromatin structure, triggers TIS by modulation of MAPK signaling and activation of p16INK4a in breast, lung and prostate cancer cell lines.[81,82] Also, the anti-CD20 antibody rituximab, which is a standard component of B-cell lymphoma therapy, as well as the CDK4/6 inhibitor palbociclib, which is approved for certain types of breast cancer, induce senescence in lymphoma, melanoma and breast cancer cell lines.[83,84] Additionally, pharmaceutical compounds which interfere with cell cycle progression, for example inhibitors of the mitosis-regulating Aurora kinase A and CDK2 inhibitors, induce senescence in various cancer cell lines.[85]

Furthermore, stabilization of p53 by MDM2 inhibitors, such as Nutlin 3, or reactivation of mutant p53 by small molecules, such as PRIMA-1, trigger TIS.[86] Alternatively, interference with MYC by genetic or pharmaceutical means may induce senescence in „MYC-addicted“ tumors, although the underlying cell-autonomous – and probably non-cell-autonomous – mechanisms remain to be elucidated. In genetic mouse models, in which c-Myc activation can be controlled, switching off c-Myc induces senescence in lymphomas, osteosarcomas or hepatocellular carcinomas.[87] Similarly, introduction of a mutant Myc protein (OmoMyc), which dimerizes with wild-type Myc or Max into complexes with reduced DNA binding efficiency and hence acts as a dominant-negative mutant of c-Myc, causes decreased proliferation and senescence in advanced lung adenocarcinomas.[88] Alternatively, inhibition of Myc expression by the small molecules JQ1 or I-BET151, which target Myc transcriptional coactivator bromodomain and extraterminal (BET) proteins and thereby block proliferation, are used as therapeutic strategy for acute myeloid leukemia (AML), mixed-lineage leukemia (MLL) and multiple myeloma (MM).[89,90,91] In particular, treatment of mouse models of multiple myeloma with JQ1 induce a senescent growth arrest.[90]

Studying cellular senescence in mouse models of cancer

Following the observation that premature senescence is a response of primary cells to oncogene activation and of cancer cells to chemotherapy *in vitro*, several mouse models of different cancer entities have underscored the relevance of OIS and TIS *in vivo*. In mouse models with inducible oncogenes, endogenous $Kras^{G12V}$ triggers senescence during the early stages of lung and pancreatic tumorigenesis.[92] Furthermore, senescence also occurs in lung tumors and melanocytic nevi in mice which endogenously express $Braf^{V600E}$.[93] Importantly, nevi progress to melanoma only after additional mutations are acquired which cancel OIS.[94] Similarly, $Hras^{G12V}$ expression from either its endogenous or tissue-specific promoter triggers OIS in papillomas, the mammary gland and the urothelium.[52,95,96] Importantly, $Hras^{G12V}$ drives hyperproliferation in the mammary gland at low expression levels, but triggers OIS at high expression levels. Furthermore, transgenic expression of $Nras^{G12V}$ in lymphoid tissue triggers OIS and thereby blocks lymphomagenesis.[97] Importantly, mice which harbour heterozygous lesions at the *Suv39h1* or *p53* locus fail to undergo OIS and develop T-cell lymphomas. In addition, only $Nras^{G12V}$ transgenic lymphomas, but not Suv39h1- or p53-deficient lymphomas undergo TIS when apoptosis is blocked by overexpression of the anti-apoptic *Bcl2* gene.[97]

This is important because the most common subtypes of Non-Hodkin's lymphoma (NHL), i.e. diffuse large B cell lymphoma (DLBCL) and follicular lymphoma (FL), frequently harbour mutations in the apoptotic pathway.[98,99] FL is characterized by *BCL2* overexpression due to the t(14;18)(q32;q21) chromosomal translocation, which occurs in about 90% of FL cases. In DLBCL *BCL2* is also frequently overexpressed either due to gene translocation (t(14;18)), gene amplification or in response to hyperactivation of the NfκB pathway.[100] In fact, constitutive activation of NfκB due to genetic alterations in B cell receptor signaling, such as CD79A/B and CARD11 mutations or A20 loss, is the predominant mechanism for lymphoid malignancies, particularly for DLBCL, to acquire resistance to apoptosis.[101] Consequently, only around 50% of the DLBCL patients experience a complete remission in response to the standard treatment, which is based on an antracycline-based chemotherapy (cyclophosphamide, doxorubicin, vincristine and prednisolone) in combination with the

monoclonal anti-CD20 antibody rituximab (R-CHOP).[102] However, lymphomas might remain susceptible to TIS. In the Eμ-*myc* mouse lymphoma model, in which primary lymphoma cells are stably transduced with *Bcl2* to block therapy-induced apoptosis, TIS occurs upon adriamycin treatment *in vitro* or cyclophosphamide treatment *in vivo* at high frequencies.[103] In this system TIS depends on the engagement of the *Cdkna* locus and a p53-mediated DNA damage response.[104] Genetic disruption of either of these pathways abolishes TIS, enforces treatment resistance and hence directly affects treatment outcome.[66]

The Eμ-*myc* mouse lymphoma model

The Eμ-*myc* mouse lymphoma model was made in 1985 by generating a transgenic mouse with a rearranged *c-myc* oncogene, which was cloned from a mouse plasmocytoma.[105] The Eμ-*myc* transgene carries an insertion 361 bp 5' to the *c-myc* gene on chromosome 15, which contains a 2.3 kb segment of the immunoglobulin heavy (H) chain locus from chromosome 12. The insertion introduces the lymphoid-specific enhancer from the Ig heavy chain locus region and disrupts a region which controls normal *c-myc* tissue expression. The resultant transgenic mice express the Eμ-*myc* transgene predominantly in B-lymphoid cells and eventually develop B cell lymphomas resembling human non-Hodgkin lymphomas.[106] The tumor burden can be easily monitored by palpation of the peripheral lymph nodes. Therefore, lymphomas become detectable upon formation of the disease and can be subjected to treatment studies, for example with the alkylating agent cyclophosphamide, which is a major component of the standard treatment regime R-CHOP for DLBCL and which induces apoptosis and senescence in the Eμ-*myc* mouse lymphoma model.[107] Similar tumor models have been developed with other oncogenes, for example the Eμ-*Nras* transgenic mouse model, which forms histiocytic sarcomas and sporadically T cell lymphomas, or the Eμ-*Tcl1* transgenic mouse model, which ressembles chronic lymphocytic leukemia (CLL).[108] To identify cooperating genetic events in Myc-driven lymphomagenesis, Eμ-*myc* mice can be further manipulated genetically, for example by crossbreeding with mice which lack tumor suppressor genes, or by insertional

mutagenesis and shRNA library screens as illustrated in Figure 2.

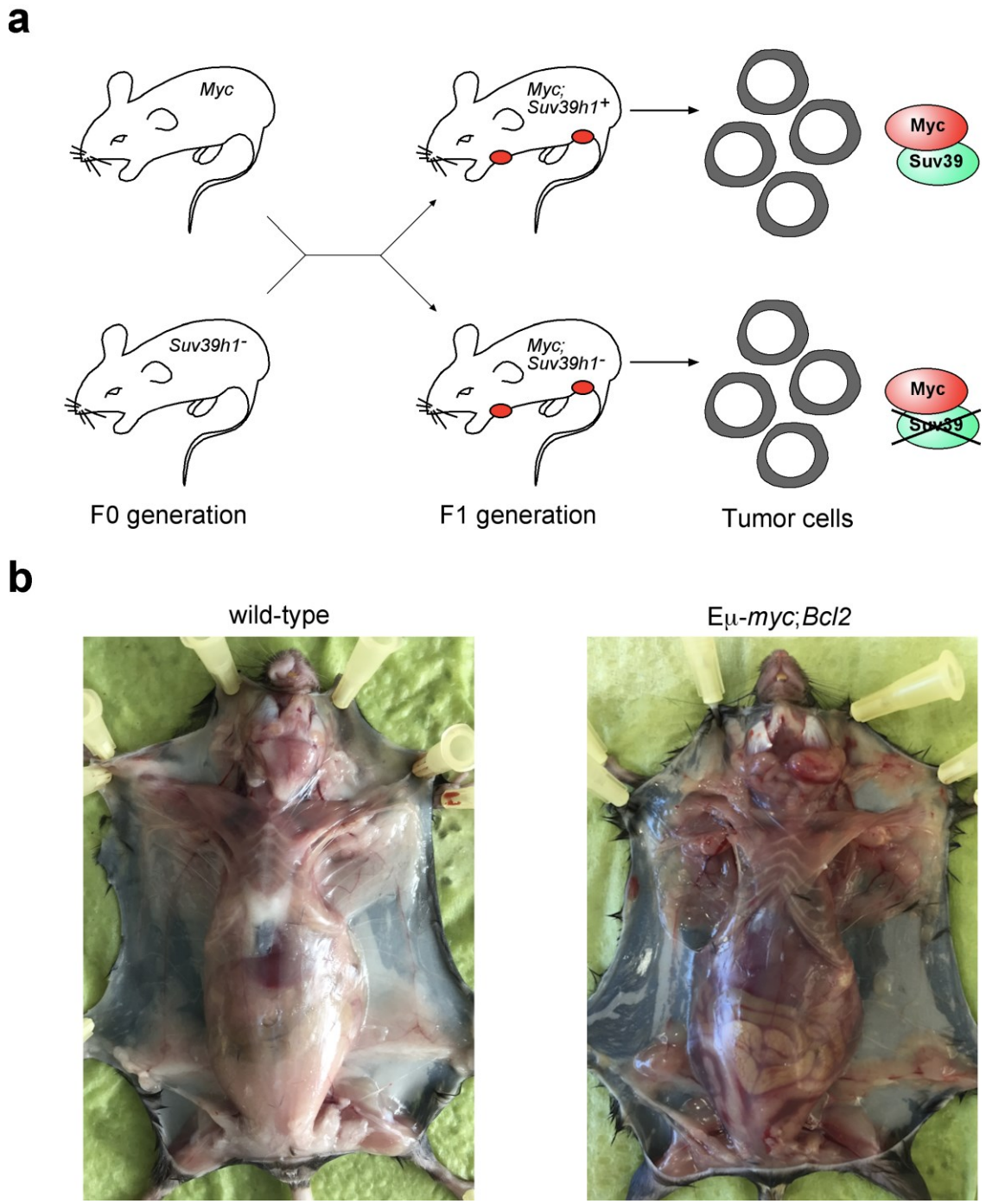

Figure 2. The Eμ-*myc* mouse lymphoma model. a, Breeding strategy to generate Eμ-*myc* lymphomas with targeted genetic lesions in the *Suv39h1* locus. Male Eμ-*myc* mice were bred to female *Suv39h1*$^{-}$ mice in a C57BL/6 background. Mice in the F1 generation were genotyped three weeks after birth and subsequently monitored for tumor latencies by palpation of peripheral lymph nodes every two days. Since the *Suv39h1* locus is X-linked, Suv39h1-deficient mice can be genotyped as either *Suv39h1*$^{-/y}$ (male) or *Suv39h1*$^{-/-}$ (female). When animals developed a palpable lymphadenopathy they were sacrificed and lymphoma cells were isolated. **b**, Representative photomicrographs of normal (left) and Eμ-*myc*;*Bcl2* lymphoma bearing (right) C57BL/6 mice. Lymphomas in wild-type mice form approximately

two weeks after tail vain injection of lymphoma cells generated as in a. Note lymphoma manifestations in the cervical, axillary and inguinal region.

These models identified a number of important regulatory genes, including the tumor supressor genes *p53* and and its regulator *p19Arf*, the transcriptional coactivator *Pim1* and the anti-apoptotic *Bcl2* oncogene.[109–111] Importantly, *E*μ-*myc* lymphomas are monoclonal and largely composed of cells with tumor initiating potential. Therefore, they can be reconstituted by as little as 10 lymphoma cells in wild-type or genetically manipulated mice by tail vain injection into syngeneic animals.[112] Furthermore, this allows investigation of tumor-host interactions by initiating lymphoma growth in mice which carry defined genetic lesions, for example in the immune system or the tumor stroma.

Histone modifications in senescence

In eukaryotic cells genomic DNA is assembled into tightly compacted, albeit dynamic chromatin structures by histone and non-histone proteins. The basic building block of chromatin is called a nucleosome. It consists of 147 base pairs of DNA and an octamer of histone proteins composed of two copies of each H2A, H2B, H3 and H4. The DNA between each nucleosome is associated with the histone H1.[113] While the core of the histone proteins is covered in the nucleosome, the N- and C-terminal tails of the histone proteins protrude from it.[114] These histone tails are subjected to site-specific post-translational modifications (PTMs), which mostly occur at the N-terminal tail. The PTMs can be classified into different groups according to the chemical modification of the amino acids, i.e. acetylation, methylation, phosphorylation, ubiquitylation, sumoylation, ADP ribosylation, deimination and proline isomerization, of which histone acetylation of lysine residues, methylation of argenine and lysine residues and phosphorylation of serine, tyrosine and threonine residues are the most abundant PTMs.[115] The PTMs can be quickly installed and removed by histone modifying enzymes, which orchestrate the highly dynamic switches in chromatin structure. The PTMs also recruit chromatin remodeling complexes, such as Swi/Snf or NURD, which alter the nucleosome structure or position and hence regulate DNA accessibility. In this way, PTMs control all biological processes related to DNA.

Importantly, combinations of different PTMs, which together form a “histone code“, result in specific chromatin structures and gene expression patterns.[116,117]

Therefore, chromatin modifications also control both proliferation and cell cycle arrest conditions, such as senescence. Mitogenic signals promote histone modifications, which set up an accessible chromatin structure around S-phase gene loci. This euchromatic structure is mainly characterized by hyperacetylated histones and methylation of H3 at lysine residues K4, K36 and K79. Conversely, arrested cells display mainly inaccessible heterochromatin structures on S-phase genes which are hypoacetylated and di- or trimethylated at histone 3 (K9, K20, K27) or histone 4 (K20).[118–120] H3K9 methylation requires removal of both H3K9 acetylation and H3K4 methylation, which is orchestrated by the histone deacetylase 3 (Hdac3) and H3K4-specific demethylases JARID1A and JARID1B.[121,122] Importantly, hypermethylated H3K9 prohibits adjacent H3K4 methylation and in the G1 and S phase of the cell cycle also H3S10 phosphorylation that would otherwise provoke transcriptional activation.[123,124] Therefore, histone lysine methylation at H3K9 plays a central role in heterochromatin formation and gene silencing in general, and it controls the repression of S-phase-relevant genes in particular.[125,]

Histone methylation is catalyzed by SET domain-containing and non-SET domain-containing histone methyltransferases (HMTs).[126] DOT1/DOTL1 is the only non-SET domain-containing HMT identified so far and targets H3K79 in the globular core of the histone. DOT1/DOT1L-mediated H3K79 methylation controls transcription, reprogramming, development, differentiation, and cell cycle progression. The SET domain-containing HMTs selectively methylate individual lysine residues on N-terminal histone tails: SET1 acts on H3K4, SUV39H1 and SUV39H2 as well as SETDB1 and RIZ1 act on H3K9, SUV420H2 on H4K20 and EZH2 on H3K27.[123,127–129] The human (SUV39H1 and SUV39H2) and murine (Suv39h1 and Suv39h2) enzymes are homologues of *Drosophila melanogaster* SU(VAR)3-9, which encodes a histone methyltransferase with specificity for H3K9. Originally, SU(VAR)3-9 was identfied as a powerful suppressor (SU) of variegation (VAR) from a group of genes which modulate position effect variegation (PEV) in *Drosophila melanogaster* and

Schizosaccharomyces pombe.[130,131] Position-effect variegation describes the inactivation of a gene in response to juxtaposition with heterochromatin by rearrangement or transposition of DNA. SUV39H enzymes control genomic stability and chromosomal segregation by stabilizing pericentric chromatin, but also mediate local gene repression by focal heterochromatinization in euchromatic regions, particularly of S-phase related genes.[132]

Therefore, SUV39H enzymes are crucial epigenetic regulators for mammalian development and cancer. Knockout mice deficient for both Suv39h1 and Suv39h2 are growth retarded and infertile and suffer from increased lethality with only one third of *Suv39h* double-knockout mice surviving to adulthood. Also, *Suv39h* double-null mice are prone to tumor development due to chromosomal missegregation and show a high incidence for B cell lymphomas.[133] As described above, in an Eμ-*Nras* mouse model genetic depletion of Suv39h1 alleles disrupted H3K9 trimethylation and heterochromatin formation.[134] Loss of Suv39h1 therefore blocked OIS and promoted lymphoma development. Furthermore, overexpression of Suv39h1 and concomitantly higher levels of H3K9me3 inhibit DMBA/TPA induced skin carcinogenesis.[135] However, primary fibroblasts, which lack Suv39h1 and Suv39h2, remain susceptible to replicative senescence and OIS. This suggests that the epigenetic marks differ in lymphocyte and fibroblast senescence.[133] Genetic alterations in other H3K9 methyltransferases, i.e. *RIZ1* and *SETDB1*, were found in human breast cancer, melanomas, lung carcinomas or colorectal tumors.[135,136] Therefore, dysregulated H3K9 methyltransferases are commonly found in cancer, although their role in senescence remains to be determined.[137]

SUV39H proteins interact with a broad variety of chromatin-associated proteins and histone modifiers, such as histone deacetylases (HDACs) and heterochromatin proteins (HPs) to set up and stablilize heterochromatin structures. Importantly, SUV39h1 also associates - albeit indirectly via HP1 - with RB, whose inactivation drives the development of retinoblastoma and other types of human cancers.[138] RB acts as a powerful tumor suppressor, because it blocks the expression of S phase relevant genes by directly inhibiting the transcription factor E2F and by transcriptional

repression of their promotor regions through SUV39H1-mediated H3K9 methylation.[43,44] As shown in Figure 3, Suv39H1-mediated H3K9 trimethylation thus controls senescence by initiating the formation of senescence-associated heterochromatin foci (SAHF).[139]

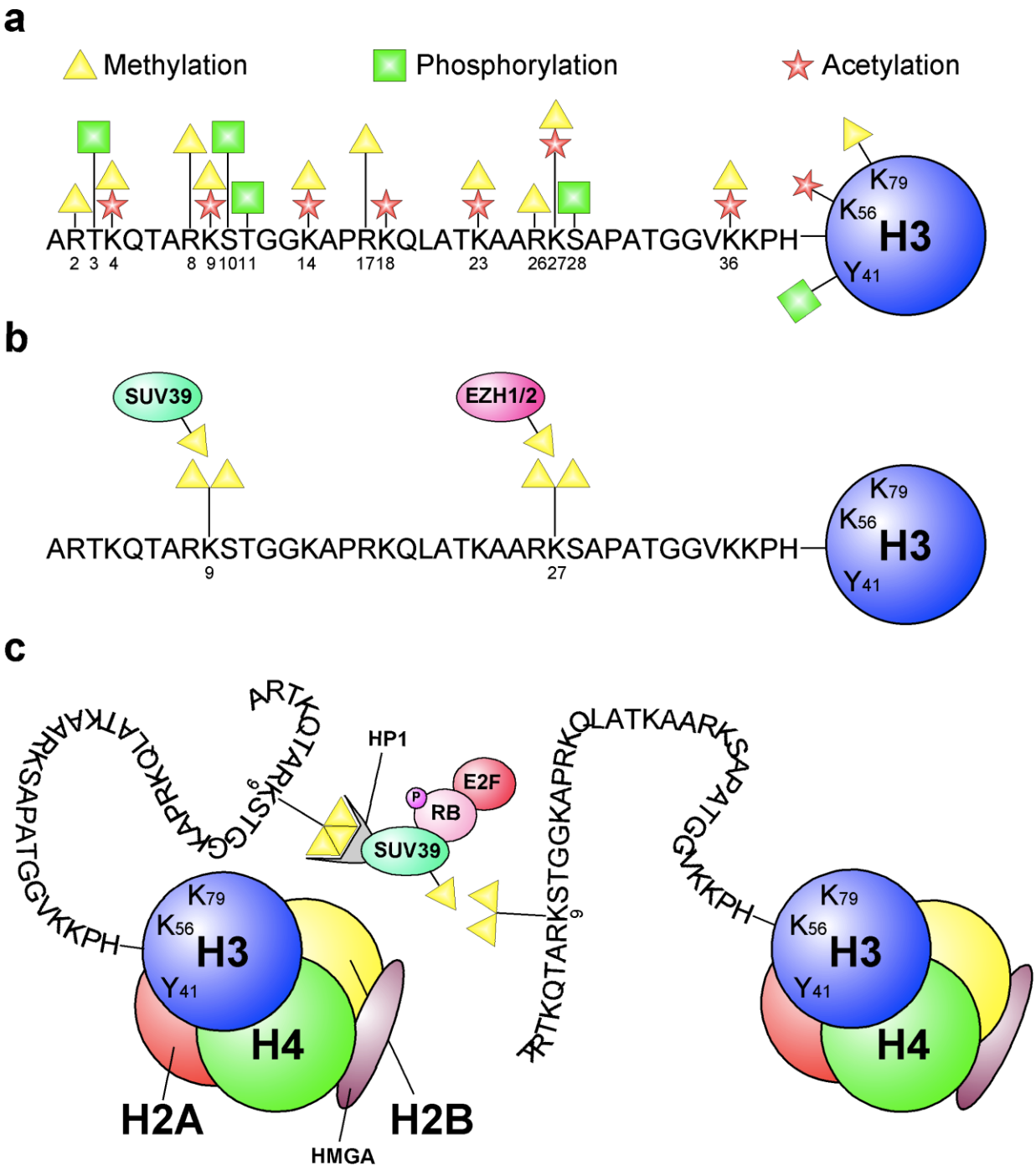

Figure 3. Histone modifications in senescence. a, Major histone modifications on histone H3, selectively showing acetylation, phosphorylation and methylation. Modifications predominantly occur on the N-terminal tail of H3 with few addtional alterations on the globular

domain. **b**, Histone methyltransferases SUV39H1/2 and EZH1/2 catalyze crucial epigenetic modifications which control constitutive (H3K9) and facultative (H3K27) heterochromatinization. **c**, Model of SAHF formation and spreading, which involves H3K9 trimethylation by SUV39H1/2 histonmethyltransferases. HP1 helps to spread the H3K9me3 mark and HMGA stabilizes the SAHF structure. EZH1/2 = Enhancer of zeste homolog 1/2, SAHF = senescence associated heterochromatin foci, HP1 = Heterochromatin protein 1, HMGA = High mobility group AT hook, H2-H4 = Histone proteins 2-4.

SAHF stably embed genomic loci of S phase genes, such as *Cyclin A* and *CDK2,* into heterochromatin structures.[14] Besides H3K9 trimethylation by SUV39H1, SAHF formation depends mainly on the activities of the p53/p21 and p16/RB pathways. Knockdown or inactivation of RB and p53 abolishes SAHF formation and senescence in primary human fibroblasts.[140] Nevertheless, it remains to be investigated how RB is structurally involved in SAHF formation: Whereas RB seems to be dispensible for SUV39H1-mediated H3K9 trimethylation of E2F target genes, it is required for the recruitment of heterochromatin protein 1 gamma (HP1γ) and stable silencing of S phase genes.[141]

SAHF are composed of layers of constitutive heterochromatin at their core, which contains trimethylated H3K9 (H3K9me3) and facultative heterochromatin in their periphery, which contains trimethylated H3K27.[142] In their core region H3K9me3 associates with components of constitutive heterochromatin such as HP1.[143] However, SAHF also comprise structures absent from constitutive heterochromatin such as the enrichment of core histone macroH2A and non-histone chromatin architectural proteins (HMGA), and the depletion of linker histone H1.[143–145] In this way SAHF segregate constitutive heterochromatin, facultative heterochromatin, and active euchromatin into exclusive layers.[146] This creates an environment in which both gene repression and gene activation can be very efficiently coordinated and maintained. Therefore, SAHF-like structures may also promote the expression of senescence-specific genes and, hence, regulate important aspects of the senescence phenotype, for example lysosomal protein degradation or inflammation. Importantly, SAHF are not always required for senescence, and they are species- and cell line-dependent.[147,148]

Mouse cells do not display SAHF-typical focal heterochromatin, although certain SAHF components, such as macroH2A, are enriched in senescence.[149] While replicative

senescence in the primary human embryonic fibroblast cell lines IMR90 and WI38 cells is associated with SAHF, replicative senescence in the primary human foreskin BJ fibroblasts does not involve SAHF formation.[140,147] Therefore, the cooperation of histone modifications, heterochromatin formation and SAHF in senescence, and their contribution to the senescent phenotype require further investigation.

The senescent phenotype

Although senescence can be induced by different stimuli, senescent cells share a number of common features beyond the abrogation of DNA synthesis and a cell cycle arrest in G1.[150] They display specific modifications at the cellular level, in particular with respect to their morphology, and at the molecular level, for example in their transcriptome, proteome and metabolome.[22,151] Senescent cells increase in cell size, change their shape and alter the structure of their organelles. Importantly, senescent cells display strongly enlarged and vaculoated endoplasmic reticulum and lysosomal compartments. Concomitantly, senescent cells display enhanced activities of many lysosomal proteins, such as the senescence-associated β-galactosidase (SA-β-gal), which serves as a key marker for senescence.[152]

Furthermore, senescent cells show marked alterations in their gene expression profile (GEP) compared to their proliferating counterparts.[153] In GEPs from OIS and TIS cells genes controlling cell cycle progression and hence cell proliferation are expectedly downregulated, particularly at the G1/S transition, while genes associated with lysosomal function and membrane biosynthesis are upregulated.[154,155] Additionally, the expression of a wide spectrum of secretory factors, which include pro-inflammatory cytokines, such as interleukin-6 (IL6) and -8 (IL8), chemokines, particularly monocyte chemoattractant proteins (MCPs) and macrophage inflammatory proteins (MIPs), and growth factors, for example granulocyte–macrophage colony-stimulating factor (GM-CSF), but also components of the extracellular matrix (ECM) and ECM proteases, is elevated in senescent cells.[156] Hence, senescence is not a mere cell cycle arrest program which limits the lifespan of a cell or acts as a cellular failsafe mechanism in cancer development and therapy, but also constitutes an individual entity within a

heterogeneous tissue or tumor environment with the potential to modulate the activity of the host immune system or the proliferation of tumor cells in their vicinity as demonstrated in Figure 4.

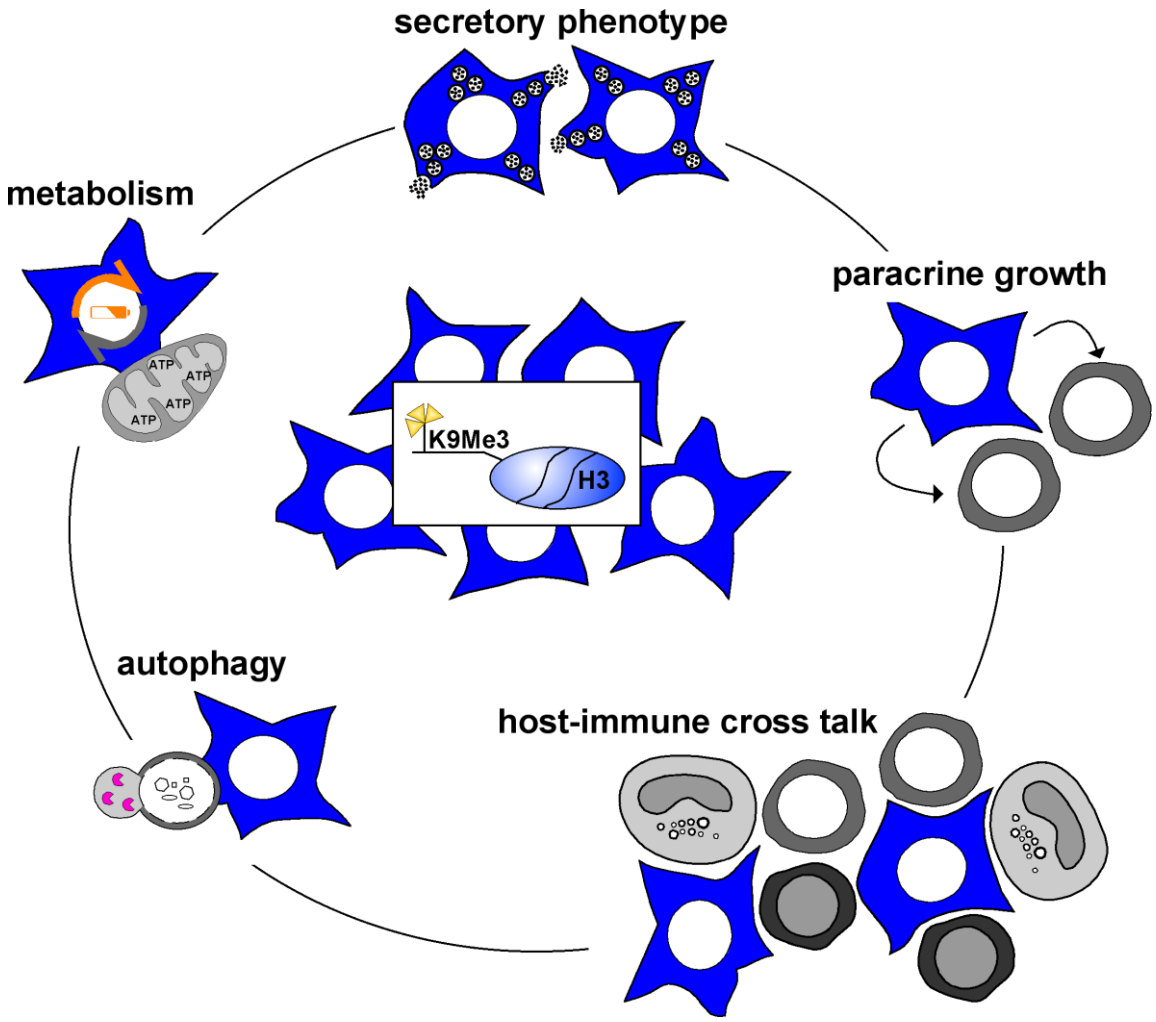

Figure 4. The senescent phenotype. H3K9me3-governed senescence initiates several senescence-associated cellular programs, for example autophagy. Senescent cells also alter their metabolism and acquire a senescence associated secretory phenotype (SASP). The SASP modulates the growth of tumor cells in the vicinity and attracts the host immune system. It remains to be determined how and to what extent H3K9 trimethylation orchestrates these changes molecularly and at what level different senescence features are interconnected. A better understanding of the senescent phenotype offers opportunities to selectively enhance, diminish and modulate senescence and its associated programs.

Senescence-associated secretory phenotype

The enhanced production of secreted factors is associated with both replicative and premature senescence and is collectively referred to as the senescence-associated

secretory phenotype (SASP).[157] Besides its influence on the tissue environment, the SASP may reinforce senescence via an autocrine feedback loop, which involves IL6, but it is not necessary for senescence induction.[103] While most senescence stimuli, particularly those which cause DNA damage, also trigger a SASP, the ectopic expression of cell cycle inhibitors, such as p16 and p21, induces senescence in primary cells, but fails to elicit a SASP.[158]

Therefore, SASP expression in response to DNA damaging stimuli requires an intact DNA damage response pathway.[157] Furthermore, SASP expression is regulated by different signaling networks, most importantly the MAPK and NF-κB signaling pathways.[159,160] NF-κB activity is stimulated by both internal cues, such as oncogene activation, and external cues, particularly B cell and cytokine receptor signaling.[161] There are five members of the nuclear factor (NF)-κB protein family (RelA or p65, c-Rel, RelB, p50 and p52), which act as dimers of different combination in transcription.[162] Their activity is controlled by IκB proteins, which bind and thereby retain NF-κB proteins in the cytoplasm. Phosphorylation of IκB by IκB kinases leads to proteasome-dependent degradation of IκB and subsequent nuclear localization of NF-κB.[163] Depending on the stimulus, the assembled protein dimers and the target genes NF-κB signaling is grouped into the classical or alternative pathway. In the classical NF-κB pathway the β subunit of the IκB kinase (IKK) complex phosphorylates IκB proteins on two N-terminal serine residues and hence triggers nuclear localization and activation of p50/p65. Truncated forms of IκB, which lack the N-terminal serine residues, act as inhibitors of NF-κB, because they bind NF-κB proteins and undergo proteasomal degradation, but fail to release p50/p65 upon NF-κB pathway activation.[164]

The classical NF-κB pathway controls the majority of the cytokines and chemokines which belong to the SASP. In OIS and TIS, SASP expression requires phosphorylation, nuclear translocation and chromatin binding of p65.[165,166] Pharmacological or genetic inhibition of NF-κB signaling by expression of a dominant-negative IκBα mutant, which lacks the 70 amino-terminal amino acids (IκBαΔN) inhibits the expression of several

SASP factors.[167] Furthermore, the transcription factor C/EBPβ controls key components of the SASP. Deletion of C/EBPβ abrogates the expression of IL6 and IL8 in BRAF-senescent fibroblasts, and licenses cells to bypass OIS. [153]

Although the SASP is a core component of senescence, the senescent secretome varies among cell types and senescence stimuli and differently impacts on its environment.[168] The secretion of cytokines and chemokines by senescent cells causes inflammation and apparently promotes the clearance of senescent cells by immune cells.[24] Other SASP components, such as IGFBP7, PAI1 or TGFβ, also trigger senescence in neighbouring cells by paracrine action or maintain the senescent phenotype in OIS and replicative senescence.[169,170] However, in heterogenous cell systems, the SASP seems to accelerate or even provoke tumorigenesis: The secretion of IL6 and IL8 by senescent fibroblasts can trigger an epithelial-mesenchymal transition (EMT) in epithelial cancer cells, which contributes to metastatic cancer progression.[171,172] Senescent fibroblasts also promote the growth of epithelial cells and xenograft tumors, which at least in part, depends on the secretion of MMP3 and VEGF.[173,174] Therefore, senescence represents an effective tumor-suppressive mechanism, but the SASP can have both deleterious and beneficial effects for cancer development and therapy due to its context-dependent influence on the tumor microenvironment.

Senescence and autophagy

Autophagy is a genetically programmed and evolutionary conserved cellular recycling system, which plays a crucial role in cellular adaptation to various different stresses.[175] While basal levels of autophagy are constantly maintained by cells, it can be stimulated during starvation and other cellular stresses. Autophagy catalyzes the endolysosomal degradation and elimination of long-lived and misfolded proteins as well as defective organelles, and thereby acts as a source for energy and building blocks by recycling metabolites and macromolecules.[176] At least three subtypes of autophagy have been documented in mammalian cells, which have been termed chaperone-mediated autophagy, microautophagy and macroautophagy. They differ in

their physiological function and the mechanism of cargo transport that they employ for the lysosomal degradation of substrates.[177] To date, senescence has predominantly been associated with macroautophagy. Macroautophagy sequesters cytoplasmic waste, such as defective organelles or protein aggregates, inside double-membraned vesicles, called autophagosomes, for degradation and recycling in a well-orchestrated program including over 30 autophagy-related (ATG) genes.[178] The formation and processing of autophagic vesicles requires the assembly and closure of an isolation membrane, called the phagophore, and can be divided into different steps, termed initiation, nucleation and maturation. Figure 5 demonstrates how autophagosomes fuse with lysosomes during autophagic turnover to degrade their cargo.

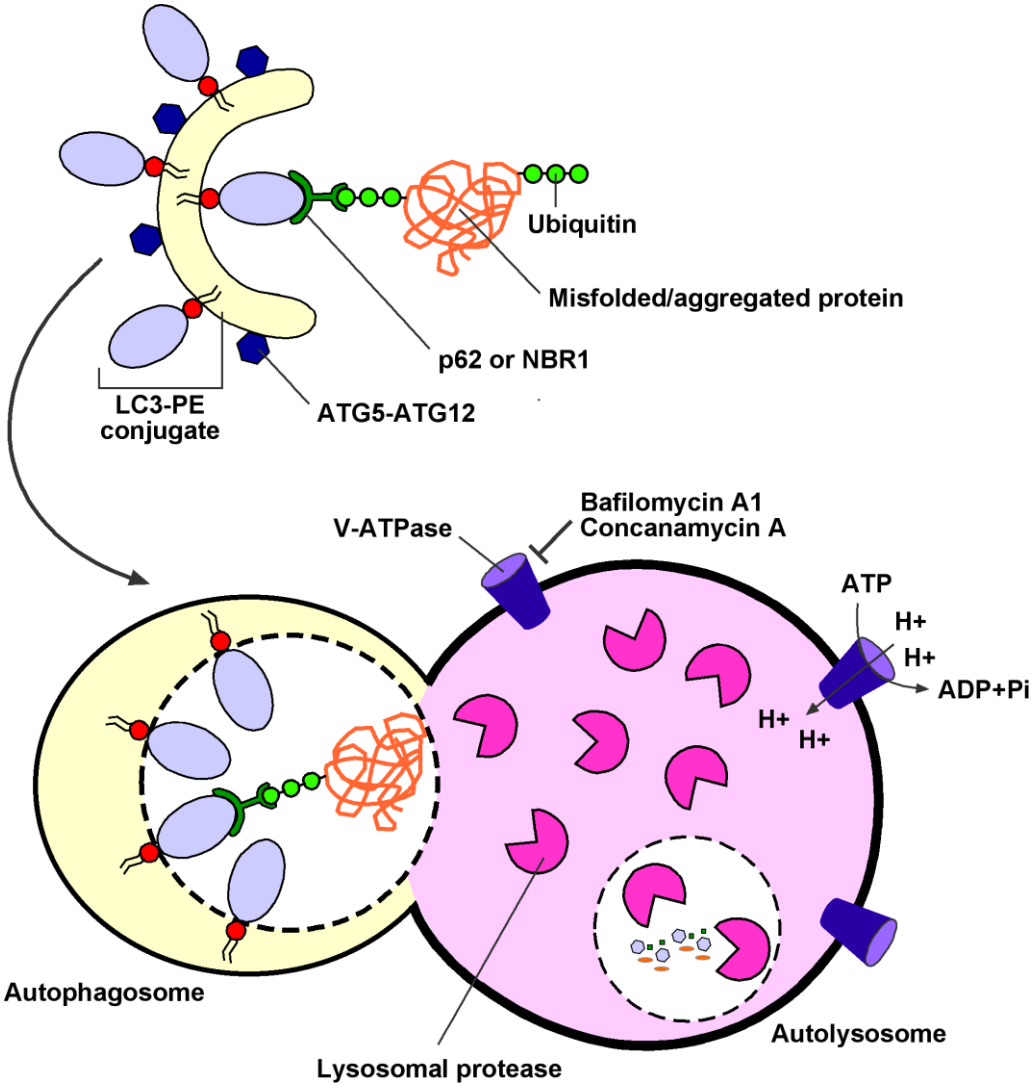

Figure 5. Protein degradation by autophagy. Degradation of misfolded and aggregated proteins by autophagy requires their selective ubiquitination by E1, E2 and E3 ubiquitinases. Ubiquitinated proteins are recognized by adaptor proteins, such as NBR1 and p62, which

directly associate with LC3. LC3 is conjugated to phosphatidyl ethanolamine (PE) in the double membrane of the autophagosome and thereby include the protein waste in the developing autophagosome. After fusion with the lysosome, the protein waste but also LC3 and p62 are degraded by hydrolytic enzymes, which work best at acidic pH levels. This is guarenteed by the activity of vacuolar-type H^+-ATPases (V-ATPase), which pump proteins into lysosomes at the expense of ATP. V-ATPase activity can be abolished by pharmacological inhibitors such as Bafilomycin A1 or Concanamycin A, which restrict lysosomal acidification and hence the formation of autophagolysosomes. Turnover or vice versa accumulation of unconjugated and lipidated LC3 as well as p62 can be measured to assess autophagic activity. NBR1 = next to BRCA1 gene 1, LC3 = light chain 3, PE = phosphatidyl ethanolamine. ATG5/12 = autophagy related protein 5/12. Figure adapted from Tyedmers et al.[179]

During initiation, lipids are sequestered from different organelles, particularly the endoplasmic reticulum, for de novo synthesis of the phagophore. This process requires the proteins ULK1 (uncoordinated 51-like kinase 1/ATG1), ATG13 and FIP200 (focal adhesion kinase interacting protein of 200 kD/ATG17).[180] During nucleation, the assembly of the phagophore is orchestrated by the class-III-phosphatidylinositol 3-kinase (PI3K) Vps34 that forms a complex with Beclin 1 (the mammalian orthologue of yeast ATG6).[181] Inhibitors of Vps34 such as methyladenine (3-MA) or wortmannin can be used to inhibit macroautophagy because they block autophagosome nucleation.[182] The maturation of the autophagosomal membrane, which includes elongation and closure of the phagophore, is orchestrated by two ubiquitin-like conjugation systems: In the first system LC3 (mammalian orthologue of ATG8) is cleaved by the ATG4 serine protease and then conjugated to phosphatidyl ethanolamine (PE) by the ATG7 and ATG3 enzymes.[183] The unmodified and lipidated forms of LC3, which are termed LC3-I and LC3-II respectively, can be distinguished by Western blot analysis and their ratio is used to asses autophagic flux.[184] The second system recruits LC3-II to the autophagophore by the ubiquitin-like activity of ATG12, which is covalently bound to ATG5 and physically associated with ATG16L. Once the formation of the autophagosome is completed, the ATG-12, -5, -16L complex dissociates from the autophagophore. Conversely, LC3-II remains associated with the autophagosome even after fusion with the lysosome.[185]

Autophagolysosome formation and turnover also depends on the proper function of vacuolar type H^+-ATPases (V-ATPase), which use the free energy of ATP hydrolysis to drive protons against the electrochemical gradient into the lumen of lysosomes.[186]

Thereby, V-ATPases generate an acidic intralysosomal pH and maintain optimal conditions for lysosomal enzymes, particularly proteases. Importantly, genetic depletion and pharmacological inhibition of V-ATPases abolishes the activity of lysosomal proteases and leads to the formation of enlarged autolysosomes with multiple single-membrane vesicles due their incomplete autophagic turnover.[187]

Whereas autophagic degradation of cytoplasmic material in response to nutrient starvation seems to be a non-selective process with the major goal to generate energy, selective protein turnover by autophagy requires the cellular ubiquitination system which specifies whether a protein will be transferred to the proteasome or an autophagosome for recycling. Proteins are targeted for degradation by E1, E2 and E3 ubiquitinases, which attach the C-terminal glycine from a ubiquitin molecule to the ε-amino group of a lysine residue in the protein being targeted.[188] Multiple molecules of ubiquitin can be added to the same protein individually, and to lysine residues on existing ubiquitin tags to form branched chains. Proteins with branched polyubiquitin chains on K48 are predominantly targeted for proteasomal degradation, while proteins with single ubiquitin moieties or branched polyubiquitin chains on other lysine residues are preferred substrates for autophagy.[189] Furthermore, the destination of ubiquitinated poteins is determined by adaptor proteins, which compete for ubiquitin binding sites with different specificity. For instance, p62 and NBR1 shuttle proteins to autophagic vesicles, whereas p97 shuttles proteins to the proteasome.[190]

Importantly, autophagy contributes to the cellular energy balance. As eluded to above, autophagy requires ATP to drive the lysosomal V-ATPase, but also for initiation, maturation and turnover of the autophagosome. However, in response to energetic needs, mainly starvation, autophagy can also mobilize different cellular energy stores such as lipids, carbohydrates and proteins to generate metabolic substrates for both energy production (catabolism) and biosynthetic reactions (anabolism). On a molecular level autophagy is directly controlled by mTORC1 (mammalian target of rapamycin complex 1), which phosphorylates and thereby inactivates ATG13 and ULK1, in respose to the nutrient state of the cell.[191] In brief, high levels of amino acids, insulin and insulin-growth factor 1 inhibit autophagy by inducing the

PI3K/AKT/mTORC1 pathway, whereas low glucose and high AMP levels induce autophagy via AMPK, which represses mTORC1 activity.[192]

Therefore, activation of autophagy in response to energetic needs, classically serum starvation, is an essential mechanism to produce ATP and hence maintain metabolic homeostasis and cell viability. In contrast, autophagy primarily acts in selective protein and organelle quality control as part of the cellular housekeeping system under nutrient-rich conditions and contributes few substrates towards cellular metabolism.[193] Interestingly, selective protein degradation by autophagy preferentially targets toxic or non-essential proteins for lysosomal breakdown while sparing proteins involved in autophagy and cell survival.[194] In this system genetic ablation of autophagy resulted in protein accumulation and subsequently cell death.[194] While the role of autophagy in cancer cells is complex and probably changes at different stages in tumor development, it can act as a critical cellular survival program in cancer cells by regulating proteotoxic and metabolic stress.

Autophagy has been associated with senescence in several different contexts. The autophagosomal marker LC3-II is significantly elevated in senescent primary human fibroblasts.[195] ATG5 and ATG7 also influence SA-β-gal activity and SASP induction, whereas their depletion attenuates senescence.[196] Furthermore, inhibition of mTOR, and subsequent activation of autophagy directly affects senescence in different ways depending on the cellular context.[197] In OIS, for example, the mTOR complex is recruited to a novel sub-cellular compartment termed TOR-autophagy spatial coupling compartment (TASCC) which affects the SASP.[198] Interference with autophagy due to pharmacological inhibition of mTOR by rapamycin induces senescence in radioresistant cancer cells and inhibits their growth in a xenograft model, but suppresses the SASP.[199,200] Therefore, autophagy directly modulates senescence and senescence-associated cellular programs. Despite a significant overlap between autophagy and senescence in cancer development and therapy, there is limited information on how these two processes cooperate to maintain cellular homeostasis and to what extent selective inhibition of either process affects cancer progression or treatment efficacy.

Senescence and metabolism

Although senescent cells stop to proliferate, they remain viable, grow in size and acquire senescence-associated functionalities.[168] These phenotypic changes, particularly the enhanced secretory capacity, require energy. Therefore, senescent cells are metabolically highly active. Furthermore, the shift from cell proliferation, which requires the synthesis of building blocks for DNA replication and cell division, to cell growth, which includes the synthesis and enlargement of organelles, also reprograms cellular metabolism.[151]

Cellular metabolism produces energy in the form of ATP primarily by glucose, amino acid and fatty acid breakdown. Their products are integrated into the tricarboxylic acid (TCA) cycle and consequently drive mitochondrial respiration. For glycolysis glucose is first transported into cells, mainly by facilitative diffusion through GLUT (SLC2A) membrane transport proteins, and then trapped intracellularly by phosphorylation in a reaction catalyzed by the enzyme hexokinase. Glucose-6-phosphate is again phosphorylated to glucose-1,6-phosphate and subsequently split into three-carbon molecules, which are either converted to glycerol for lipid synthesis or further processed to form pyruvate. Additionally, glucose generates ribose for nucleic acid synthesis and NADPH for reductive biosynthesis through the pentose phosphate pathway (PPP).[201] Pyruvate can be converted to acetyl-CoA, which is shuttled across the mitochondrial membrane. There it associates with the TCA intermediate oxaloacetate to form citrate. This initiates a new round of the TCA cycle, which generates high-energy electrons as NADH and FADH2 for redox reactions and efficient ATP production (36 ATP molecules per glucose molecule) during oxidative phosphorylation as well as carbon skeletons for biosynthesis and CO_2. Alternatively, pyruvate can be converted to lactate in a cytosolic fermentation reaction, which is mediated by the lactate dehydrogenase and generates little ATP (2 ATP molecule per glucose molecule). The breakdown of fatty acids by beta oxidation in the mitochondrion also generates NADH and FADH2 as well as acetyl-CoA, which is integrated into the TCA cycle to support ATP production.

In addition to glucose, the amino acid glutamine provides carbon backbones and ATP for cell growth. Furthermore, glutaminolysis, in which glutamine is converted to glutamate and then integrated in the TCA cycle as α-ketoglutarate (αKG), produces nitrogen for hexosamines and nucleotides of proliferating cells.[202] When glucose levels suffice to meet cellular energy demands, αKG produces nonessential amino acids in transamination reactions either in the cytosol or in the mitochondrion.[203] However, when the energy supply from glucose is scarce, αKG participates in the TCA cycle to generate FADH2 and NADH for oxidative phosphorylation and hence ATP production.[203]

From a bioenergetic standpoint, TCA cycle flux and mitochondrial respiration are induced in response to energetic needs, which are indicated by a high AMP:ATP ratio.[204] This activates the AMP-activated protein kinase (AMPK), which acts as the principal energy sensor in eukaryotic cells.[205,206] AMPK subsequently restores energy homeostasis by boostering catabolic pathways generating ATP, such as glycolysis, glutaminolysis or beta oxidation as well as mitochondrial biogenesis and oxidative phosphorylation, while inhibiting biosynthetic, ATP-consuming processes, such as triglyceride or glycogen synthesis.

Cells frequently adapt their metabolism to nutrient and oxygen availability and the energetic needs required to perform specialized tasks, for example during excercise or infection. Metabolic reprogramming is one of the hallmarks of cancer and several enzymes involved in glycolysis or the TCA are either mutated in cancer or upregulated by oncogenes to increase glucose turnover.[207] A paradigm of tumor cell metabolism, called the „Warburg effect“, is aerobic glycolysis, i.e. even in the presence of oxygen tumor cells favor glycolysis and the production of lactate over mitochondrial respiration.[208] In comparison to mitochondrial oxidative phosphorylation in normal cells this is the much less efficient route to produce energy. Despite the discovery of aerobic glycolysis in cancer cells almost a century ago many questions remain as to its function. A popular theory is that it facilitates the production of macromolecules, for example lipids, proteins or DNA, which are needed for cell division, by shuttling glucose carbon into biosynthetic side branches of glycolysis, such as the pentose

phosphate pathway or the hexosamine pathway.[209] Importantly, inhibition of AMPK boosters Warburg metabolism, lactate production and thereby supports tumor growth.[210] Of note, glycolysis also produces less reactive oxygen species (ROS) than the TCA cycle. Therefore, aerobic glycolysis might protect cancer cells from toxic DNA damage and hence contribute to apoptosis resistance.[211]

The metabolic reprogramming of cancer cells provides the opportunity for therapeutic interventions.[212,213] Several different strategies are successfully used in clinical treatment regimes or currently tested in clinical trials. The enzyme L-asparaginase is part of the standard chemotherapeutic regimen in the treatment of acute lymphoblastic leukemia (ALL), because it reduces asparagine availability to ALL cells and thereby suppresses their growth.[214] Furthermore, the type II diabetes drug metformin, which increases AMP levels and induces AMPK by complex action, directly inhibits cancer cell growth in cell lines and preclinical models *in vitro* and *in vivo*.[215] In addition, various inhibitors of glycolysis demonstrate anticancer efficacy. The pyruvate dehydrogenase kinase (PDK) inhibitor dichloroacetate reactivates the pyruvate dehydrogenase (PDH) and hence induces a metabolic switch from aerobic glycolysis and lactate production to increased TCA cycle activity and mitochondrial respiration. Thereby, dichloroacetate triggers apoptosis and tumor shrinkage in clinical trials, for example in glioblastoma patients.[216] Interestingly, the combinatorial treatment of dichloroacetate and radiotherapy improves treatment efficacy, since radiotherapy augments aerobic glycolysis in tumors.[217] Similarly, 2-deoxyglucose, which reversibly inhibits the enzyme hexokinase and hence blocks glycolysis, shows limited therapeutic efficacy as a single drug, but exhibits synergistic treatment effects if combined with standard chemotherapy or irradiation.[218]

As illustrated in Figure 6 senescent cells also alter their metabolism, but implement modifications which differ from proliferating cancer cells. Due to high energetic needs OIS cells increase the flux of glucose carbon into the TCA cycle and induce oxidative phosphorylation to booster energy production. Importantly, hyperactive mitochondrial respiration also elevates cellular ROS levels, which are typically associated with senescence.[219]

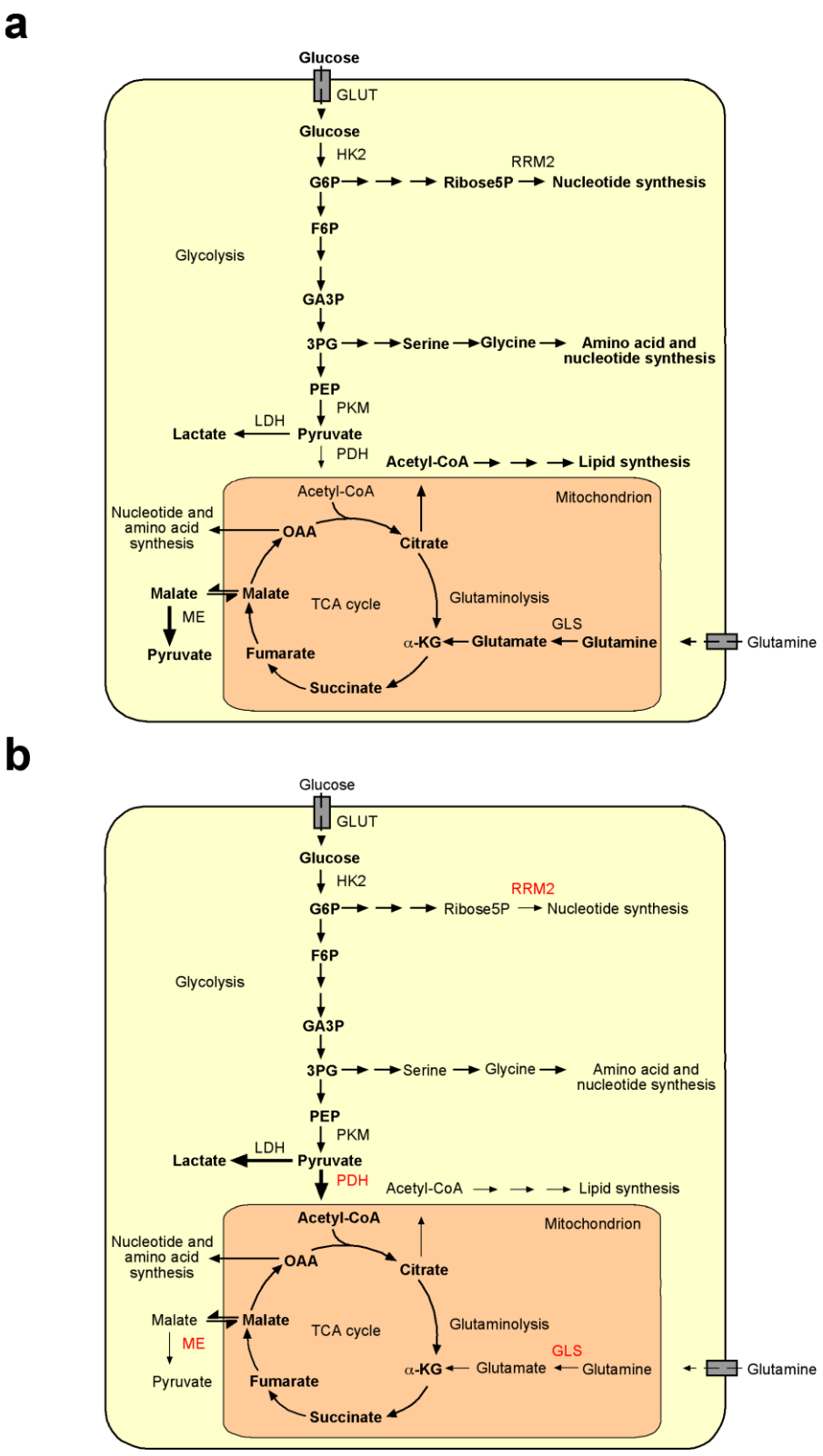

Figure 6. Metabolic reprogramming in senescence. a, Proliferating tumor cells increase the uptake of glucose and glutamine. Glutamine serves as a nitrogen donor for sugars and nucleotides and fuels the TCA cycle for energy production and the generation of precursors for transamination and biosynthetic reactions. Glucose is predominantly used in aerobic glycolysis (Warburg effect), which produces lactate, to support biosynthetic pathways. For this purpose

the PKM2 isoform of the pyruvate kinase is expressed in favor over PKM1. This slows the conversion of phosphoenolpyruvate to pyruvate and thereby allows branching of glycolytic intermediates into biosynthetic reactions. Furthermore, tumor cells suppress PDH activity to reduce glucose flux into the TCA cycle. **b**, Senescent tumor cells reprogram their metabolism to increase glucose flux into the TCA. This is achieved by stimulating PDH activity and by enforced expression of PKM1. Lactate is at least temporarily produced at elevated levels (see results). At the same time, glutamine uptake as well as the synthesis of lipids and nucleotides is reduced in part by downregulation of GLS and RRM2 activity.[219] Key enzymes which are differentially regulated in senescence are shown in red. Big or small arrows as well as plain and bold font indicate pathways of high and low flux in proliferating and cancer cells. GLUT = Glucose transporters, HK2 = hexokinase, G6P = glucose-6-phosphate, G6PDH = glucose-6-phosphate dehydrogenase, Ribose-5P = ribose-5-phosphate, F6P = fructose-6-phosphate, GA3P = glyceraldehyde-3-phosphate, 3PG = 3-phosphoglycerat, PEP = phosphoenolpyruvate, LDH = lactate dehydrogenase, PKM = pyruvate kinase muscle isoenzyme, PDH = pyruvate dehydrogenase, RRM2 = Ribonucleoside-diphosphate reductase subunit M2, GLS = glutaminase, α-KG = alpha-ketoglutarate, OAA = oxaloacetate, TCA = tricarboxylic acid, ME = malic enzyme. Figure adopted from Boroughs et al.[220]

The increased TCA cycle activity in senescent cells is mediated by the upregulation of PDH, which converts pyruvate to acetyl-CoA.[219] Additionally, the repression of malic enzymes, which otherwise divert carbon backbones from mitochondrial respiration, facilitates TCA cycle flux and contributes to p53-mediated senescence induction.[221] Furthermore, OIS cells exhibit reduced lipid synthesis and increased fatty acid oxidation, which also augments mitochondrial respiration.[222] Therefore, senescence-associated regulation of both carbohydrate and lipid metabolism increase mitochondrial respiration and ATP production.

Conversely, depolarization of the mitochondrial membrane potential and hence mitochondrial dysfunction also occurs in models of replicative senescence and OIS.[223,224] In fact, dysfunctional mitochondria have been tightly linked to the process of ageing. Old or damaged mitochondria produce less ATP despite high oxygen consumption rates due to the uncoupling of oxidative phosphorylation from ATP synthesis.[225] At the same time, however, mitochondrial biogenesis is increased as a countermeasure to restore full mitochondrial function.[226] Interestingly, damaged mitochondria in OIS seem to be degraded by autophagy.[227] Therefore, it remains to be determined whether mitochondrial dysfunction is a permanent attribute of OIS or part of a cellular reprogramming process towards high mitochondrial respiration and energy production. Also, the cellular programs, which require the high metabolic expenditure of senescent cells, require further investigation.

Senescence and synthetic lethality

An important principle of cellular homeostasis and survival is synthetic lethality. The phenomenon derives from observations in the model organism *Drosophila melanogaster* and has been extended to yeast, mice and men.[228–230] Synthetic lethality is a consequence of the functional redundancy provided mainly by non-homologous genes, which operate in the same cellular process or in parallel pathways and which thereby increase the robustness of an organism to genetic and environmental challenges. In classical genetics two genes are synthetically lethal if mutation of either alone is compatible with viability while mutation of both induces cell death.

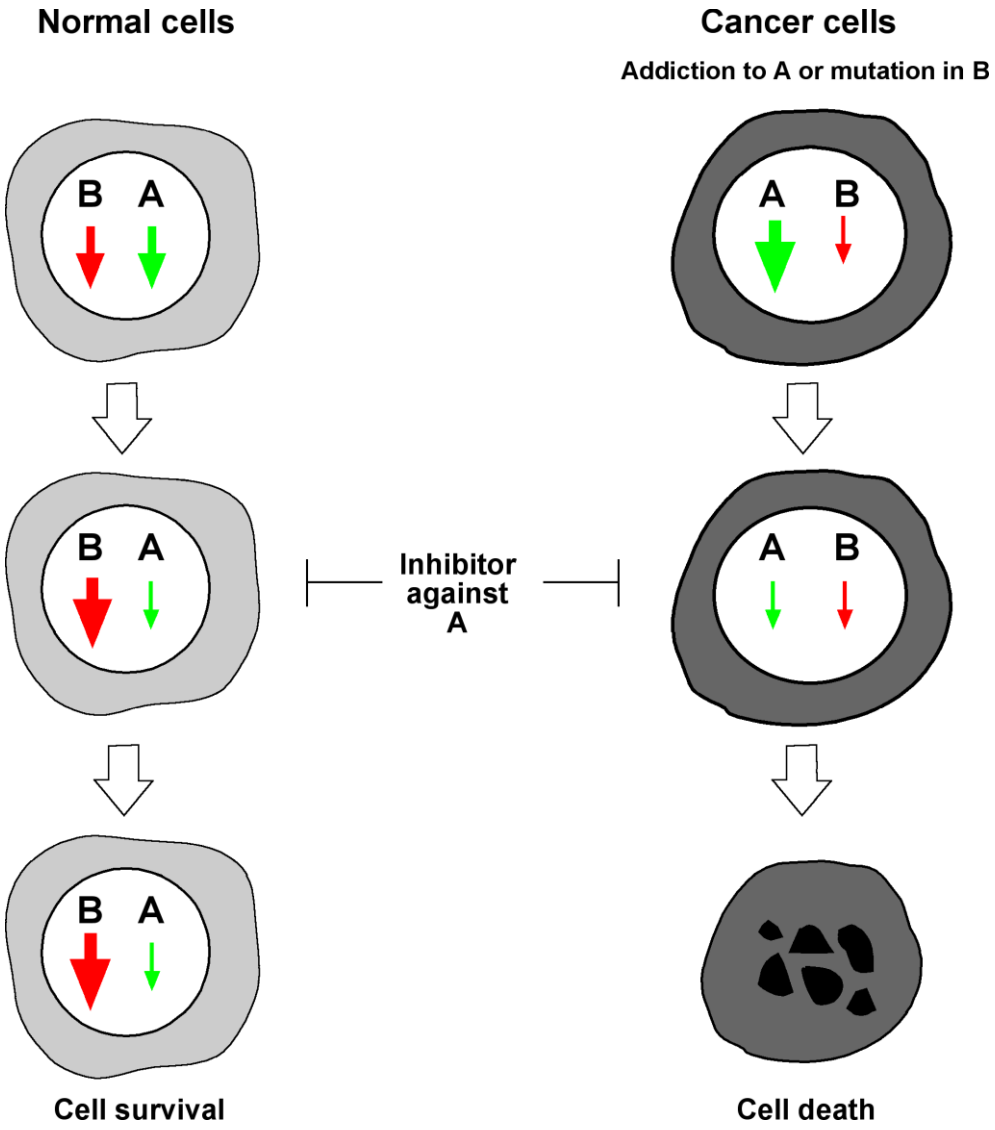

Figure 7. Synthetic lethality in cancer therapy. In normal cells inhibition of pathway A is compensated by the activation of a parallel pathway B, for example to initiate a DNA damage

response. In this way, the cell tolerates the inhibition of A and survives. Conversely, cancer cells can become addicted to pathway A or rely on its activity due to a mutation in pathway B. Therefore, inhibition of pathway A leads to intolerable stress, i.e. irreversible breakdown of DNA repair mechanisms, and cancer cell death. In this way synthetic lethal treatments selectively kill cancer cells.

As illustrated in Figure 7 the concept can also be applied to the situation, in which the combination of a mutation and the action of a chemical compound causes lethality and even to situations in which specific triggers, such as epigenetic changes, alterations in the microenvironment and a mutation or a chemical inhibitor act synergistically and induce cell death.[231] Therefore, the inhbition of a gene which is synthetically lethal to a cancer-relevant mutation, for example in an oncogene or in a tumor suppressor, should selectively kill cancer cells, while normal cells should remain unaffected.

In this regard synthetic lethality provides a conceptual framework for the development of cancer-specific cytotoxic drugs.[232] For instance, cancer cells with genetic defects in the signaling and repair of DNA double strand breaks (DSB) by homologous recombination, for example due to mutations in *ATM* or *BRCA1/2*, show increased susceptibility to inhibitors of the poly(ADP-ribose) polymerase (PARP), which is mainly involved in the repair of single strand breaks (SSB), because defects in both DSB and SSB repair lead to accumulation of intolarable DNA damage and subsequently cell death.[233,234] Consequently, PARP inhibitors are currently evaluated in several clinical trials against different cancer entities.[235]

Whereas pharmaceutical interventions to exploit synthetic lethality for cancer therapy usually rely on the addiction to signaling pathways and their concomitant inhibition, the concept can be extended to a cancer-specific phenotype and the associated cellular programs which maintain this condition. An example of such a process is OIS in premalignant cells. Therefore, targeted pharmaceutical inhibition of OIS-specific liabilities, such as autophagy, might selectively remove premalignant cells in case non-malignant host cells in the environment do not rely on the same program for cell survival. The same principle could be applied to TIS under the assumption that cancer cells react differently to the applied therapeutic challenge, i.e. induction of senescence, than non-malignant bystander cells.

In fact, the activation of oncogenes or the loss of tumor suppressors fundamentally rewire gene expression, signaling networks and hence the response to chemotherapy.[236] For instance, most *TP53* mutations in human tumors are missense mutations in the DNA-binding domain, which cluster at six 'hot-spot' residues (R175, G245, R248, R249, R273 and R282).[237] Many of these mutants do not only impose a dominant-negative effect on wild-type p53, but they also display gain-of-function properties.[238] Despite the mutation in the DNA binding domain p53 mutants retain transcriptional activity due to the interaction with transcription factors or the recognition of new promoter elements. Thereby, individual p53 mutants display different gene expression profiles and altered stress responses. In fact, cells which contain the mutant p53R175P protein, or its mouse homologue p53R172P respectively, cannot initiate apoptosis in response to DNA damaging treatment, but retain the ability to induce senescence by transcriptional activation of *p21*. Similarly, mouse cells, which expresses $Trp53^{E177R}$ (the orthologue of $TP53^{E180R}$), fail to execute apoptosis in response to ionizing radiation or serum starvation, but retain the capacity to induce senescence.[239] Therefore, TIS is specifically induced in tumor cells which harbor specific p53 mutations, while p53 wild-type bystander cells undergo apoptosis. Thus, OIS and TIS provide a cancer-specific condition, and drugs that selectively eliminate senescent cells confer to the principle of context-dependent synthetic lethality.

6. Materials and Methods

Mouse strains and lymphoma generation

The animal work in this project was approved by the governmental review board (Landesamt für Gesundheit und Soziales, LAGeSo, Berlin) and carried out according to the appropriate regulatory standards. To generate lymphomas with defined genetic defects in a C57BL/6 background Eμ-*myc* transgenic (hereafter referred to as 'control') mice were intercrossed with mice carrying loss-of-function alleles at the *Suv39h1* locus. *Suv39h1*$^{-}$ lymphomas can be generated from Eμ-*myc* lymphomas that arose in *Suv39h1*$^{-/-}$ females or in *Suv39h1*$^{y/-}$ males due to the X-linkage of the *Suv39h1* locus. Control and *Suv39h1*$^{-}$ lymphomas used for *in vitro* experiments were pre-screened for defects in the DNA damage pathway by phospho-S18-p53, p53 and p21^{CIP1} immunoblot analyses six hours after γ-irradiation at a dose of 4 gray (Gy). Samples which failed to activate the p53 pathway in response to DNA-damaging γ-irradiation were excluded from further analysis. Mice were monitored for lymphoma onset at least every two days by palpation of the prescapular and cervical lymph nodes and sacrificied when lymphomas became palpable greater than 5mm in diameter or according to the Lageso score sheet (see Supplementary Figure 1). After CO_2 euthanasia of the mice, enlarged lymph nodes were excised and manually dissected using scissors, knives and forceps and subsequently dissociated with a semi-automated benchtop instrument (gentleMACS^{TM}, Miltenyi) to produce single cell suspensions, which were directly used for *in vitro* experiments or conserved in a freezing solution in liquid nitrogen. Preservation of snap-frozen or formalin-fixed tissues for subsequent histopathological analyses were carried out as described previously.[107,103] Briefly, lymph nodes or spleen were fixed in 4% formaldehyde or cryoconserved in liquid nitrogen.

Lymphoma cell culture and retroviral gene transfer

Lymphoma cells (LC) were cultured in B cell medium (BCM) on feeder layers generated from irradiated NIH3T3 fibroblasts.[104] Retroviral gene transfer was carried

out as described previously.[107] Briefly, low passage Phoenix cells were grown in a 10cm petri-dish to approximately 70% confluency. For one transfection reaction 20μg retroviral plasmid, 15μg helper plasmid and 62.5μg $CaCl_2$ were mixed in a Falcon tube and adjusted to 500μl with sterile water. Subsequently, 500μl 2x HEPES buffered saline (HBS) was added dropwise under constant agitation. The reaction mix was allowed to settle for 10 minutes at room temperature until DNA precipitation occured and subsequently transferred onto Phoenix cells grown in 10ml DMEM with 25μM chloroquine.

After incubation for 12 hours the supernatant was exchanged by 5ml BCM to start virus collection. For retroviral infection, the virus supernatant was collected four times over a period of 48 hours. For each step the medium was supplemented with 20μg polybrene and filtered through a 0.45μm filter before it was transferred to LC. The stably infected LC were subsequently selected by antibiotic treatment or purified by fluorescence-activated cell sorting.

All retroviruses were murine stem cell virus (MSCV)-based constructs that either co-express puromycin (i.e. MSCV-Bcl2-puro, MSCV-RasV12-puro) or GFP (i.e. MSCV-Bcl2-IRES-GFP), including the corresponding empty vectors as controls (i.e. MSCV-puro, or MSCV-IRES-GFP). For the transfection of Phoenix cells maxi-preparations of the plasmids from individual DH5α E.coli colonies inoculated in 200ml LB medium were prepared with the Invitrogen maxi-preparation kit. For long-term storage plasmid DNA was stored after mini-preparations. For this purpose an individual bacterial colony was incubated in 3ml LB medium overnight. Bacteria were centrifuged and pelleted, lysed and their pellet precipitated by sequentially adding 100μl ice-cold Solution I, 200μl freshly prepared Solution II and finally 150μl of ice-cold Solution III. After centrifugation the supernatant was transferred to a fresh Eppendorf tube and plasmid DNA precipitated by addition of 1ml absolute ethanol. The precipitate was centrifuged, washed in 70% ethanol and again pelleted. Finally, the DNA was air-dried, resuspended in 30μl dH_2O and stored at -20°C or -80°C.

Stable knockdown of caspase 3 and caspase 12 was achieved by retroviral infection of

LC with the pSuperRetro plasmid system (Oligo Engine) as described above. For lentiviral knockdown of hexokinase 2 and p62/SQSTM1, individual complementary DNA constructs from the human pGIPz lentiviral shRNA library, version 13 (CSHL RNAmir, Open Biosystems) were used. Viral particles were generated according to the manufacturer's instructions, using second generation helper plasmids (psPAX2, pMA2-VSVG) and the HEK293T packaging cell line.

shRNA constructs:
Caspse 3 shRNA: 5'-GGATCTATCT GGACAGTAGTT-3'
Caspase 12 shRNA: 5'-GCTCTCATCATCTGCAA CAAA-3'

Lentiviral constructs:
Hexokinase 2 lentiviral plasmid ID: V3LHS_344623
p62/SQSTM1 lentiviral plasmid ID: V2LMM_77135

Genomic DNA to genotype offspring was isolated from mouse tails. For each offspring a small part of the tail was cut off and incubated in 450µl lysis buffer, containing 100mM Tris-HCl, 5mM Ethylenediaminetetraacetic Acid (EDTA), 0.2% SDS, 200mM NaCl and 1mg/ml Proteinase K (Roche Diagnostics), in an Eppendorf tube at 55°C for at least two hours. Afterwards the reaction product was spun down to separate DNA in the supernatant from undigested remnants in the pellet. The supernatant was then transferred to a new tube and DNA was precipitated by adding 100µl isopropanol. The precipated DNA was again transferred to a new tube containing 100µl TE buffer (10mM TrisCL, 1mM EDTA) and stored at -20°C for PCR genotyping

Primer sequences for the detection of the Eμ-*myc* transgene, *Suv39h1, p53, Atg5* and α-*Tubulin* (as an internal control) were as follows:

Eμ-*myc* transgene: 5'-CAGCTGGCGTAATAGCGAAGAG-3'
5'-CTGTGACTGGTGAGTACTCAACC-3'

Suv39h1: 5'-GTTGATGCTTCCTGGTGTGTAGG-3'

5’-TTTGAGGGGACGACGACAGTATG-3’
5’-AACAGATGTGGGGTTGGTGGAG-3’

p53: 5’-TAT ACT CAG AGC CGG CCT-3’
5’-ACA GCG TGG TGG TAC CTT AT-3’
5’-TCC TCG TGC TTT ACG GTA TC-3’

Atg5: 5’-ACA ACG TCG AGC ACA GCT GCG CAA GG-3’
5’-GAA TAT GAA GGC ACA CCC CTG AAA TG-3’
5’-GTA CTG CAT AAT GGT TTA ACT CTT GC-3’

α-Tubulin: 5’-CGC GAG TGC ATT TCA GTC C-3’
5´-TCC CAG TGA TAA GCT GCT CT-3’

For PCR amplification the DNA samples were combined with a PCR mastermix containing 1x DreamTaq buffer (Fermentas), a dNTP mix (10mM of each nucleotide, Roth) and DreamTaq Polymerase [5U/µl] (Fermentas) and the respective primers in a total volume of 25µl and incubated in a cell cycler according the following protocols:

Genotype	**Temperature (°C)**	**Time (minutes)**	**Number of cycles**
Eμ-*myc*	94 94, 64, 72 72	5 1, 1, 1 5	1 32 1
Suv39h1	94 94, 56, 72 72	5 0.5, 0.5, 0.5 10	1 35 1
p53	92 92, 62, 72 72	5 0.5, 1, 1 5	1 34 1
Atg5	94 94, 57, 72 72	3 0.5, 0.5, 1 5	1 30 1

The resulting bands were visualized on an agarose gel after gel electrophoresis at 100V. For *Suv39h1* the PCR reaction produces a *Suv39h1* wild-type band at 417bp and a *Suv39h1* mutant band at 588bp. For *p53* the PCR reaction yields a *p53* wild-type band at 450bp and a *p53* mutant band at 600bp. For *Atg5* the PCR reaction produces an *Atg5* wild-type band at 351bp and an *Atg5* mutant band at 574bp.

In vitro and *in vivo* treatments

For *in vitro* drug treatments, adriamycin (ADR, Sigma), a topoisomerase II inhibitor, was added once in senescence-related experiments at a concentration of 0.05μg/ml for *Bcl2*-protected LC and removed after incubation for three days. The serine/threonine-protein kinase mTOR inhibitor rapamycin (Sigma) was added at a concentration of 5μM and replenished every 48 hours to induce senescence.

For *in vivo* experiments individual lymphomas were propagated by intravenous injection in C57/BL6 strain-matched, non-transgenic, fully immunocompetent mice and treated with a single intraperitoneal dose of cyclophosphamide (CTX, Sigma, 300mg/kg body weight) when cervical lymphomas became palpable. Although CTX cannot be used *in vitro*, it was preferred to ADR *in vivo* due to lower organ toxicity. In some experiments, mice were exposed to a single dose of the following drugs five days after CTX treatment: 2DG (Sigma, 250mg/kg body weight intraperitoneally), Bafilomycin A1 (Sigma, 1μg in 150ml phosphate buffer intraperitoneally), or phosphate buffer as mock treatment. Treatment responses *in vivo* were monitored by palpation of the prescapular and cervical lymph nodes every two days. Time to death as a means to determine overall survival was defined as the latency between treatment and a terminal stage of the disease as defined by the LAGeSo score sheet (see Supplementary Figure 1).

Mouse fluorescence and FDG- and FLT-PET imaging

Fluorescence-based whole-body imaging was performed with a charge-coupled device (CCD)-camera-equipped bioimaging system (LAS-4000, Fujifilm). For *in vivo* imaging,

mice were anaesthetized with isoflurane (Abbott) using a veterinary anaesthesia system (Vetland Medical Sales and Services, and Harvard Apparatus). The FDG- and FLT-PET imaging were carried out at the Technische Universität in Munich by Prof. Dr. Andreas Buck. The glucose analogue FDG was produced at the cyclotron unit using a standard procedure according to good manufacturing practice (GMP) guidelines. The nucleoside FLT was produced as described previously with minor modifications using an automated radiotracer synthesizer (General Electric Medical Systems).[240] FDG- and FLT-PET were performed in a dedicated small animal PET system (INVEON, Siemens Preclinical Solutions) within 24 hours before treatment, and on day 5 or day 6 after CTX therapy. Static imaging was started 45 minutes after intravenous injection of 3.7–7.4 megabecquerels (MBq) FLT or FDG per mouse. Data were acquired over 15 minutes, normalized and corrected for random coincidence events, dead time, and decay. To assess tracer accumulation at tumor sites, tumor-to-background ratios (TBRs) were calculated for all tumor manifestations that showed focal tracer accumulation prior to therapy. Circular two-dimensional regions of interest (ROIs), not covering the entire tumor to avoid partial volume effects, were placed manually in the area with the highest tumor activity. To determine background activity, a corresponding ROI was set at the muscle of the right thigh. Corresponding TBR values were calculated as mean count rates within the tumor and the matching background ROI.

Cell growth, apoptosis, autophagy and cellular senescence *in vitro* and *in vivo*

Viability and cell numbers were analyzed by trypan blue dye exclusion (0.04% trypan blue stain in PBS, Sigma) using a Neubauer counting chamber. 200 cells were counted for each sample and viability was indicated as the percentage of living cells. DNA synthesis was assessed by immunohistochemical staining of incorporated 5-bromo-2'-deoxyuridine (BrdU, Sigma). For this purpose, 20μM BrdU was added to the lymphoma cell culture two hours before harvesting the cells. Afterwards, LC were pelleted, washed in PBS and fixed in 80% ice-cold ethanol at -20° for at least 24 hours. Subsequently, LC were washed and incubated in 2M HCl at room temperature for 30

minutes following pH neutralization with 0.1M sodium borate for 15 minutes. LC which contain stably incorporated BrdU were then labeled using a FITC-conjugated anti-BrdU antibody (Molecular Probes, 1:2000) in the dark overnight. As the final step, LC were incubated with 100µg/ml propidium iodide (in PBS) for 10 minutes and analyzed by fluorescence-activated cell sorting (FACS, BD FACSCalibur).

Senescence was assessed by SA-β-gal activity at pH 5.5 (mouse) or pH 6.0 (human) in cryosections or cytospin preparations of cell suspensions. For SA-β-gal staining, tissue slices and cells were incubated in freshly prepared SA-β-gal fixation solution for 15 minutes at room temperature. Subsequently, cells were washed twice in PBS and incubated in SA-β-gal staining solution in a humidified atmosphere at 37°C for approximately 8 hours. Cell proliferation was detected by BrdU and Ki67 staining. For proliferation analysis of lymphomas *in vivo* 2mg BrdU were injected intraperitoneally 6 hours before the mice were sacrificed. Formaldehyde-fixed lymph nodes were subsequently deparaffinized in alcohol and stained with anti-BrdU antibody (AbD Serotec, #OBT0030G, 1:100), followed by biotinylated donkey anti-rat antibody (Dianova, #712-066-003, 1:1000) and streptavidin peroxidase-bottle rtu (DAKO –Kit K5001). For Ki67 staining *in situ* lymph nodes were deparaffinized in bond dewax solution (Leica), pretreated in ER2 solution (Leica) and subsequently stained with anti-Ki67 antibody (Dako, TEC3, 1:100) followed by rabbit anti-rat antibody (Dako, 1:100). For Ki67 staining *in vitro* LC were fixed in ICC staining buffer for ten minutes at room temperature and subsequently permeabilized in PBS with 0.2%Triton X-100 for 10 minutes at room temperature. Following two washing steps in TBS LC were incubated with anti-Ki67 antibody (Dako, MIB-5, 1:150) in antibody diluent (Zymed) for 30 minutes. Further staining was carried out with the LSAB 2 System AP-Kit (DAKO) according to the manufactorer's protocol. Apoptotic DNA strand breaks were detected by TUNEL staining in paraffin-embedded tissue sections in accordance with the manufacturer's protocol (Roche).

Global protein synthesis, immunofluorescence and immunoblot analyses

Total protein synthesis was detected by the Click-iT AHA Alexa Fluor 488 Protein

Synthesis HCS Assay (Invitrogen) according to the manufacturer's protocol. Briefly, LC were incubated with medium containing Click-iT-labeled L-methionine for 30 minutes, washed and subsequently loaded with Click-iT-reactive Alexa Fluor 488 dye. 4',6-diamidino-2-phenylindole (DAPI) was used as a nuclear and chromosome counterstain. Images were automatically acquired using a Pathway 855 high-content bioimager confocal microscope (Becton Dickinson) and subsequently analysed using the AttoVision software package (version 1.6) as a threshold-based single-cell densitometric measurement of the Alexa Fluor 488 signal.

For immunoblot analyses whole-cell extracts were generated by lysing cells in NP-40 protein lysis buffer (150mM NaCl, 50mM Tris-HCl, 1% NP-40, pH 8.0) including proteinase inhibitors and phosphatase inhibitors. Equal aliquots corresponding to 30-60μg of protein were resolved on SDS-polyacrylamide gels and transferred to Immobilon-P membranes (Millipore) using a semi-dry transfer chamber (BioRad). Afterwards, membranes were blocked with 5% milk in phosphate buffered saline with Tween-20 (PBST) for one hour and then incubated with primary antibodies against AMPK (no. 2603, Cell Signaling Technology (CST)), 1:1000 in 5% BSA in PBST), AMPK-P-T172 (no. 2535, CST, 1:1000), ATF4 (c20, Santa-Cruz Biotechnology (SCBT), 1:250), BrdU (Molecular Probes, 1:2000), Bcl2 (SCBT, 1:500), CHOP (sc-7351, Santa Cruz, 1:200), Caspase 4 (no. 4450, CST, 1:1000), Caspase 12 (no. 2202, CST, 1:1000), cleaved (D175) Caspase 3 (no. 9661, CST, 1:1000), JNK (no. 9258, CST, 1:1000), JNK-P-T183/T185 (no. 4671, CST, 1:1000), p62/SQSTM1 (no. 5114, CST, 1:1000), PKM1 and PKM2 (from the laboratory of M. Vander Heiden; 1:1000), microtubule-associated protein 1 light chain 3 (2G6, Nanotools, 1:1000), α-tubulin (T5168, Sigma-Aldrich, 1:8000), ubiquitin (no. 3933, CST, 1:1000), and V-ATPase A1 (sc28801, Santa Cruz, 1:250) at 4°C overnight. Subsequently, the blot was washed in PBST and then incubated with the appropriate corresponding anti-mouse and anti-rabbit peroxidase-conjugated secondary antibodies (GE Healthcare; 1:1000 and 1:2000, respectively) for one hour at room temperature. After addition of chemiluminescent peroxidase substrate images were visualized by a chemiluminescence imaging system (Intas Chemocam Imager).

Gene-expression analyses

For RT–PCR analyses cell pellets were lysed in 1ml Trizol (Invitrogen). Following a short incubation, 0.2ml chloroform was added. Subsequently, samples were centrifuged in a table-top centrifuge at 12,000g for 15 minutes at 4°C to achieve phase separation. After isolation of the aqueous phase RNA was precipitated by adding 0.5ml isopropanol and incubating the mixture for ten minutes. RNA was sedimented by centrifugation at 12,000g for ten minutes at 4°C, washed with 70% ethanol and redissolved in DEPC-treated H_2O. The RNA concentration was determined by spectrophotometry at a wavelength of 260nm with a NanoDrop-1000 instrument (NanoDrop Technologies). To synthesize cDNA 1µg RNA was transcribed with random hexamer primers in a 20µl reaction using Superscript® II Reverse Transcriptase (Promega). A mixture of 150ng random hexamer primer, 1µl 10mM dNTP, 1µl RNA and DEPC-treated H_2O was heated to 65°C for five minutes. Subsequently, 4µl 5x First-Strand-Buffer (Promega), 2µl 0.1M Dithiothreitol (DTT, Promega) and 1µl Ribonuclease Inhibitor Recombinant RNasin® (Promega) were added to the reaction mixture and heated to 42°C after incubation at room-temperature for ten minutes. Reverse Transcription was started by adding 1µl Superscript® II Reverse Transcriptase and subsequently maintained at 42°C for 50 minutes. The PCR was heat-inactivated at 70°C for 15 minutes and cDNA was stored at -20°C.

For quantitative RT–PCR (qRT– PCR) analyses of murine Gapdh, Casp3, Casp12, Cpt1a, Cxcl5, Glut1, Glut3, Hk2, Igfbp7, Il-6, Mcp1, Mmp2, p62/SQSTM1, Serpine1 (also known as Pai-1), Pfk1, and Sco2 as well as human GAPDH, CXCL1, HGF, IL-6, IL-8, and MMP3 100ng cDNA were amplified in a 10µl volume containing 0.5µl gene-specific TaqMan® Assays (Applied Biosystems) and 1x Real-time PCR master Mix (Applied Biosystems) in a StepOnePlusTM Real-Time PCR System (Applied Biosystems). For every sample, the difference in cycle threshold (ΔCt) values were determined as the difference between the Ct value of a specific transcript and the Ct value of GAPDH, serving as the housekeeping control messenger RNA, and relative transcript levels (for example, treated versus untreated) were calculated based on $2^{(-\Delta\Delta Ct)}$ with $\Delta\Delta Ct = \Delta Ct_{treated} - \Delta Ct_{untreated}$. For detailed primer information see below:

Gene	Company and Catalogue number
Glucose transporter 1 (Glut1, Slc2a1)	Applied Biosystems, Mm00441480_m1
Glucose transporter 3 (Glut3)	Applied Biosystems, Mm00441480_m1
Hexokinase 2 (Hk2)	Applied Biosystems, Mm00443385_m1
Phosphofructokinase 1(Pfk1)	Applied Biosystems, Mm00435587_m1
Pyruvate dehydrogenase kinase 1 (Pdk1)	Applied Biosystems, Mm00554306_m1
Gapdh, 20x	Applied Biosystems, Mm99999915_g1
Sco2	Applied Biosystems, Mm00460357_m1
Cpt1a	Applied Biosystems, Mm00550438_m1
p62/SQSTM1	Applied Biosystems, Mm00448091_m1
Interleukin 6, human (IL6)	Applied Biosystems, Hs99999032_m1
Interleukin 8, human (IL8)	Applied Biosystems, Hs00174103_m1
Cxcl1, human	Applied Biosystems, Hs00236937_m1
Matrix metalloproteinase 3, human (Mmp3)	Applied Biosystems, Hs00233962_m1
Human growth factor, human (HGF)	Applied Biosystems, Hs00300159_m1
Cxcl5	Applied Biosystems, Mm00436451_g1
Igfbp7	Applied Biosystems, Mm00514987_m1
Matrix metalloproteinase 2 (Mmp2)	Applied Biosystems, Mm00439506_m1
Macrophage chemoattractant protein (Mcp1, Ccl2)	Applied Biosystems, Mm00441243_g1
Interleukin 6, mouse (IL6)	Applied Biosystems, Mm99999064_m1
SerpineE1 (Pai-1)	Applied Biosystems, Mm00435858_m1
Caspase 3 (Casp3)	Applied Biosystems, Mm01195085_m1
Caspase 12 (Casp12)	Applied Biosystems, Mm00438038_m1
GAPDH, 20x (human)	Applied Biosystems, Hs02758991_g1

Detection of *Xbp1* gene splicing was carried out as described previously.[241] Briefly, cDNA was synthesised from LC as described for RT–PCR analyses above and used as a template for a PCR reaction with primers flanking the splice site:

Xbp1: 5’-AAACAGAGTAGCAGCTCAGACTGC-3’
5’-TCCTTCTGGGTAGACCTCTGGGA-3’

For PCR amplification of spliced und unspliced *Xbp1* 35 PCR cycles were carried out in a PCR thermal cycler, in which the DNA was denatured at 94°C for 10 seconds, annealed at 66°C for 30 seconds and extended at 72° for 30 seconds. The primers generate an unspliced band of 480bp and a spliced band of 454bp. α-Tubulin was used as a control as described above. The PCR reaction was carried out in 25µl with 1x DreamTaq buffer (Fermentas), a dNTP mix (Roth) and DreamTaq Polymerase [5U/µl] (Fermentas) and the resulting bands were visualized on an agarose gel after gel electrophoresis at 100V for four hours.

Microarray-based gene-expression profiling was performed by Dr. Dido Lenze in the laboratory of Prof. Michael Hummel at the Institute of Pathology at the Charité-Universitätsmedizin Berlin. For microarray analyses RNA was isolated from LC with the RNAeasy Mini kit (Qiagen). Subsequently, RNA was hybridized to Affymetrix Mouse Genome 430 2.0 microarrays (Affymetrix), washed and scanned according to standard Affymetrix protocols. The resulting CEL files were imported into Partek Genomic Suite Software (Version 6.4, Partek), and the data were processed by the implemented default workflow. The raw microarray data were deposited at the Gene Expression Omnibus (GEO) repository of the National Center for Biotechnology Information under accession numbers GSE31099 and GSEA44355. The enrichment of distinct gene sets defined by Gene Ontology within the global transcript signals from matched pairs of untreated vs. ADR-treated control*;Bcl2* or *Suv39h1^{-};Bcl2* LC was analysed with the GSEA v2.0 software (Broad Institute of the Massachusetts Institute of Technology (MIT) and Harvard, http://www.broad.mit.edu/gsea). Normalized enrichment scores (NES) reflect a statistically significant enrichment for *P* values below 0.05 and false discovery rate (FDR) values below 0.25.[33]

Analysis of cell metabolism

In situ analyses of glucose and lactate levels in cryopreserved lymphoma tissue sections were performed by Dr. Stefan Walanta in the laboratory of Prof. Dr. Müller-Klieser at the Johannes Gutenberg University in Mainz using bioluminescence imaging as previously described.[242] To measure glucose and lactate concentrations, the

substrates were enzymatically linked to the luciferase enzyme to obtain a light emission signal whose intensity is proportional to the tissue glucose or lactate concentration respectively. The spatial distribution of the bioluminescence intensity was registered directly by a microscope (Axiophot, Zeiss) with a low-light imaging camera which contains an electron multiplying charge coupled device (iXon, Andor Technology). The light intensity was calibrated as weight-related tissue concentrations (μmol/g) by appropriate tissue standards.

Metabolic flux analysis was carried out by Christin Zasada in the laboratory of Dr. Stefan Kempa at the Max Delbrück-Center for Molecular Medicine (MDC) in Berlin. For stable isotope-resolved metabolomics (SIRM), LC were pooled and centrifuged at 300g for five minutes. Subsequently, cell pellets were resuspended in pre-warmed labelling medium containing $^{13}C_6$-glucose (2.5g/l, Sigma) as a labeled carbon source and incubated for three minutes at 37°C. Cell suspensions were centrifuged at 3,000g for five minutes at 4°C. The supernatants were discarded and the cell pellets were quenched in liquid nitrogen to stop all metabolic processes. Intracellular metabolites were prepared by methanol–chloroform–water extraction. For extracellular metabolites, LC were propagated in 24-well plates. 200μl of medium was collected from independent wells at different time points (e.g. after 18 hours) and stored at -25°C until sample extraction. 50μl of each media sample were extracted with 1ml pre-chilled methanol-chloroform-water buffer (5:2:1 v/v) under agitation for 30 minutes at 4°C. For both intra- and extracellular metabolites, 0.5ml water was then added to each sample. The upper polar phase was dried and stored at -20°C for subsequent analyses. For gas chromatography–mass spectrometry (GC-MS) analysis of intracellular and extracellular metabolites, cell pellets were prepared and measured as described.[243] The GC-MS chromatograms were processed with the ChromaTOF software (LECO). Data matrices for the relative quantification were extracted from the mass spectra using the MetMax software.[243,244]

Global metabolite analyses was performed by Dr. Jan Lisec in the laboratory of Prof. Lothar Willmitzer at the Max Planck Institute of Molecular Plant Physiology in Potsdam. For this purpose lymphoma cells were subjected to a methanol– chloroform–water

extraction as reported[245]. The polar fraction with a volume of 150µl was dried, derivatized and analysed by GC-MS as described.[246] The R software package TargetSearch was used to compare measured data against a reference library (Golm Metabolome Database, http://gmd.mpimp-golm.mpg.de), and to extract the intensity of quantification ions for 109 metabolites. The non-polar fraction with a volume of 500µl was analysed using an Exactive mass spectrometer (Thermo-Fisher). The intensity of 140 representative ion masses was retained after filtering for non-redundancy, abundance, assignable sum formulas and matching isotopic peaks using custom-made R scripts. Both raw data matrices were log10 transformed to improve normality and corrected for run-order effects and differences in sample median intensity using an appropriate analysis of variance (ANOVA) model.[247] For statistical analyses, normalized metabolite data were subjected to a principal com- ponent analysis (PCA) using the nipals algorithm from the pcaMethods package available for the statistical software framework R (http://www.r-project.org/) following an initial Pareto scaling.[248]

Analysis of fatty acid metabolism was performed by Dr. Markus Grähler at the Charité-Universitätsmedizin in Berlin. Fatty acid oxidiation was assessed by quantification of 16:0 phosphatidylcholine and its oxidized form lyso-phosphatidylcholine. Measurements of lymphoma cell lysates were performed according to an established protocol using liquid chromatography coupled to triple-quadrupole mass spectrometry (LC–MS–MS).[249] Multiple reaction monitoring transitions were as follows: phosphatidylcholine (16:0/18:2) m/z 758/184, lyso-phosphatidylcholine (16:0) m/z 496/184. Liquid chromatography resolution of all analytes was achieved using a 2x60 mm MultoHigh C18 reversed phase column with 3µm particle size (CS-Chromatographie Service). Linearity of the standard curves and correlation coefficients were obtained by linear regression analyses. Data analyses were performed using Analyst 1.4 (ABSciex).

In vitro analyses of metabolites were carried out by enzyme-linked absorbance or luminescence kits for glucose (Amplex Red Glucose/Glucose Oxidase kit, Invitrogen), lactate (Lactate assay kit, BioVision) and ATP (APOSensor ATP luminescence assay kit, Biovision, or ATP colorimetic/fluorometric assay kit, Biovision) according to the

manufacturers' protocols. Glucose uptake was assessed by flow cytometry after exposure to 10mM of the fluorescent glucose analogue 2-(N-(7-nitrobenz-2-oxa-1,3-diazol-4-yl)amino)-2-deoxyglucose (2NBDG; Molecular Probes) for two hours. Oxygen consumption rates (OCRs) and extracellular acidification rates (ECARs) were measured in an extracellular flux analyzer in accordance with the manufacturer's standard protocol (XF24, Seahorse Biosciences). In all assays equal cell numbers of untreated and ADR-treated control;*Bcl2* or *Suv39h1^{-};Bcl2* LC were compared. To analyze short-term changes in ATP levels upon inhibition of the lysosomal V-ATPase control;*Bcl2* and *Suv39h1^{-};Bcl2* LC were subjected to ADR treatment for five days. Subsequently LC were seeded in 384-well plates at equal numbers, where they were either exposed to 100nM Concanamycin A for ten minutes or left untreated. ATP levels were measured by an ATP luminometric assay kit (Promega) according to the manufacturer's instructions.

In vitro glucose metabolism was blocked by glucose transport inhibitors phloretin (Sigma, 50μM) or cytochalasin B (Sigma, 10μM) or by 2-deoxy-D-glucose (Sigma, 5mM). Glucose-free medium was supplemented with D-Glucose (Sigma, 5mM). The lactate dehydrogenase enzyme was inhibited by sodium oxamate (Sigma, 25mM). The electron transport chain was interrupted with antimycin A (Sigma, 1μM). AMPK was inhibited by Compound C (Sigma, 10mM). The carnitine palmitoyltransferase I inhibitor etomoxir (Sigma, 100μM) was used to block fatty acid oxidation. In LC lysosomal V-ATPases were inhibited by Bafilomycin A1 (Sigma, 5μM) or Concanamycin A (Sigma, 50nM). Lysosomal proteases were blocked using an inhibitor cocktail composed of pepstatin A, ZPAD (N-CBZ-l-phenylalanyl-l-alanine-diazomethylketone), and E64d (all from Sigma, 10μM). The final inhibitor concentrations were determined for each cell type (for primary AML samples and cancer cell lines see below) by dose-response experiments with serial dilutions, so that the selected concentration specifically killed senescent cells. Inhibitors were added once 48 hours prior to the analyses.

Autophagosome, endoplasmic reticulum and lysosome structure

Cellular ultrastructure and formation of autophagosomes were assessed by electron

microscopy in cooperation with Bettina Purfürst at the electron microscopy facility of the Max Delbrück Center (MDC) in Berlin. LC were fixed in a 0.1M phosphate buffer containing 4% formaldehyde and 1% glutaraldehyde for 24 hours. Samples were stained with 1% OsO4 for two hours, dehydrated in a graded ethanol series and propylene oxide and embedded in Poly/Bed 812 (Polysciences). Ultrathin sections were contrasted with uranyl acetate and lead citrate. For cryosectioning, cells were fixed in a 0.1M phosphate buffer containing 4% formaldehyde and 0.5% glutaraldehyde for one hour, subsequently embedded in 10% gelatine, and infiltrated with 2.3M sucrose. Ultrathin cryosections were contrasted and stabilized with a mixture of 3% tungstosilicic acid hydrate (Fluka) and 2.5% polyvinyl alcohol (Sigma). Sections were examined with a transmission electron microscope (Morgagni, FEI). Digital images were taken with a CCD camera (Morada), equipped with the iTEM software package (Olympus Soft Imaging Solutions).

Lysosomes were stained with LysoTracker Red DND-99 (Molecular Probes) as recommended by the manufacturer's protocol. LC were incubated with 100nM LysoTracker for one hour in cell culture medium. Subsequently, cytospin preparations were produced from LC on microscope slides by centrifugation at 800g for ten minutes. The slides were washed with PBS, stained with DAPI to obtain a nuclear counterstain and finally mounted with Mowiol 4-88 (Roth). The LC were imaged and analyzed by fluorescence microscopy (Axioplan, Zeiss).

Calcium efflux

Intracellular Ca^{2+} efflux was measured in accordance with the manufacturer's protocol (Fluo-4 NW Assay, Invitrogen). Cells were resuspended in assay buffer and seeded onto a poly-l-lysine-coated 96-well imaging plate. After incubation at 37°C for one hour, the calcium-sensitive dye Fluo-4 was added to each well. Following equilibration of the plate for 30 minutes to obtain a stable baseline intensity, 5mM 2-deoxy-D-glucose or 5μM Bafilomycin A1 were injected to the respective wells and the cells were automatically analyzed every 20 to 40 seconds. Fluorescence intensity curves were normalized against the values obtained from untreated LC.

Adherent cell culture

Human diploid fibroblasts, murine embryonic fibroblasts (MEFs), cancer cell lines, NIH 3T3 and Phoenix cells were cultured at 37°C in an incubator set at 5% CO2, 20% O2 and 95% humidity. Cells were grown in tissue-culture treated petri dishes and splitted onto new dishes at 80-90% confluency using 1% Trypsin/EDTA. Cell culture media were renewed every two to three days.

Primary AML samples

The use of human peripheral blood and bone marrow primarily obtained for the initial diagnosis of acute myeloid leukemia (AML) as anonymous samples was based on informed patient consent, and was specifically approved by the local ethics commission of the Charité – Universitätsmedizin Berlin (reference EA4/061/11). Mononuclear cells were isolated by Ficoll density-gradient centrifugation and red cell lysis. Briefly, the blood or bone marrow samples were diluted with PBS and subsequently mixed with a Biocoll Separating Solution (Merck Millipore) in a 3:1 ratio. The solution was centrifuged for 20 minutes at 1800rpm to achieve phase separation and the mononuclear cells (MNC) at the interphase were isolated by aspiration. Following red cell lysis the MNC were washed in PBS and either directly used for *in vitro* experiments or frozen as single cell suspensions. For *in vitro* experiments the cells were cultured on feeder layers as described for murine LC.[104] For synthetic lethal treatments primary AML samples were treated with 5μM Bafilomycin A1 or 5mM 2-deoxy-D-glucose respectively.

Human cell lines

The human B-cell lymphoma (Mec1, RCK8) and colon carcinoma (CaCo2, HCT116), obtained from local partner laboratories, were cultured in RPMI and DMEM respectively and exposed to ADR (lymphomas: 10ng/ml; colon carcinomas: 50ng/ml) to induce TIS. Six days after initiation of the treatment, cells were analyzed for SA-β-gal activity and subjected to additional experiments. For synthetic lethal treatments the

cell lines were incubated with Bafilomycin A1 (lymphomas: 10nM, colon carcinomas: 100nM) or 2-deoxy-D-glucose (lymphomas and colon carcinomas: 5mM) respectively. Mec1 and RCK8 were authenticated using multiplex cell authentication (Multiplexion).[250] The SNP profiles matched known profiles or were unique. Moreover, no mycoplasma contamination was detected in the cell lines.

Oncogene-induced senescence

Wild-type, *p53*$^{-/-}$ and *atg5*$^{-/-}$ mouse embryo fibroblasts (MEFs) were produced from E13.5 mouse embryos in accordance with regulatory standards of the governmental review board (LAGeSo, Berlin). MEFs and the human diploid fibroblast cell line Tig3 (a gift from D. Peeper) were cultured in accordance with published protocols.[43,20] Oncogene-induced senescence was established by stable transduction of cells with a MSCV-Hras^{G12V}-blasticidin (abbreviated as *RasV12*) retrovirus, or infection with a 4-hydroxytamoxifen (4-OHT)-inducible MSCV-Hras^{G12V}•ER-blasticidin retrovirus, encoding an oncogenic Ras-to-oestrogen receptor (ER) fusion (abbreviated as RasV12•ER; a gift from P. A. Khavari). The RasV12•ER fusion protein was activated by addition of 1μM of 4-OHT. In some experiments, Tig3 cells were infected with the pSuperRetro plasmid system for stable knockdown of IL6 (*shIL6*) or p53 (*shp53*).[153,251] Senescence was detected by SA-β-gal staining at day 5 after successful antibiotic selection or 4-OHT addition. Synthetic lethal treatments were performed with 50nM Bafilomycin A1 and 5mM 2-deoxy-D-glucose respectively.

Statistics

Based on previous experience with the Eμ-*myc* transgenic mouse lymphoma model, sample sizes typically reflect three to five individual primary tumors (that is, biological, not technical replicates), or even ten or more tumor-bearing animals per arm in investigator-blinded survival analyses of long-term outcome to treatment *in vivo*. If not stated otherwise, data are presented as arithmetic means ± standard deviation (s.d.) or standard error of the mean (s.e.m.). Statistical analyses of the generally normally

distributed (as assessed by the Shapiro–Wilk test) and variance-homogeneous (as assessed by the Levene test) data were based on paired or unpaired t-tests. The survival of mouse subcohorts was calculated using the Kaplan–Meier estimation and compared with the log-rank (Mantel–Cox) test. For GSEA, the non-parametric Kolmogorov–Smirnov test was applied. All quantifications from staining reactions were carried out by an independent and blinded second examiner, and reflect at least three samples with at least 200 events counted (typically in three different areas) each. Unless otherwise stated, a *P* value of 0.05 was considered statistically significant.

Further materials

Chemicals and reagents

Name	Company
2-propranol	Sigma
5-bromo-2'-deoxyuridine (BrdU)	Sigma
30% Acrylamide/Bis-acrylamide	Carl Roth
Adriamycin	Sigma
Agar	Carl Roth
Agarose	Carl Roth
Albumin Fraktion V	Carl Roth
Ammoniumperoxisulfat (APS)	Carl Roth
Ampicilin, sodium salt	Carl Roth
Bromphenol blue	Eurobio
Calcein	Sigma
Calcium chloride ($CaCl_2$)	Carl Roth
Chloroform	Merck
Chloroquine-diphosphate	Sigma
DAPI	Sigma
Diethyl pyrocarbonate (DEPC)	Sigma
Dimethylsulfoxid (DMSO)	Merck
Dulbecco's MEM	Invitrogen

DTT	Eurobio
ECL reagent	Millipore
Ethylenediaminetetraacetate (EDTA)	Carl Roth
Ethanol, absolute	Carl Roth
Ethidium-bromide powder	Sigma
Fetal bovine serum (FBS)	Biochrom
Formaldehyde solution 37%	Carl Roth
Gel Ruler 1-kb ladder plus	Fermentas
Glucose	Carl Roth
Glutaraldehyde	Carl Roth
Glyerol	Carl Roth
Glycine	Carl Roth
Hydrogen peroxide, H_2O_2	Sigma
Hydrochloric Acid, Hcl	Merck
HEPES	Carl Roth
Iscove's modified Eagle's media	Invitrogen
L-glutamine (solution)	Invitrogen
L-glutamine (powder)	Biochrom
Magnesium chloride ($MgCl_2x6H_2O$)	Carl Roth
β-Mercaptoethanol	Carl Roth
Methanol	Carl Roth
Milk powder	Carl Roth
Mowiol 4-88	Carl Roth
Nonident 40 (NP-40)	Fluka
PageRuler Plus Prestained Protein Ladder	Thermo Scientific
Penicillin-streptomycin	Biochrom
Phosphate Buffered Saline (PBS)	Carl Roth
Phenylmethylsulfonylfluoride (PMSF)	Sigma
Polybrene	Sigma
Potassium bicarbonate (KHCO3)	Sigma
Potassium ferricyanide (K3Fe(CN)6)	Sigma

Potassium ferrocyanide (K4Fe(CN)6x3H2O)	Sigma
Potassium chloride (KCl)	Sigma
Potassium acetate (KAc)	Carl Roth
Propridium iodide	Sigma
Protease inhibitor tablet	Roche
Puromycin	Calbiochem
ROTI-prestained	Invitrogen
RotiQuant, Bradford reagent	Carl Roth
RPMI 1640	Invitrogen
Salmon sperm DNA	Invitrogen
SDS 2326.2 Roth	Carl Roth
Sodium chloride (NaCl)	Carl Roth
Sodium citrate (C6H5Na3O7x2H2O)	Carl Roth
Sodium-desoxycholate	Sigma
Sodium fluoride (NaF)	Sigma
Sodium hydroxide (NaOH)	Carl Roth
Sodiumorthovanadate	Sigma
Sodium pyrophosphate	Sigma
Tris(hydroxymethyl) base	Invitrogen
TEMED	Sigma
Triton-X 100	Merck
TRIZOL	Invitrogen
Trypan-blue solution	Sigma
Trypsin-EDTA	Biochrom
Trypton/Pepton	Carl Roth
Tween 20	Carl Roth
Vecta-Shield	Vector
X-Gal	Carl Roth
Yeast extract	Carl Roth

Additional equipment

Name	Company and Model
Agarose gel electrophoresis chamber	Peqlab
Agarose UV gel imager	Gene Flash Syngene Bio Imaging
Digital camera	Diagnostic Instruments SPOT RT
Cell culture dishes and falcons	TPP
Cell culture incubator	Binder
Centrifuge	Hereus Megafuge 1.0R and Hettich Rotina 35R
Cryotubes	Sefar company
Frosted slides (76 x 26 mm)	Engelbrecht
Flow Hood Typ UVF 6.18S	BDK
Light microscope	Krüss MBL3100
Microcentrifuge	Roth
Microscopy immersion oil	Merck
Microwave	Siemens
Mr. Frosty Freezing Container	Thermo Scientific
NanoDrop	Peqlab ND-2000
Neubauer cell-counting chamber (Improved 0.025 mm, Depth 0.1mm)	Superior Marienfeld
Needles for single-use, sterile	Neoject
Nylon mesh (35μm)	Simport Plastics
PCR machine	Eppendorf
pH-meter	Mettler Toledo MP-220
Pipettes	Eppendorf
Polysterene tubes	BD Falcon
PVDF membrane (Immobilon P)	Millipore
Real-time PCR machine	Applied Biosystems StepOne Plus
Rotilabo filter, sterile (0.45μm PVDF)	Carl Roth
Rotilabo filter, sterile (0.22μm PVDF)	Carl Roth
Scalpel for single use	Feather

SDS-PAGE gel electrophoresis chamber	C.B.S. Scientific
Semi-dry transfer system	Biorad
Table top centrifuge	Eppendorf Centrifuge 5415D
Thermal shaker	Eppendorf Thermomixer comfort 1.5 ml
Tissue dissociator	Miltenyi Biotec, gentleMACS
Whatman paper (3MM)	Schleicher-Schuell

Commercial kits

Name	Company and Catalogue number
DAKO REAL™ Detection System, Alkaline Phosphatase_RED, Rabbit_Mouse	Dako, K5005
SuperScript® III First-Strand Synthesis system	Invitrogen, 18080-051
Immobilon Western Chemiluminescent AP substrate	Millipore, P36600
PureLink® HiPure Plasmid Filter Maxiprep Kit	Invitrogen, K2100-17
QIAprep Spin Miniprep Kit	Qiagen, 27104
RNeasy Mini Kit	Qiagen, 74104
TaqMan® Gene Expression Master Mix	Applied Biosystems, 4369016
LSAB 2 System AP-Kit	Dako, K0676

Media

Name	Composition
LB medium	10g tryptone 5g yeast extract 10g NaCl 1l dH_2O (pH 7.0) store at +4°C

LB agar plate	LB-medium + 15g Agar Autoclaved, cooled to approx. 55°C, antibiotic added and poured into petridish
DMEM	DMEM + 10% FCS + Penicillin-streptomycin (100U/ml) store at 4°C (sterile)
B cell medium	DMEM + IMDM (1:1) + 10% FCS + Penicillin-streptomycin (100U/ml) + 4mM L-glutamine +25μM β-Mercaptoethanol store at 4°C (sterile)
RPMI medium	RPMI 1640 + 10% FCS + Penicillin-streptomycin (100U/ml) store at 4°C (sterile)
Freezing medium	BCM + FCS (1:1) + 10% DMSO store at 4°C (sterile)

Solutions and buffers

Name	**Composition**
Plasmid Preparation Solution 1	25mM Tris (pH 8.0) 50mM Glucose 10mM EDTA
Plasmid Preparation Solution 2	0.2 N NaOH 0.5% SDS
Plasmid Preparation Solution 3	5M KAc 15% acetic acid

Transfection solution	2 x Hepes buffered saline (HBS): 280mM NaCl 10mM KCl 1.5mM Na_2HPO_4 x $2H_2O$ 12mM Dextrose 50mM HEPES 100ml dH_2O (pH 7.05) + 2M $CaCl_2$ store at -20°C (sterile)
Protein lysis buffer (NP-40)	1% NP-40 50mM Tris-HCl (pH 7.4) 150mM NaCl 5mM MgCl2 proteinase inhibitor cocktail (Roche) phosphatase inhibitor cocktail (Roche) store at -20°C
SDS sample buffer	1ml 0.5M Tris-HCl (pH 6.8) 0.8ml Glycerol 1.6ml 10% SDS 0.4ml 14.3M β-mercaptoethanol 0.4ml 1% Bromphenol blue store at -20°C
10% APS	1g Ammonium peroxysulfate in 10ml dH_2O
10x Running buffer (pH 8.3)	30g Tris base 144g Glycine 10g SDS 1l dH_2O (pH 6.8)
25x TBS	60g Tris base 200g NaCl 9.5ml 10N HCl 1l dH_2O

Transfer buffer	2.9g Tris base 14.5g Glycine 200ml Methanol 1l dH_2O store at 4°C
Blocking solution	5% dry milk in 1x TBS + 0.2% Tween 20, prepared freshly
Sa-β-gal fixation solution	0.25% Glutaraldehyde 2% Paraformaldehyde in PBS, prepared freshly
20x Potassium cyanide (KC) stock	20mg K3Fe(CN)6 1.05mg K4Fe(CN)6 x 3H2O in 25ml 1x PBS
Sa-β-gal staining solution (10ml)	9.25ml PBS + 1mM $MgCl_2$ (pH 5.5) +0.5ml 20x KC solution +0.25ml 40x X-Gal solution (40mg X-Gal in 1ml DMSO) prepared freshly
Immunofluorescence (IF)/ immuncytochemistry (ICC) fixation solution	4% Paraformaldehyde in 1x PBS prepared freshly
IF and ICC permeabilization solution	0.2% Triton X-100 in 1xPBS
IF and ICC blocking solution	1% BSA in 1x PBS
IF and ICC washing buffer	0.01% Tween 20 in 1x PBS

7. Results

Role of Suv39h1 in TIS

To assess the role of Suv39h1 in TIS, Eμ-*myc* lymphomas in a Suv39h1-proficient (hereafter referred to as 'control' lymphomas) and in a Suv39h1-deficient context (*Suv39h1*$^{-}$ lymphomas) were generated. Upon lymphoma formation, lymphoma cells (LC) were isolated and stably transduced with the anti-apoptotic *Bcl2* moiety *in vitro* prior to the senescence-inducing treatment with the DNA-damaging anticancer agents adriamycin (ADR) *in vitro* or cyclophosphamide (CTX) *in vivo* to investigate TIS in the absence of an apoptotic response.

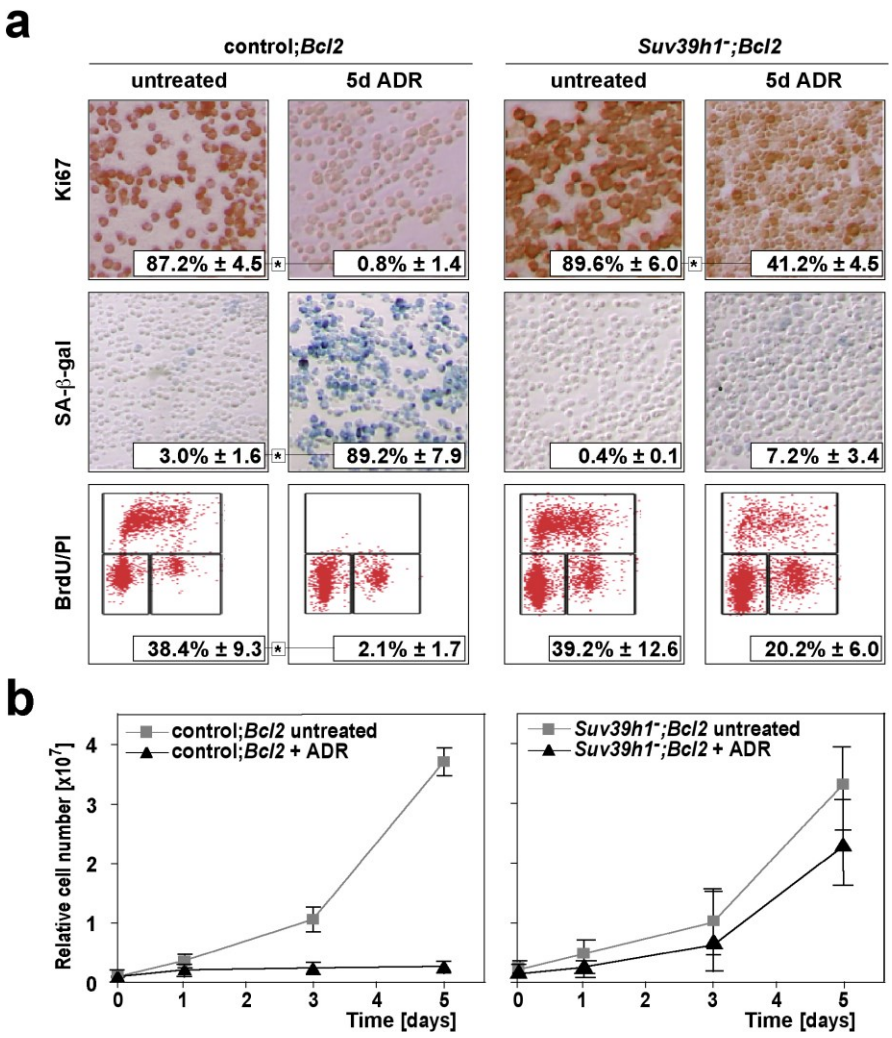

Figure 8. The histone methyltransferase Suv39h1 is an essential mediator of TIS *in vitro*. **a**, Features of ADR-induced senescence, i.e Ki67, SA-β-gal staining and BrdU/PI cell cycle

analyses, in ADR-senescent *vs.* untreated control;*Bcl2* LC as compared to ADR-treated *vs.* untreated *Suv39h1⁻;Bcl2* LC. Data represent means ± s.d. (n = 5 each). *P < 0.05. **b**, Growth curve analyses of control;*Bcl2* LC as compared to *Suv39h1⁻;Bcl2* LC exposed to ADR (black line) or left untreated (grey line). Notably, only ADR-treated control;*Bcl2* LC display features of senescence and stop to proliferate, while ADR-treated *Suv39h1⁻;Bcl2* LC remain SA-β-gal negative and maintain most of their proliferative capacity. Results represent means ± s.d. (n = 5 each).

As presented in Figure 8, control;*Bcl2* LC entered senescence after ADR-exposure for five days at very high frequencies. This is illustrated by a strong reduction of LC, which remained positive for the cell-cycle marker Ki67 as well as the high frequency of SA-β-gal positive LC, and the shift of DNA synthesis/S-phase activity towards the G1-phase of the cell-cycle. In contrast, *Bcl2*-protected LC, which lack Suv39h1, failed to display features of TIS following ADR treatment (Figure 8a). In addition, growth curve analyses confirmed growth cessation upon chemotherapy in control;*Bcl2*, but showed sustained exponential growth in *Suv39h1⁻;Bcl2* lymphomas (Figure 8b).

To evaluate the role of Suv39h1 function in TIS in lymphoma bearing mice *in vivo*, control;*Bcl2* and *Suv39h1⁻;Bcl2* lymphomas, which express the green fluorescent protein (GFP) to visualize the tumor burden, were propagated in non-transgenic recipient animals. A single dose of the alkylating agent cyclophosphamide (CTX) was administered when a significant lymphadenopathy became palpable. As shown in Figure 9 control;*Bcl2* lymphomas remained stable in size in response to CTX treatment after five days when compared to the lymphoma burden before treatment. In contrast, *Suv39h1⁻;Bcl2* lymphomas progressed to significantly larger and more disseminated tumor manifestations at this timepoint irrespective of CTX treatment (Figure 9a).

To determine whether this observation relates to a TIS defect due to Suv39h1 deficiency, lymphoma sections from untreated mice *vs.* mice five days post CTX treatment were assessed for SA-β-gal activity, Ki67 and incorporation of the thymidine analogue 5-bromodeoxyuridine (BrdU) *in situ*. Indeed, only CTX-exposed control;*Bcl2*, but not *Suv39h1⁻;Bcl2* lymphomas displayed significant SA-β-gal activity. Additionally, the spleen from CTX-exposed wild-type mice remained SA-β-gal negative and hence

did not display a TIS phenotype. Furthermore, whereas control;*Bcl2* lymphomas exhibited growth cessation with low fractions of Ki67- and BrdU-positive cells, *Suv39h1*$^{-}$*;Bcl2* lymphomas preserved S-phase activity as indicated by positive Ki67 staining and retained incorporation of BrdU (Figure 9b). Therefore, Eμ-*myc* lymphomas lacking *Suv39h1* alleles lost the ability to enter cellular senescence in response to DNA-damaging chemotherapy *in vivo*.

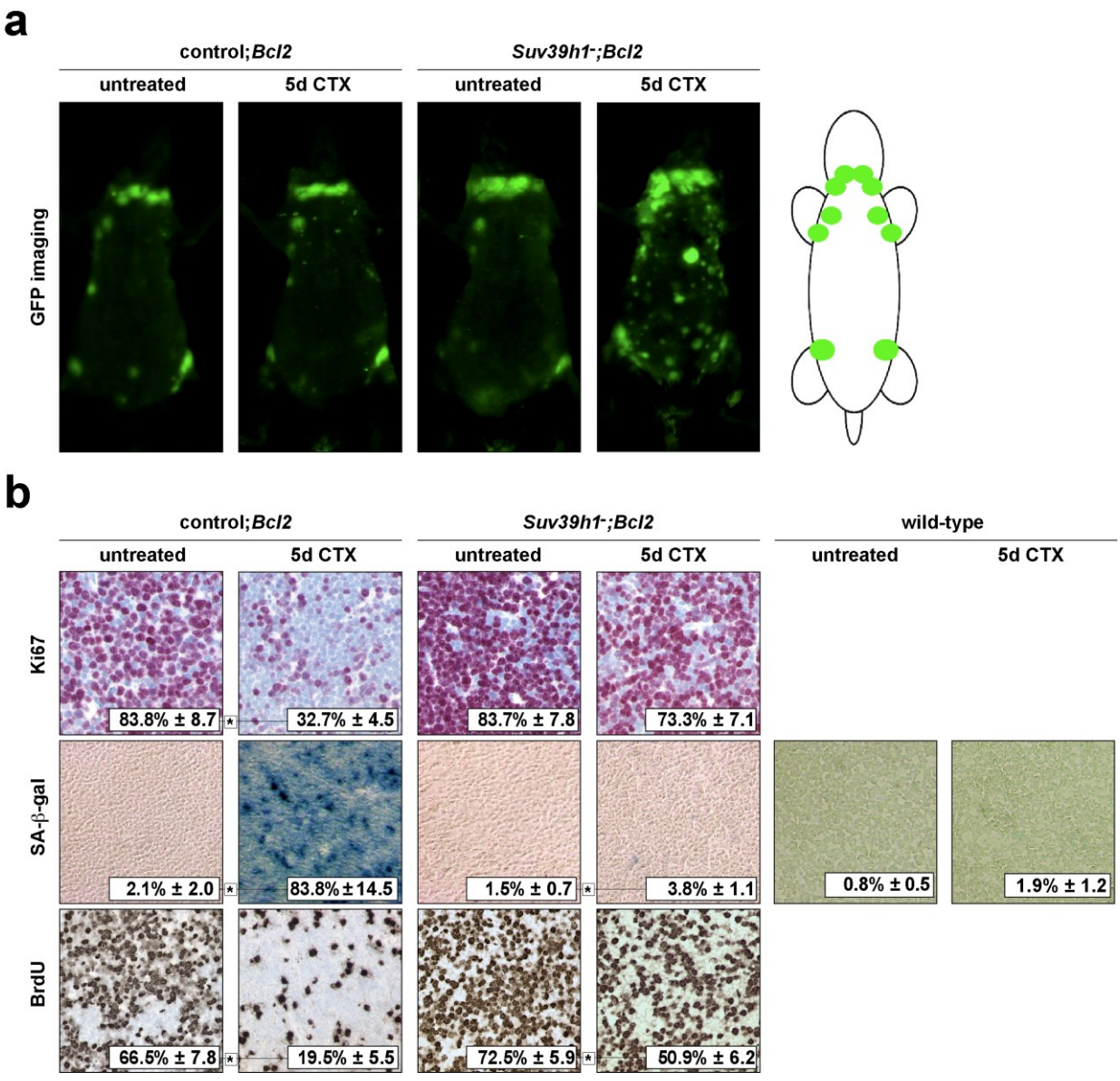

Figure 9. Loss of Suv39h1 selectively disables TIS *in vivo*. **a**, Representative photomicrographs of lymphoma growth in CTX-treated mice harboring GFP-tagged control;*Bcl2 vs. Suv39h1*$^{-}$*;Bcl2* lymphomas by whole body fluorescence imaging. **b**, Control;*Bcl2*, but not *Suv39h1*$^{-}$*;Bcl2* lymphomas or wild-type spleen exhibit features of TIS as measured by SA-β-gal, Ki67 and BrdU staining five days after CTX therapy *in vivo*. Results represent means ± s.d. (n = 5 each). *P < 0.05.

Metabolic alterations in TIS

Since diagnostic procedures to non-invasively detect a senescent proliferation arrest of cancer lesions in response to chemotherapy *in vivo* are still missing, functional lymphoma parameters in response to CTX therapy were monitored by [18F] fluorothymidine (FLT)-positron emission tomography (PET) to assess proliferation and by [18F] fluorodeoxyglucose (FDG)-PET to judge metabolism. Consistent with the SA-β-gal reactivity and the reduction in proliferation markers BrdU and Ki67 *in situ*, the FLT-PET analysis of lymphoma-bearing mice before and six days after CTX treatment in Figure 10 displayed significantly lower FLT tracer uptake after CTX treatment in the control;*Bcl2* lymphomas, but not in the *Suv39h1*$^{-}$*;Bcl2* lymphomas.

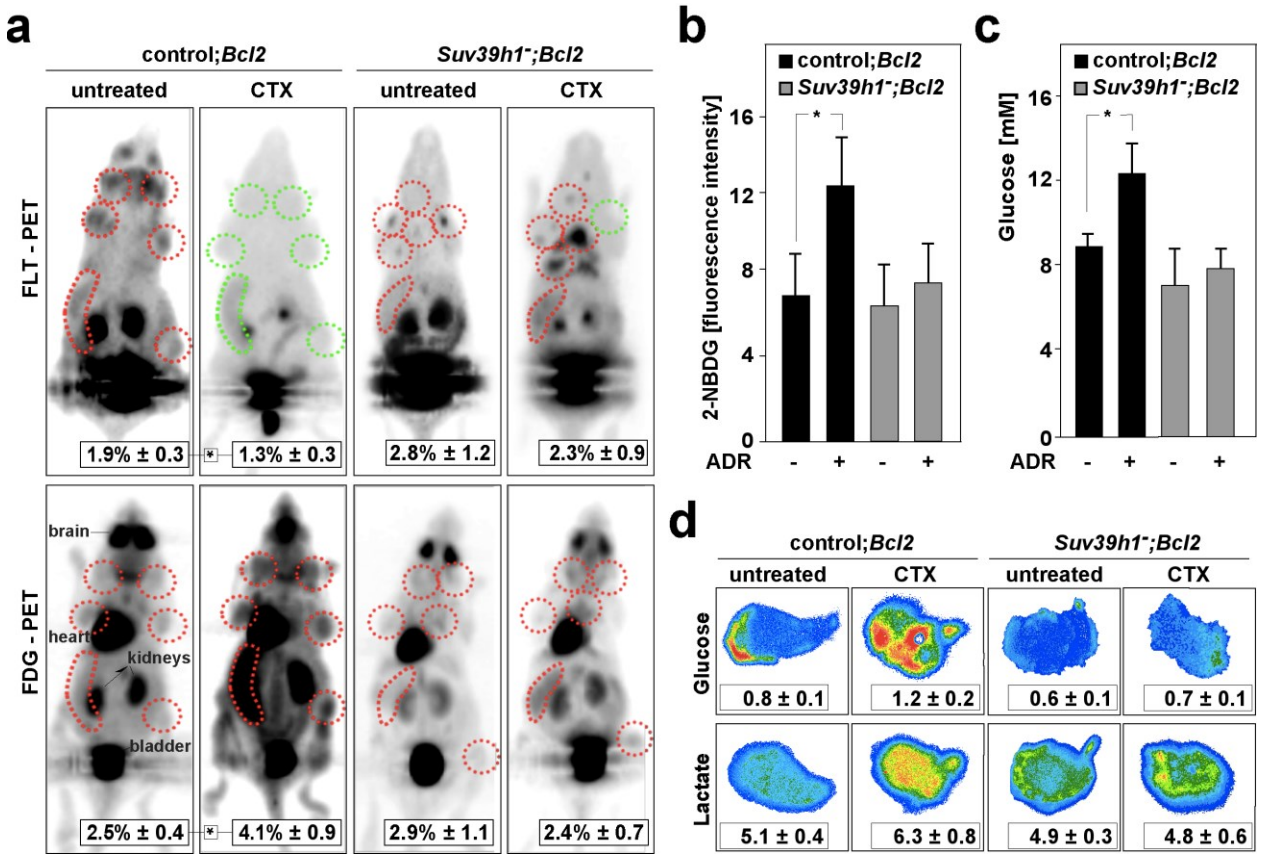

Figure 10. **TIS is a highly glucose-consuming condition. a**, Representative whole-body FLT- and FDG-PET images of individual control*;Bcl2* and *Suv39h1*$^{-}$*;Bcl2* lymphoma-bearing mice at tumor manifestation (untreated) and at day 6 after CTX treatment. Red circles indicate areas of specific tracer retention; green circles highlight matching areas with lost retentions. Specific tracer uptake was assessed by calculation of tumor-to-background ratios. Data represent mean ratios ± s.d. ($n \geq 5$ mice for FLT-PET and FDG-PET scans). *$P < 0.05$. **b**, 2-(N-[7- nitrobenz-2-oxa-1,3-diazol-4-yl]amino)-2-deoxyglucose (2-NBDG) uptake by flow cytometry in untreated and ADR-senescent control;*Bcl2 vs.* ADR-treated *Suv39h1*$^{-}$*;Bcl2* LC at

day 5 *in vitro*. Results represent mean ± s.d. (*n* = 5 each). **P* < 0.05. **c**, Intracellular glucose concentrations of LC as in b. Results represent means ± s.d. (*n* = 5 each). **P* < 0.05. **d**, Representative, color-calibrated bioluminescence images of glucose and lactate levels in tissue sections of untreated *vs.* CTX-treated control;*Bcl2* and *Suv39h1*$^{-}$*;Bcl2* lymphomas *in situ* (red – highest, blue – lowest intensities). Note that only TIS-capable lymphomas display both increased glucose and lactate levels. Data represent means ± s.d. (control;*Bcl2*: *n* = 8, *Suv39h1*$^{-}$*;Bcl2*: *n* = 4). Figure adapted from Dörr et al..[103]

Unexpectedly, the same TIS control;*Bcl2* lymphomas showed an enhanced glucose uptake by [18F] fluorodeoxyglucose (FDG)-PET (Figure 10a). The increased glucose avidity of TIS lymphomas was confirmed *in vitro* in a PET-independent glucose uptake assay with the fluorescent glucose analogue 2-(N-(7-nitrobenz-2-oxa-l,3-diazol-4-yl)amino)-2- deoxyglucose (2NBDG) (Figure 10b). In accordance with this observation, higher glucose levels were detected *in vitro* in ADR-treated vs. untreated control;*Bcl2* lymphomas and *in situ* in CTX-treated vs. untreated control;*Bcl2* lymphomas, whereas no difference was seen in TIS-incompetent *Suv39h1*$^{-}$*;Bcl2* lymphomas upon ADR or CTX treatment (Figure 10c, d). Hence, TIS lymphomas are characterized by an enhanced glucose uptake and can be non-invasively detected by a discordant negative FLT-PET and positive FDG-PET scan post treatment.

Interestingly, TIS lymphomas, but not TIS-incompetent *Suv39h1*$^{-}$*;Bcl2* lymphomas also display higher lactate levels *in situ* upon CTX treatment (Figure 10d). To assess whether the increased glucose uptake and the higher glucose and lactate levels in TIS lymphomas are indicative of an increased glucose metabolism in senescence, glycolysis metabolites were measured at different timepoints in the supernatant of ADR-treated vs untreated *control;Bcl2* as well as *Suv39h1*$^{-}$*;Bcl2* LC *in vitro* as indicated in Figure 11. Furthermore, metabolic flux analysis with 13C-labeled glucose was performed in LC in the same setting (Figure 11a). The analyses show that TIS cells metabolized glucose rapidly to pyruvate, lactate and citrate, such that these metabolites became detectable at much higher concentrations relative to glucose, despite the resting state of these cells. In addition, only TIS LC, but not untreated, proliferating *control;Bcl2* LC, or *Suv39h1*$^{-}$*;Bcl2* LC, irrespective of treatment, exhibited increased glucose transporter and glycolytic enzyme expression levels as well as higher steady- state glucose concentrations after ADR treatment *in vitro* (Figure 11b).

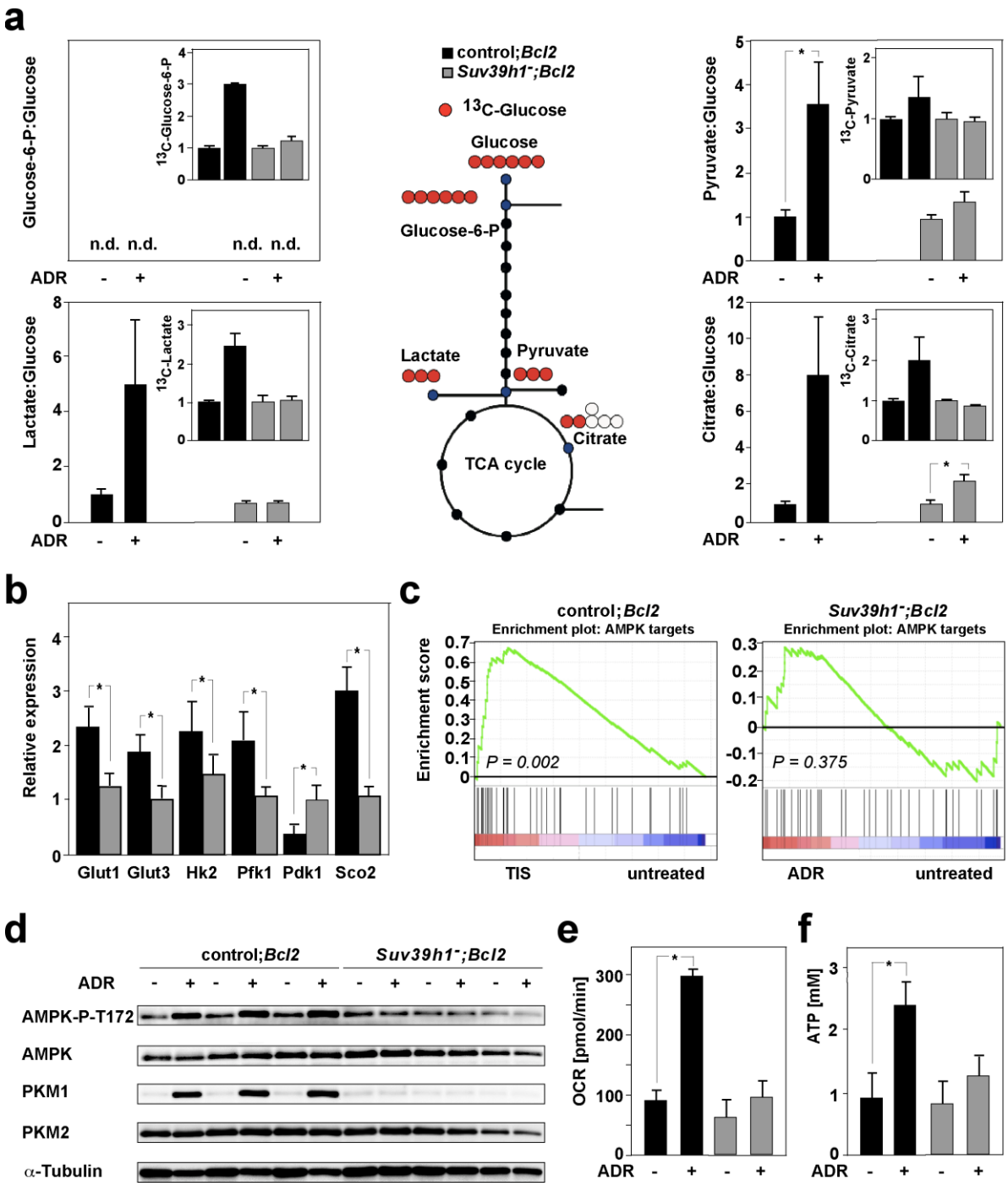

Figure 11. **TIS is an energy-producing condition. a**, Extracellular levels of the specified metabolite-to-glucose ratios in the indicated LC relative to untreated control;*Bcl2* LC after 18 hours of cultivation. Data represent mean ratios ± s.d. (*n* = 4 each, measurements were carried out in duplicate). Note that glucose-6-phosphate is not detectable (n.d.) in the medium. Insets show mean ratios (ADR-treated relative to untreated) of intracellular levels of the respective metabolites after labelling with $^{13}C_6$-glucose for one representative lymphoma from each group. **b**, Relative expression levels (ADR-treated normalized to the untreated condition) of the glucose transporters Glut1 and Glut3, the glycolytic enzymes hexokinase 2 (Hk2) and phosphofructokinase 1 (Pfk1), the pyruvate dehydrogenase kinase 1 (Pdk1) and the synthesis of cytochrome c oxidase 2 assembly gene (Sco2) in control;*Bcl2 vs. Suv39h1-;Bcl2* LC at day

5 *in vitro*. Results represent means ± s.d. (*n* = 5 each). **c**, Gene set enrichment analysis (GSEA) of AMPK target genes (gene set taken without further changes from Greer et al.[252]) in gene expression profiles of ADR-senescent *vs.* untreated control;*Bcl2* LC (*n* = 12 matched pairs), and ADR-treated *vs.* untreated *Suv39h1*$^{-}$*;Bcl2* LC (*n* = 5 matched pairs), which demonstrates a selective enrichment of the module in TIS LC. **d**, Immunoblot analyses of phosphorylated AMP-activated protein kinase (AMPK-P-T172), total AMPK, and pyruvate kinase isoforms M1 and M2 in ADR-senescent *vs.* untreated control;*Bcl2* and ADR-treated *vs.* untreated *Suv39h1*$^{-}$*;Bcl2* LC *in vitro* (*n* = 3 each); α-Tubulin as a loading control. Gels were cropped to ease presentation; full-length blots are provided in Supplementary Figure 2. **e**, Mean oxygen consumption rates (OCR) in ADR-senescent *vs.* untreated control;*Bcl2* and ADR-treated *vs.* untreated *Suv39h1*$^{-}$*;Bcl2* LC *in vitro*. Results represent means ± s.d. (*n* = 5 each). **f**, Intracellular ATP concentrations in LC as in e. Results represent means ± s.d. (*n* = 5 each). Where indicated **P* < 0.05. Figure adapted from Dörr et al..[103]

Furthermore, RQ-PCR revealed a TIS-dependent increase in the expression of the cytochrome c oxidase 2 assembly gene (Sco2), which promotes energy generation *via* mitochondrial respiration upon adenosine mono-phosphate (AMP)-activated protein kinase (AMPK) activation.[253] AMPK is a central energy sensor of the cell, which responds to changes in the AMP/ATP and ADP/ATP ratios. Gene set enrichment analyses and immunoblot analysis of control;*Bcl2* and *Suv39h1*$^{-}$*;Bcl2* LC before and after ADR treatment showed enhanced expression of AMPK target genes and activating phosphorylation of AMPK only in TIS LC indicating their increased energetic demands (Figure 11c, d).[254]

Besides the accumulation of lactate, which is according to the Warburg effect the predominant endpoint of glucose breakdown in cancer cells, TIS cells also increase pyruvate metabolism in the tri-carboxylic acid (TCA) cycle (Figure 11a).[255] On a molecular level this is catalyzed by decreased expression of the pyruvate dehydrogenase kinase 1 (Pdk1) only in TIS LC, but not in untreated, proliferating *control;Bcl2* LC, or in *Suv39h1*$^{-}$*;Bcl2* LC, irrespective of treatment (Figure 11b). Pdk1 inactivates the pyruvate dehyrogenase (Pdh) by phosphorylation and thereby prevents the oxidative decarboxylation of pyruvate to acetyl-CoA.[256] Therefore, reduced expression of Pdk1 in TIS increases Pdh activity and enhances the flux of glucose carbon into the TCA cycle. Furthermore, the M1 isoform of the pyruvate kinase (Pkm1) is induced in senescence as shown by immunoblot analysis of ADR-treated vs. untreated control;*Bcl2* and Suv39h1^{-};*Bcl2* LC (Figure 11d; for full length blots see Supplementary Figure 2). PKM1 is found predominantly in differentiated tissues with

high ATP requirements and increases oxygen consumption.[257] In fact, a strongly elevated oxygen consumption rate (OCR) and higher intracellular ATP levels were detected selectively in TIS LC (Figure 11e, f).

Furthermore, transcriptome and metabolome analysis of ADR treated vs. untreated control;*Bcl2* and *Suv39h1*$^{-}$*;Bcl2* was performed as demonstrated in Figure 12.

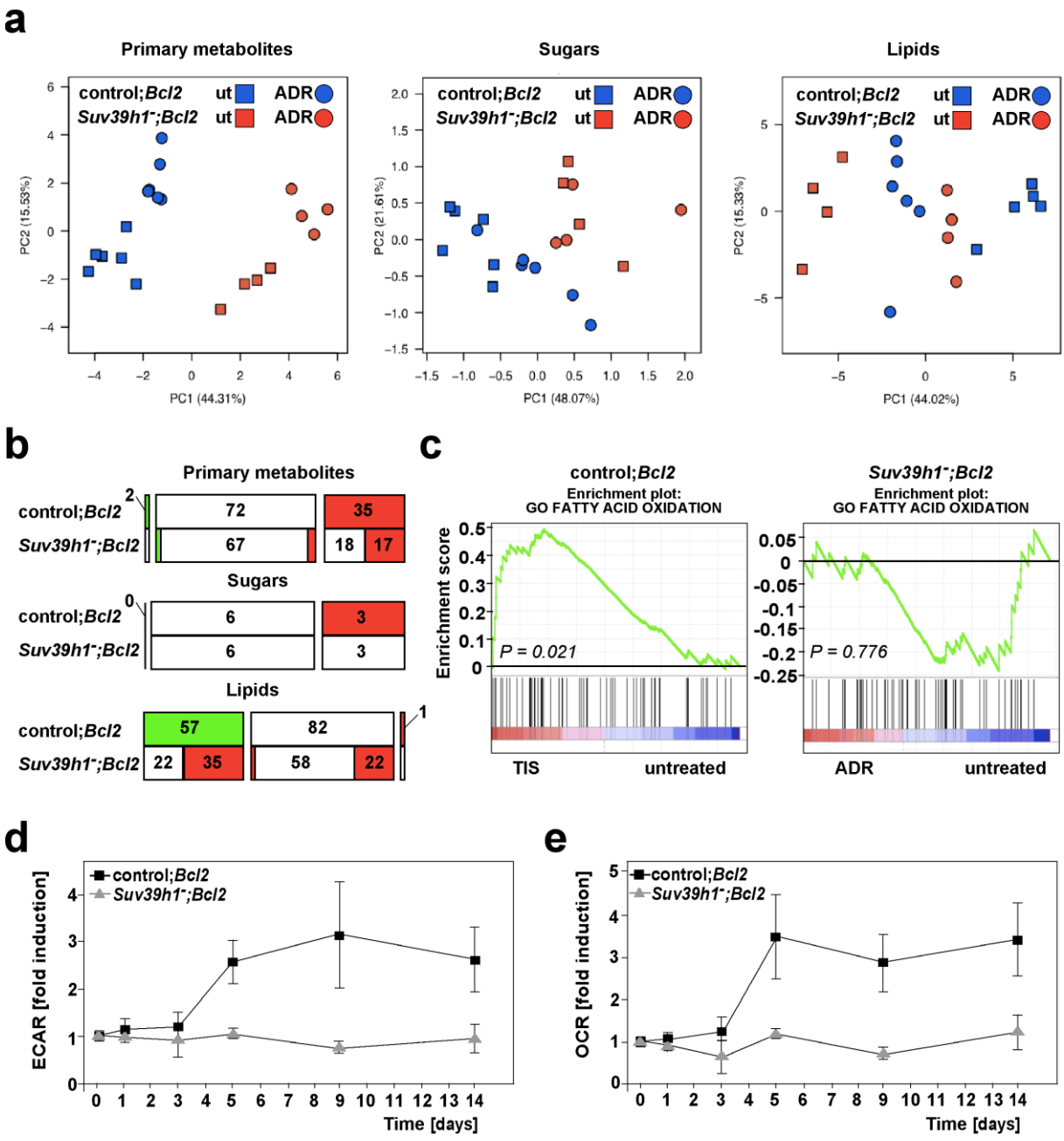

Figure 12. **Global metabolic changes in TIS. a-c**, Metabolomics and GSEA analyses of ADR-senescent control;*Bcl2 vs.* ADR-treated *Suv39h1*$^{-}$*;Bcl2* LC at day 5 as compared to the matching untreated LC *in vitro*. **a**, Principal component analysis (PCA) of all primary

metabolites, sugars (as a subgroup of primary metabolites), and lipids measured by GC- and LC-MS, respectively. Note the distinctly different clustering of TIS cells when compared to any other group (control;*Bcl2*: *n* = 6; *Suv39h1*$^{-}$*;Bcl2*: *n* = 4). **b**, Graphical representation of metabolite changes measured by metabolomics (as in a). The red color code indicates the number of metabolites detected at significantly higher quantities in ADR-treated cells, whereas the green color code indicates the number of metabolites detected at significantly lower quantities according to a *t*-test (presented as absolute number of metabolites per group; metabolites that did not change significantly [$P \geq 0.05$] are shown in white). Changes within three metabolic subgroups (*i.e.* primary metabolites, sugars [within primary metabolites], lipids) detected in the control;*Bcl2* group can be directly compared to changes in the *Suv39h1*$^{-}$*;Bcl2* group. Note that primary metabolites are predominantly elevated in ADR-senescent control;*Bcl2* LC (X^2-test significant at $P < 0.05$ if compared to the number of elevated metabolites in ADR-treated *Suv39h1*$^{-}$*;Bcl2* LC), while lipids are reduced in TIS LC to fuel primary metabolism and energy production, but not in ADR-treated *Suv39h1*$^{-}$*;Bcl2* LC. **c**, GSEA of transcripts related to the gene ontology term "fatty acid oxidation", showing selective enrichment of the module in TIS cells. Underlying gene expression profiles as in Figure 11c. **d**, Extracellular acidification rates (ECAR) of LC in ADR-senescent control;*Bcl2* vs. ADR-treated *Suv39h1*$^{-}$*;Bcl2* LC monitored for 14 days *in vitro*. The values were normalized to the untreated condition at the indicated time points. Results represent means ± s.e.m. (*n* = 3 each). **e**, OCR as in d. Results represent means ± s.e.m. (*n* = 3 each). Figure adapted from Dörr et al..[103]

The metabolome profile shows a significant elevation of primary metabolites, such as sugars, and reduction of lipids to fuel energy production only in TIS LC, but not in ADR-treated *Suv39h1*$^{-}$*;Bcl2* LC (Figure 12a, b). On the transcriptome and gene expression level, gene set enrichment analysis of the gene ontology term "fatty acid oxidation showed selective enrichment of the module in TIS cells (Figure 12c). Furthermore, measurement of glycolysis as well as oxidative phosphorylation over a timespan of 14 days shows that energy production is stably elevated only in TIS LC, but not in untreated, proliferating *control;Bcl2* LC, or in *Suv39h1*$^{-}$*;Bcl2* LC, irrespective of treatment (Figure 12d, e). In summary, TIS lymphomas are characterized by an unexpected hypermetabolic phenotype composed of enhanced glycolysis, fatty acid catabolism and ATP-boosting oxidative phosphorylation.

TIS addiction to increased energy demands

To test whether TIS lymphomas do not only show a hypermetabolic condition but also depend on it, energy production in TIS LC and untreated control;*Bcl2* LC as well as ADR-treated and untreated *Suv39h1*$^{-}$*;Bcl2* was inhibited by pharmacological and short-hairpin RNA approaches. As shown in Figure 13 senescent LC were indeed selectively susceptible to inhibition of glucose transporters by phloretin or cytochalasin

B as well as to a block in glycolysis by either stable knockdown of hexokinase 2 with a short hairpin RNA (*shHk2*) or by pharmacological means with 2-deoxy-D-glucose (2-DG) as a false substrate and sodium oxamate as an inhibitor of the lactate dehydrogenase (Figure 13a-d). TIS-selective toxicity was also observed after inhibition of the energy sensor AMPK by compound C (Figure 13e). Furthermore, suppressing fatty acid oxidation by etomoxir, or ATP depletion after poisoning of the respiratory chain by antimycin A exert a TIS-specific cytotoxicity (Figure 13f, g). Therefore, high energy demands in TIS LC present a critical senescence-associated liability, which may be therapeutically exploitable.

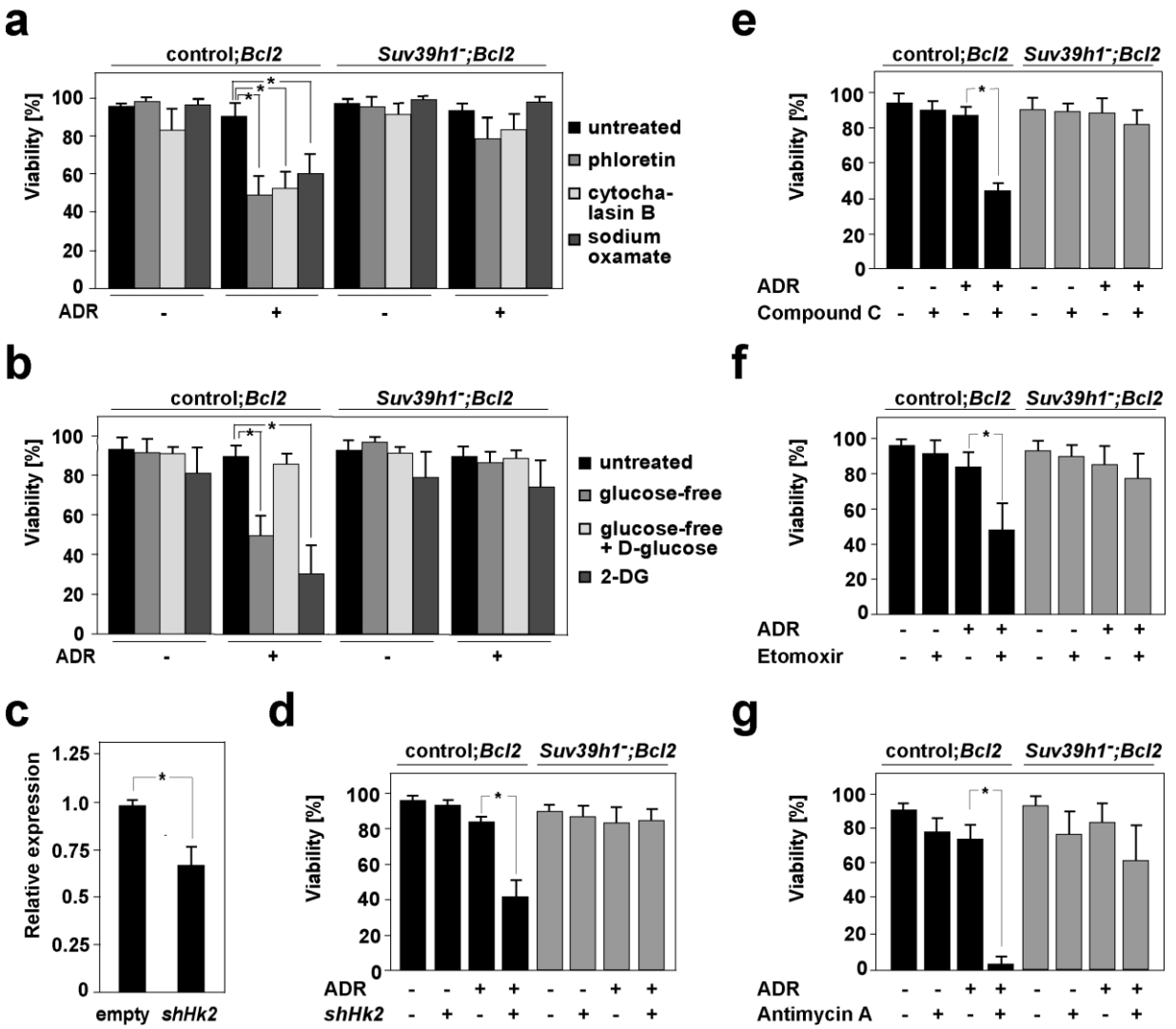

Figure 13. **Selective vulnerability of TIS LC to inhibition of energy-generating catabolic pathways. a**, Inhibition of glucose metabolism by phloretin, cytochalasin B, and sodium oxamate in ADR-senescent *vs.* untreated control;*Bcl2* and ADR-treated *vs.* untreated *Suv39h1*$^{-}$*;Bcl2* LC. **b**, Exposure to 2-deoxy-D-glucose (2-DG) or switch to glucose-free medium with or without glucose replenishment of cells as in a. **c**, Knock-down efficacy of

lentiviral small-hairpin RNA against *hexokinase 2* (*shHk2*) by RQ-PCR analysis. **d**, Viability of ADR-senescent *vs.* untreated control;*Bcl2* and ADR-treated *vs.* untreated *Suv39h1*$^{-}$*;Bcl2* LC with and without sh*Hk2*. **e**, Inhibition of AMPK by compound C of cells as in a. **f**, Block of fatty acid oxidation by the carnitine palmitoyltransferase I inhibitor etomoxir of cells as in a. **g**, Inhibition of the electron transport chain by antimycin A of cells as in a. All results represent means ± s.d. (n = 5 each). *P < 0.01, except b (n = 8 each), c (*P < 0.05) and f (*P < 0.05). Figure adapted from Dörr et al..[103]

Autophagy in TIS

Despite the lack of a compelling analysis that quantitates global ATP consumption in biosynthetic and degradative processes in a cell, it is commonly believed that protein synthesis and turnover consume large parts of the cellular energy pool.[258] Protein turnover is predominantly mediated by the ubiquitin-proteasome system and by autophagic degradation in the lysosome. Both mechanisms require ATP.[259,260] A key feature of senescent cells is their enlarged lysosomal compartment, which is, at least in part, associated with the activation of autophagy.[261] Autophagy serves as a cellular stress response that degrades and recycles cellular components.[262] In this context, a link between higher protein quantities and the induction of autophagy in Ras-senescent fibroblasts has been reported.[196] In autophagy protein cargo is marked by ubiquitination for lysosomal degradation. The ubiquitinated proteins are transported to the autophagosome by intracellular adaptor proteins, such as p62, which bind to both the protein cargo as well as the forming autophagosome.[263]

As shown in Figure 14, a significantly higher protein synthesis rate was detected in TIS LC as measured by global incorporation of a fluorescent methionine, which is the first amino acid incorporated in each protein chain (Figure 14a). Furthermore, gene set enrichment analyses (GSEA) for the gene ontology terms “protein maturation“ and “protein processing“ were significantly enriched in TIS LC (Figure 14b). However, the TIS-associated increase in protein synthesis induced substantial proteotoxic stress as shown by ultrastructural endoplasmic reticulum alterations reminiscent of endoplasmic reticulum stress (Figure 14c). Additionally, a significant enrichment of transcripts involved in the unfolded protein response (UPR), as well as UPR-related phosphorylation of Jun N-terminal kinases (JNK), alternative splicing of XBP1

transcripts, and enhanced expression of the transcription factors ATF4 (cyclic AMP-dependent transcription factor ATF-4) and CHOP (also known as DNA damage-inducible transcript 3 protein) were detected only in TIS control;*Bcl2* LC, but neither in untreated control;*Bcl2* LC nor in ADR-treated or untreated *Suv39h1*$^{-}$*;Bcl2* LC (Figure 14d).

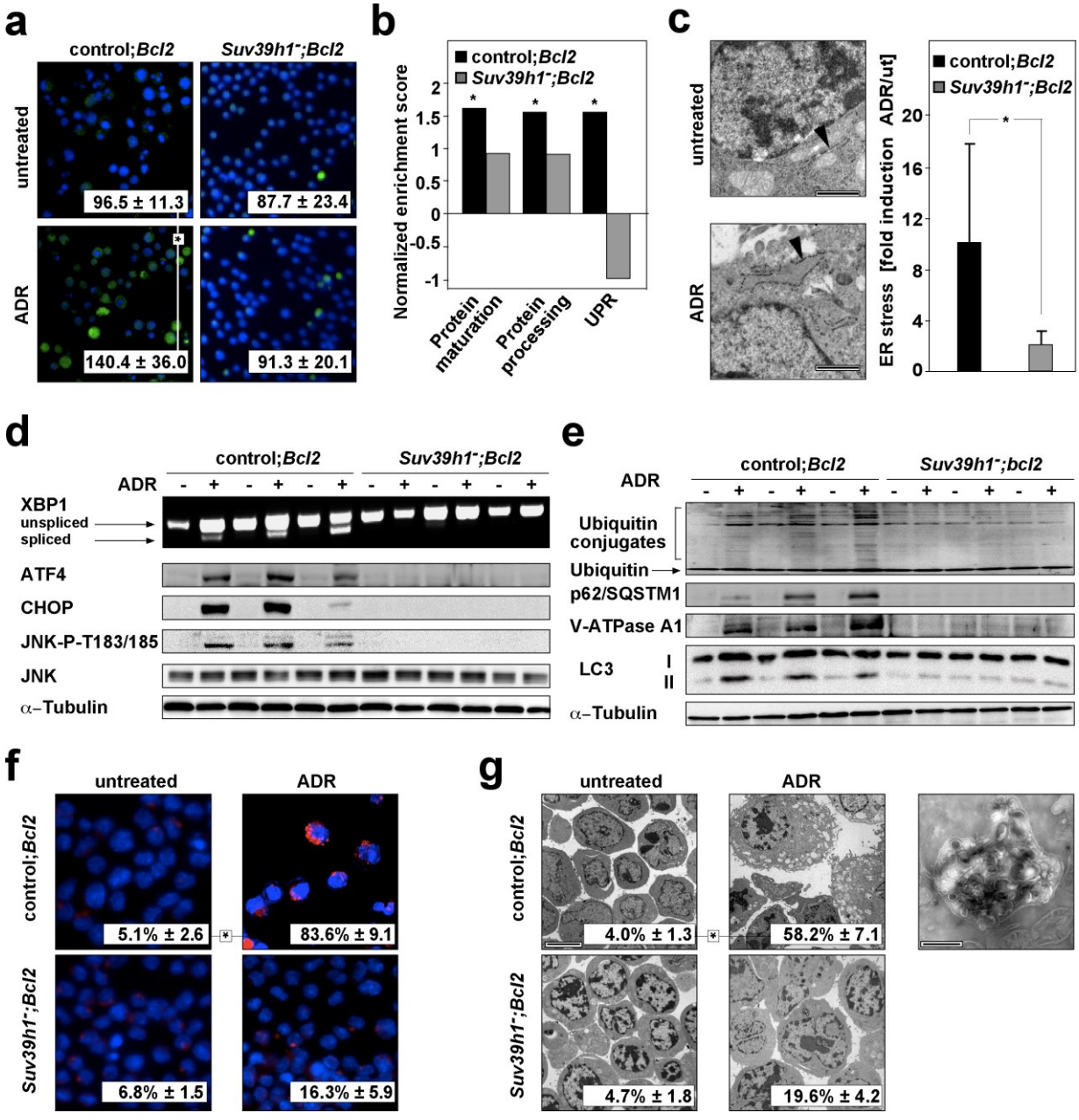

Figure 14. **TIS-evoked proteotoxicity induces ER stress, and it enforces lysosomal expansion and autophagy. a**–**g**, Proteostasis analysis in TIS LC vs. ADR-treated *Suv39h1*$^{-}$*;Bcl2* LC *in vitro*. **a**, Global protein synthesis rate, measured by incorporation of green-fluorescent methionine. Mean fluorescent intensities reflect newly synthesized protein within two hours (DAPI used as a counterstain). Data represent means ± s.d. (*n* = 5 each). **b**, GSEA of transcripts related to the GO terms “protein maturation”, “protein processing” and

"endoplasmic reticulum unfolded protein response (UPR)". Underlying gene expression profiles as in Figure 11c. **c**, Ultrastructural alterations in TIS LC by electron microscopy (*left*; note the dilated and disorganized cisternae of the rough ER in TIS LC reminiscent of ER stress as compared to the narrow and regularly organized cisternae in untreated LC [arrow heads]). Representative photomicrographs (bar = 2µm; *n* = 3 each). Quantification of ER stress (*right*) in ADR-senescent *vs.* untreated control;*Bcl2* and ADR-treated *vs.* untreated *Suv39h1*$^{-}$*;Bcl2* LC, which reflects the relative changes in the percentages of LC with dilated cisternae. Data represent means ± s.d. (*n* = 3 each; measurements were done in duplicates). **d**, Expression of the transcription factors Xbp1 (by RT–PCR; the lower band reflects the UPR-related splice form; top), ATF4, CHOP, phospho-Jun N-terminal kinase (JNK-P-Thr183/Thr185) and total JNK (by immunoblot analyses, with α-Tubulin as a loading control; bottom) in LC as indicated (*n* = 3 each). Gels were cropped to ease presentation; full-length blots are provided in Supplementary Figure 2. **e**, Global protein ubiquitination, expression of p62/SQSTM1 and of the V-ATPase subunit A1, and conversion of MAP1-LC3-I to MAP1-LC3-II by immunoblot analyses, demonstrating autophagosome formation in LC as in d (*n* = 3 each; α-Tubulin as a loading control). Gels were cropped to ease presentation; full-length blots are provided in Supplementary Figure 2. **f**, TIS-associated changes of the lysosomal compartment by Red DND-99-based fluorescence in LC as in a. The red staining marks LC with an expanded lysosomal compartment. Data represent means ± s.d. (*n* = 3 each). **f**, Representative photomicrographs of TIS-associated changes of the lysosomal compartment by electron microscopy in cells as in a (*left*) (bar = 5µm). Numbers reflect the mean fraction of LC ± s.d. (*n* = 3 each) that scored positive by containing at least 5 autophagosomes per cell section; representative example of TIS-associated autophagosomes (*right*) (bar = 500nm). **P* < 0.05 except f, where **P* < 0.01. Figure adapted from Dörr et al..[103]

Consistent with the idea that protein homeostasis is mediated by autophagy in OIS, global ubiquitination and expression of the microtubule- associated protein light chain 3 (MAP1-LC3)-binding protein SQSTM1 (also known as p62) were strongly induced in TIS (Figure 14e). In addition, only TIS control;*Bcl2* LC, but neither untreated control;*Bcl2* LC nor *Suv39h1*$^{-}$*;Bcl2* LC irrespective of ADR treatment, displayed a greatly expanded lysosomal compartment as well as signs of autophagy as indicated by enhanced conversion of the MAP1-LC3-I-protein isoform to the MAP1-LC3-II-protein isoform, elevated autophagic flux, and activation of the lysosomal vacuolar type ATPase (V-ATPase) A1 (Figure 14e). In support of the immunoblot results, only TIS LC show structural alterations indicative of enlarged lysosomal and autophagic compartments as indicated by fluorescence and electron microscopy (Figure 14f, g).

Role of SASP in TIS-related proteotoxicity

Therefore, it could be possible that the increased protein production in senescence fuels the nuclear factor-kB (NFκ-B)-driven SASP which in turn requires autophagy for

degradation of misfolded SASP components. To test whether the increased proteotoxicity and autophagic turnover is induced by NF-κB-driven cytokine production and causally linked to the observed hypermetabolism, control;*Bcl2* LC were stably transduced with an NF-κB super-repressor (SR) IκBαΔN. SR lymphomas have previously been shown to repress the expression of SASP-associated cytokines in response to ADR treatment without affecting TIS *in vitro*.[166] As demonstrated in Figure 15, SR lymphomas did not show a significantly increased protein synthesis rate and lacked elevated levels of proteotoxicity and autophagy after senescence-inducing ADR treatment (Figure 15a, b). Furthermore, senescent SR lymphomas lacked signs of the TIS-associated hypermetabolism as displayed by much lower gains in glucose uptake, OCR and ATP generation (Figure 15c-e).

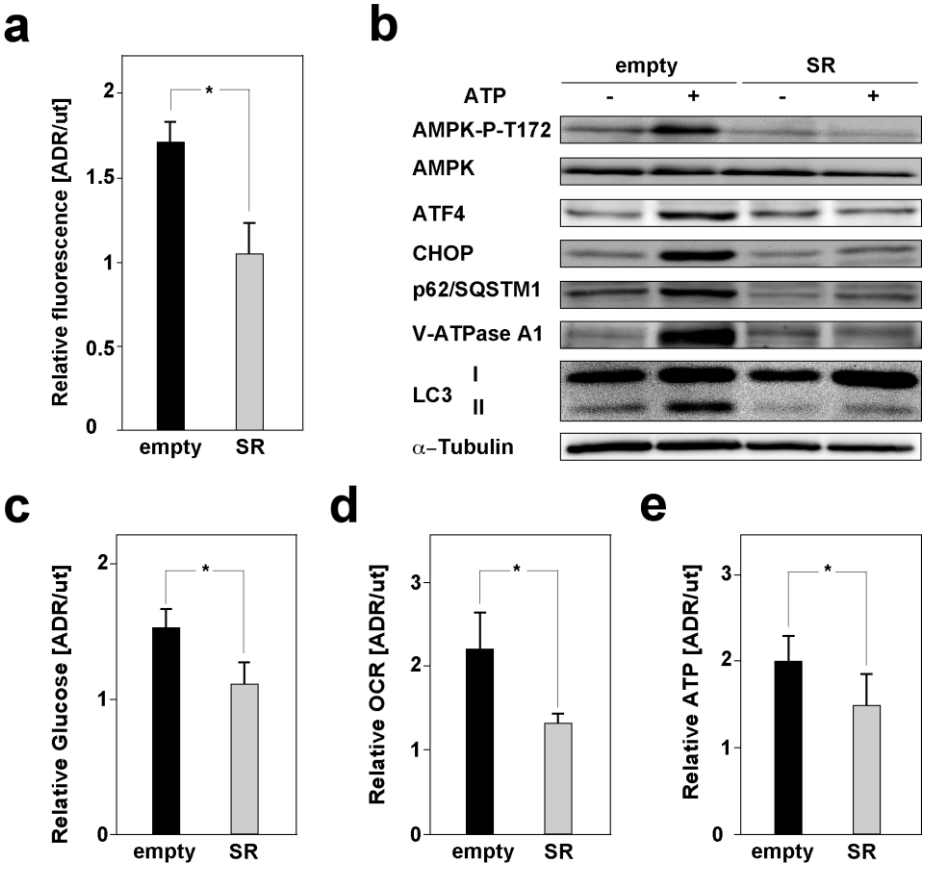

Figure 15. SASP-related proteotoxicity is mirrored by ER stress, enhanced autophagy and hypermetabolism. a, Rate of global protein synthesis as measured in Figure 14a in ADR-senescent relative to untreated control;*Bcl2* LC, which are either empty vector-infected or which stably express the NF-κB super-repressor IκBαΔN (SR). Results represent means ± s.d. (*n* = 5 each). **b**, Immunoblot analyses of phosphorylated AMPK (AMPK-P-T172), AMPK, ATF4, CHOP, p62/SQSTM1, V-ATPase A1 and MAP1-LC3-I/II in one representative empty vector-infected *vs.* SR-infected LC suggesting proteotoxicity-evoked ER stress mediating autophagosome formation as indicated by conversion of the MAP1-LC3 isoform I to II only in

TIS control;*Bcl2* LC, but not in TIS SR LC (α-Tubulin as a loading control). Gels were cropped to ease presentation. **c**, Relative intracellular glucose concentrations of LC as in a. **d**, Relative OCR of LC as in a. **e**, Relative intracellular ATP concentrations of LC as in a. Results represent means ± s.d. (n = 5 each). *P < 0.05. Figure adapted from Dörr et al..[103]

The connection between senescence and the energy-consuming autophagic degradation of proteotoxic waste was further substantiated in a model of oncogene-induced senescence in human diploid fibroblasts as shown in Figure 16.

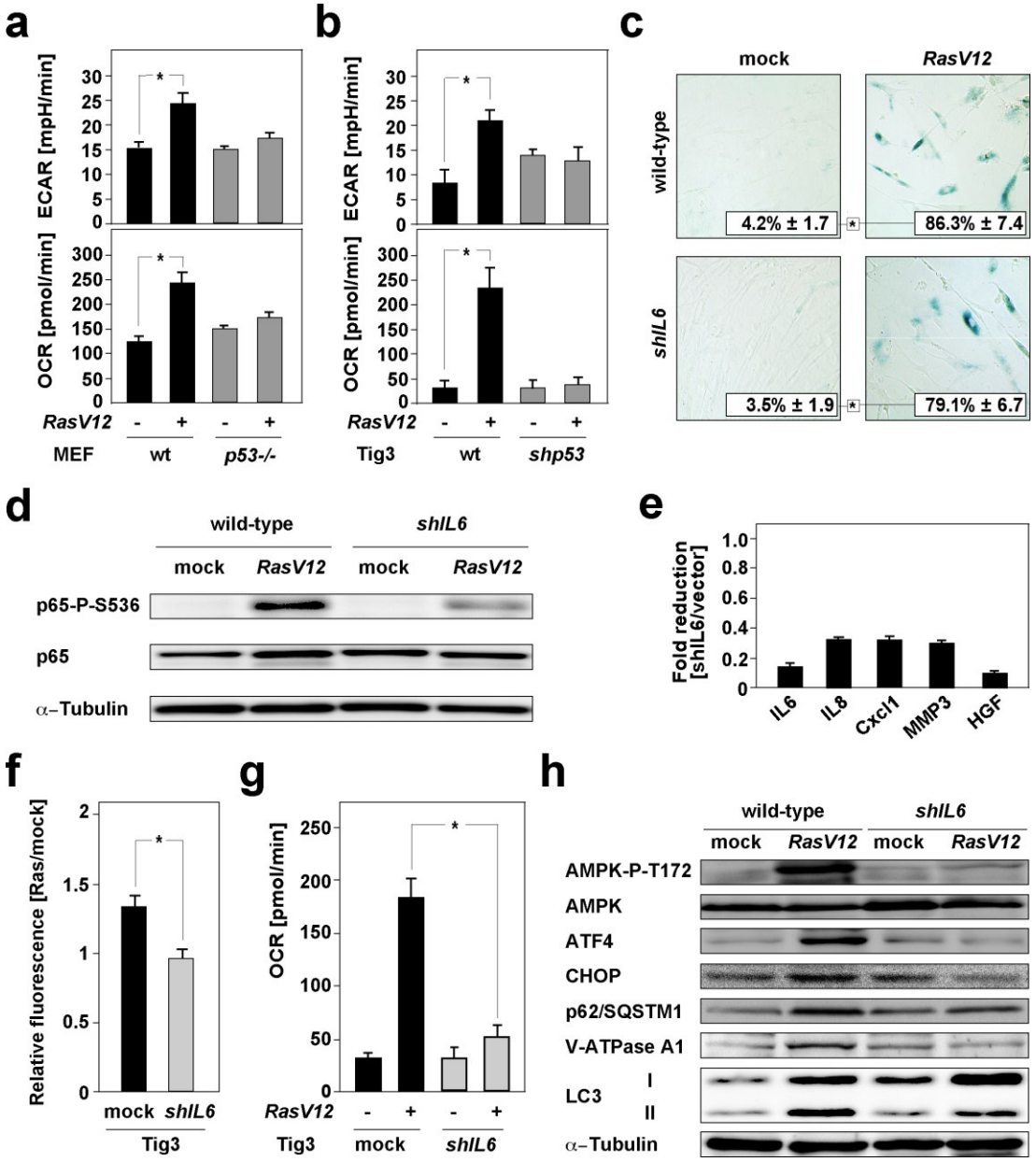

Figure 16. Glucose metabolism, proteotoxicity-related ER stress and autophagy in OIS. **a,** ECAR and OCR of stably *RasV12*-transduced senescence-proficient fibroblasts (wild-type MEFs) or senescence-incapable counterparts (*p53-/-* MEFs). Results represent means ± s.d. (n = 5 each). **b**, ECAR and OCR of stably *RasV12*-transduced senescence-proficient human

Tig3 fibroblasts or senescence-incapable counterparts (Tig3 stably transduced with a short hairpin RNA against *p53* [sh*p53*]). Experiments were conducted in triplicate, for which the results represent means ± s.d. **c**, SA-β-gal staining of *RasV12- vs.* mock-infected Tig3 cells stably transduced with a shRNA against *IL6* (*shIL6*) to block NF-κB-dependent SASP production or an empty vector as a control. Note that *RasV12*-expressing cells senesce despite efficient knockdown of IL6. Experiments were conducted in triplicate, for which the results represent means ± s.d.. **d**, Representative immunoblot analyses of phosphorylated p65 (p65-P-S536) and p65 in lysates from cells as in c (α-Tubulin as a loading control). Gels were cropped to ease presentation. Note that phosphorylation of p65 at residue S536 indicates enhanced activity of the classical NF-κB pathway and increases the transcriptional activity of p65.[264] **e**, Relative transcript levels (*shIL6- vs.* empty vector- transduced) of the indicated senescence-associated cytokines in RasV12-senescent cells (as in c) showing markedly reduced SASP expression in cells with reduced IL6 expression. Results represent means ± s.d. (*n* = 3 each). **f**, Relative protein synthesis rate of cells as in c. **g**, OCR of cells as in c. **h**, Representative immunoblot analyses of phosphorylated AMPK (AMPK-P-T172), AMPK, ATF4, CHOP, p62/SQSTM1, V-ATPase A1 and MAP1-LC3- I/II in cells as in c, mechanistically dissecting the previously reported ER stress in Ras-senescent fibroblasts[265] (α-Tubulin as a loading control). Gels were cropped to ease presentation. **P* < 0.05. Figure adapted from Dörr et al..[103]

Only wild-type, but not p53-deficient *RasV12- vs.* mock-infected mouse embryo fibroblasts (MEFs) and human Tig3 fibroblasts showed increased levels of glycolysis and oxygen consumption rates (Figure 16a, b). Furthermore, Tig3 cells were stably transduced with a shRNA against *IL6* (*shIL6*) or an empty vector as a control. While reportedly sh*IL6* may block OIS in p16INK4a-deficient Tig3 cells[153], senescence was not affected in RasV12-driven, sh*IL6*- vs. empty-infected p16INK4a-proficient Tig3 cells as measured by SA-β-gal activity (Figure 16c). However, NF-κB-activation and NF-κB dependent SASP production was markedly reduced in RasV12-senescent Tig3 expressing *shIL6* as shown on RNA and protein level (Figure 16d-f). As a result, much lower levels of proteotoxicity-related ER stress and autophagy as well as reduced oxygen consumption rates were observed in Ras-senescent sh*IL6*- (and hence SASP proteotoxicity-blunted) vs. empty-infected Tig3 cells despite full OIS capacity (Figure 16g, h).

The V-ATPase A1 acidifies the lysosome by pumping protons across the lysosomal membrane in an ATP-dependent fashion. The low lumenal pH of the lysosome stimulates the activity of a range of lysosomal proteases, which degrade nonselective and selective cargos delivered by autophagy.[266] Therefore, the enhanced activity of the V-ATPase as a means to boost autophagic degradation of proteins could present a

major energy sink in senescence. As demonstrated in Figure 17 the inhibition of the V-ATPase by Concanamycin A acutely increased ATP levels only in TIS control;*Bcl2* LC, but not in untreated control;*Bcl2* LC or *Suv39h1*$^{-}$*;Bcl2* LC irrespective of ADR treatment (Figure 17a).

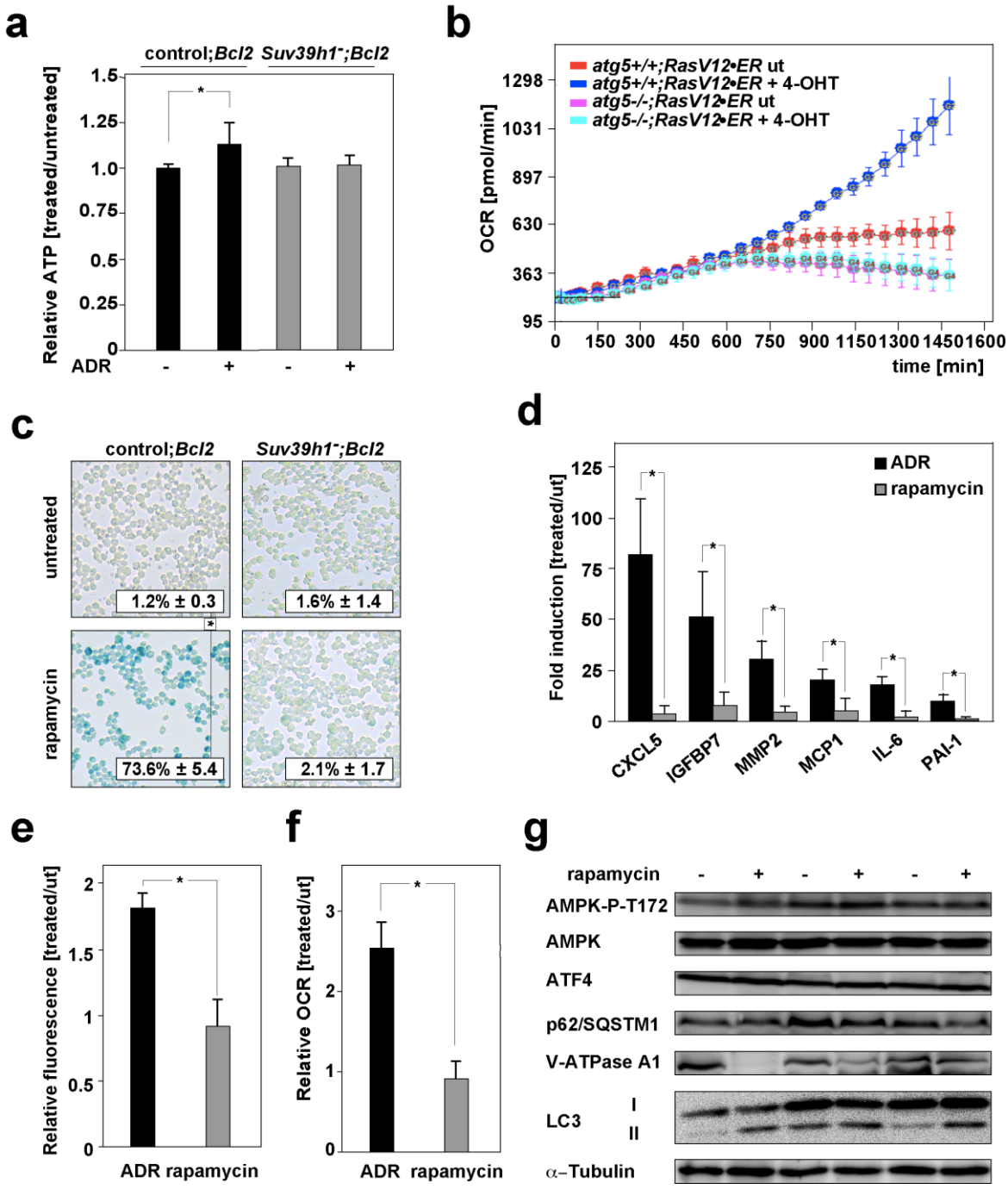

Figure 17. Proteotoxicity-related autophagy and its energetic demands. a, Relative change in ATP levels in ADR-pretreated or untreated control;*Bcl2* and *Suv39h1*$^{-}$*;Bcl2* LC after exposure to Concanamycin A for 10 minutes. Note that ATP levels rise only after inhibition of V-ATPase in TIS cells indicating the high senescence-associated ATP consumption by this enzymatic activity. Data represent means ± s.d. (*n* = 4, measurements were done in triplicate).

b, OCR of autophagy- competent (*atg5*$^{+/+}$) *vs.* autophagy-defective (*atg*$^{-/-}$) solvent-only *vs.* 4-OHT-induced *RasV12•ER*-infected MEFs. Note that only senescence-primed, autophagy-competent MEFs exhibit an OCR boost reflecting the energy-consuming induction of autophagy in OIS. Data represent means ± s.d. (*n* = 5 technical replicates). **c**, Exposure to the mTOR inhibitor and autophagy inducer rapamycin selectively evokes senescence in control;*Bcl2* LC but not in *Suv39h1*$^{-}$*;Bcl2* LC as indicated by SA-β-gal staining.[267,268] Results represent means ± s.d. (*n* = 5 each). **d**, RQ-PCR analysis (treated relative to untreated [ut]) of senescence-associated cytokines showing that ADR-evoked TIS, but not rapamycin-induced senescence of control;*Bcl2* LC presents with a SASP. Results represent means ± s.d. (*n* = 3 each). **e**, Relative changes of the protein synthesis rate in ADR- or rapamycin-treated *vs.* untreated LC. Results represent means ± s.d. (*n* = 3 each). **f**, Relative changes of the OCR in ADR- or rapamycin-treated *vs.* untreated LC. Results represent means ± s.d. (*n* = 3 each). **g**, Immunoblot analyses of p-AMPK (AMPK-P-T172), AMPK, ATF4, p62/SQSTM1, V-ATPase A1 and MAP1-LC3-I/II of untreated *vs.* rapamycin-senescent control;*Bcl2* LC, showing that SASP-blunted rapamycin-induced senescence is accompanied by direct elevation of autophagic activity that does not involve energy-demanding proteotoxicity-driven ER stress (*n* = 3; α-Tubulin as a loading control). Gels were cropped to ease presentation. **P* < 0.05. Figure adapted from Dörr et al..[103]

Also, the elevated OCR in RasV12-driven senescence strictly depends on the induction of autophagy since MEFs, which harbor a defect in autophagy due to genetic ablation of the autophagy related gene 5 (Atg5)[269] fail to exhibit an OCR boost in response to RasV12 activation (Figure 17b). Moreover, induction of senescence by the mammalian target of rapamycin (mTOR) inhibitor rapamycin[270], which is known to induce autophagy, displayed an attenuated SASP response (Figure 17c, d). Consequently, rapamycin-induced senesence did not show signs of proteotoxicity-driven endoplasmic reticulum stress and occurred with an unchanged OCR (Figure 17e-g).

TIS addiction to protein turnover and autophagic clearance

To examine whether senescent cells rely on the lysosomal degradation of proteins, untreated and TIS control;*Bcl2* LC were exposed to the V-ATPase inhibitors Bafilomycin A1 and Concanamycin A, which disturb the autolysosomal pH, or to a cocktail of lysosomal protease inhibitors, which disrupt autolysosomal digestion. As demonstrated in Figure 18 in all of these inhibitor settings death of TIS cells occurred at significantly higher rates compared to untreated control;*Bcl2* LC or *Suv39h1*$^{-}$*;Bcl2* LC irrespective of ADR treatment (Figure 18a). Similarly, lentiviral knockdown of p62/SQSTM1 which compromises the delivery of ubiquitinated proteins to the

lysosome[271], only sensitized TIS control;*Bcl2* LC to cell death, whereas untreated control;*Bcl2* LC and *Suv39h1*$^{-}$*;Bcl2* LC irrespective of treatment remained unaffected by diminished p62 function (Figure 18b, c).

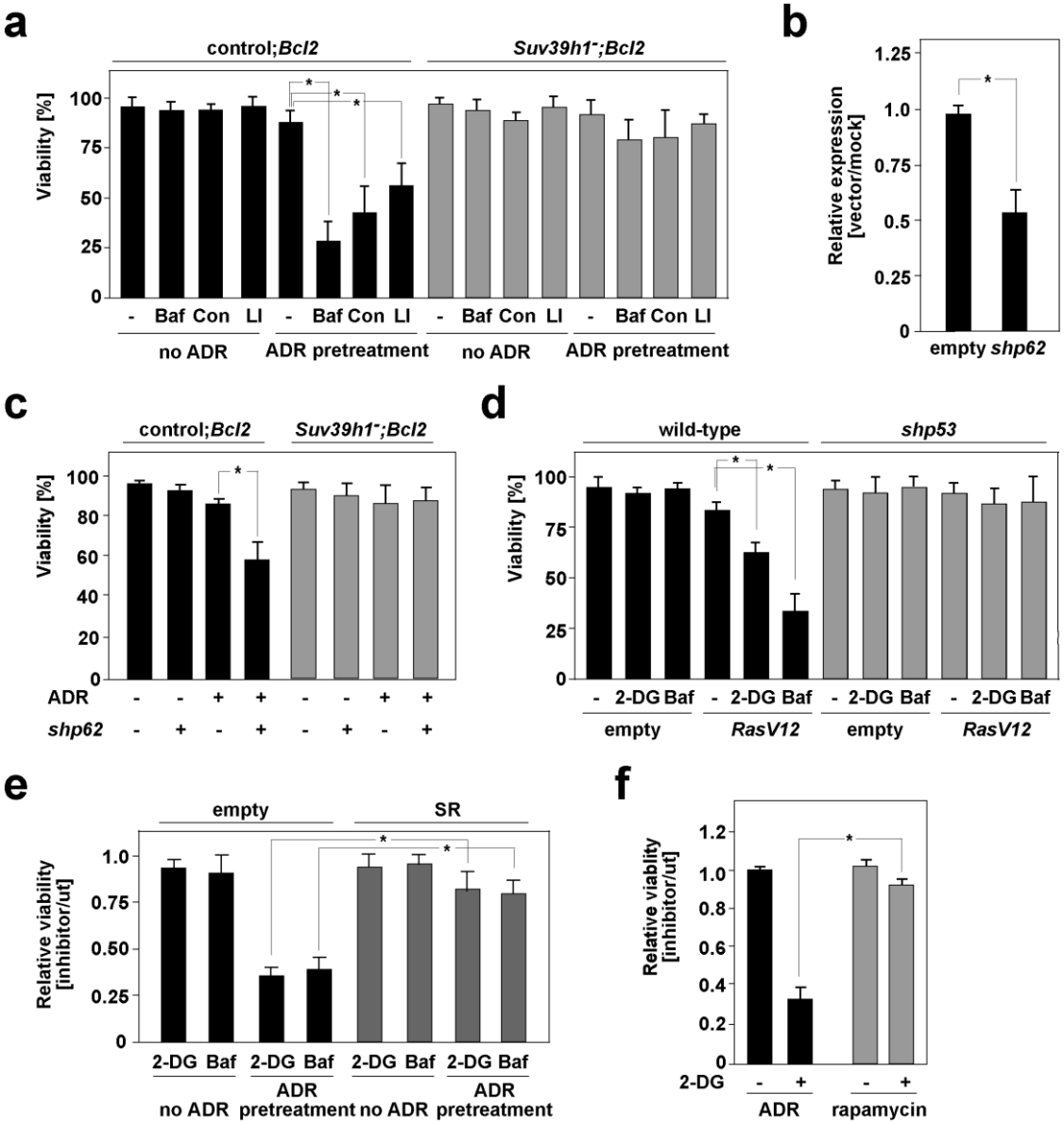

Figure 18. SASP-producing senescence requires autophagy for proteotoxic stress release. a, Cellular viability by trypan blue dye exclusion of LC as in Figure 12 after exposure to the V-ATPase inhibitors Bafilomycin A1 (Baf), Concanamycin A (Con) or a cocktail of lysosomal protease inhibitors (LI) at day 7 (*i.e.* 2 days after addition of inhibitors) *in vitro*. The respective inhibitors were added at day 5 after ADR or without any ADR pre-treatment. Results represent means ± s.d. (*n* = 5 each). **b**, Knockdown efficacy of lentiviral shRNA against *p62/SQSTM1* (sh*p62*) in LC by RQ-PCR analysis. Results represent means ± s.d. (*n* = 4 each). **c**, Cell viability by trypan blue dye exclusion after lentiviral knockdown of *p62/SQSTM1* in ADR-senescent control;*Bcl2 vs.* ADR-exposed *Suv39h1*$^{-}$*;Bcl2* LC at day 5 as compared to the untreated condition. Results represent means ± s.d. (*n* = 4 each). **d**, Cell viability by trypan blue dye exclusion of senescence-competent (wild-type) or senescence-compromised (*shp53*) Tig3 cells after Ras or mock infection followed by exposure to the

glycolysis inhibitor 2-DG or the autophagy inhibitor Bafilomycin A1 (Baf), demonstrating selective vulnerability of OIS cells. Experiments were conducted in triplicate, for which the results represent means ± s.d.. **e**, Cellular viability of SR- or empty-vector-infected control;*Bcl2* LC treated with ADR or untreated for five days, then exposed for two days to the inhibitors 2-DG or Bafilomycin A1, compared to no inhibitor (ut) *in vitro*. Results represent means ± s.d. (n = 5 each). **f**, Relative (ADR- or rapamycin-treated *vs.* untreated) changes in viability of control;*Bcl2* with or without subsequent exposure to 2-DG (2-DG/ut), demonstrating a strong reduction in viability only in ADR-senescent but not in rapamycin-senescent LC (relative to no rapamycin or no ADR, respectively) in response to the inhibition of glycolysis. Results represent means ± s.d. (n = 5 each). ***** indicates $P < 0.05$, except for a, in which $*P < 0.01$. Figure adapted from Dörr et al..[103]

Furthermore, the viability of RasV12-senescent Tig3 fibroblasts was more strongly reduced after incubation with 2-DG or the V-ATPase inhibitor Bafilomycin A1 than of *RasV12*-infected, senescence-compromised *shp53* Tig3 fibroblasts (Figure 18d). Similarly, the viability of senescent SR lymphomas, which lack signs of proteotoxicity, autophagy and enhanced energy production, was hardly affected by exposure to 2-DG or the V-ATPase inhibitor Bafilomycin A1 (Figure 18e). Finally, only SASP-inducing ADR-senescent LC, but not SASP ignorant rapamycin-senescent LC showed strong reduction in viability (relative to no rapamycin or no ADR, respectively) after exposure to 2-DG (Figure 18f).

This indicates that proper autolysosomal function is crucial for the survival of senescent cells, whereas non-senescent cells can tolerate defects in autolysosomal degradation at least temporarily. In conclusion, OIS and TIS cells engage in a broad secretory program that seems to overwhelm the cellular capacity for accurate protein biosynthesis, processing and secretion. This induces a strong proteotoxic stress response that triggers energy-consuming autophagy to maintain cellular integrity. Importantly, the increased energy demands of OIS and TIS cells and their boosted autophagic machinery are mechanistically linked at the level of V-ATPase function and lysosomal degradation and account for the vulnerability of OIS and TIS cells to either inhibitors of metabolism or autophagy.

As shown in Figure 19 inhibition of glycolysis by 2-DG or of V-ATPases by Bafilomycin A1 in SASP-producing TIS cells resulted in further accumulation of misfolded proteins.

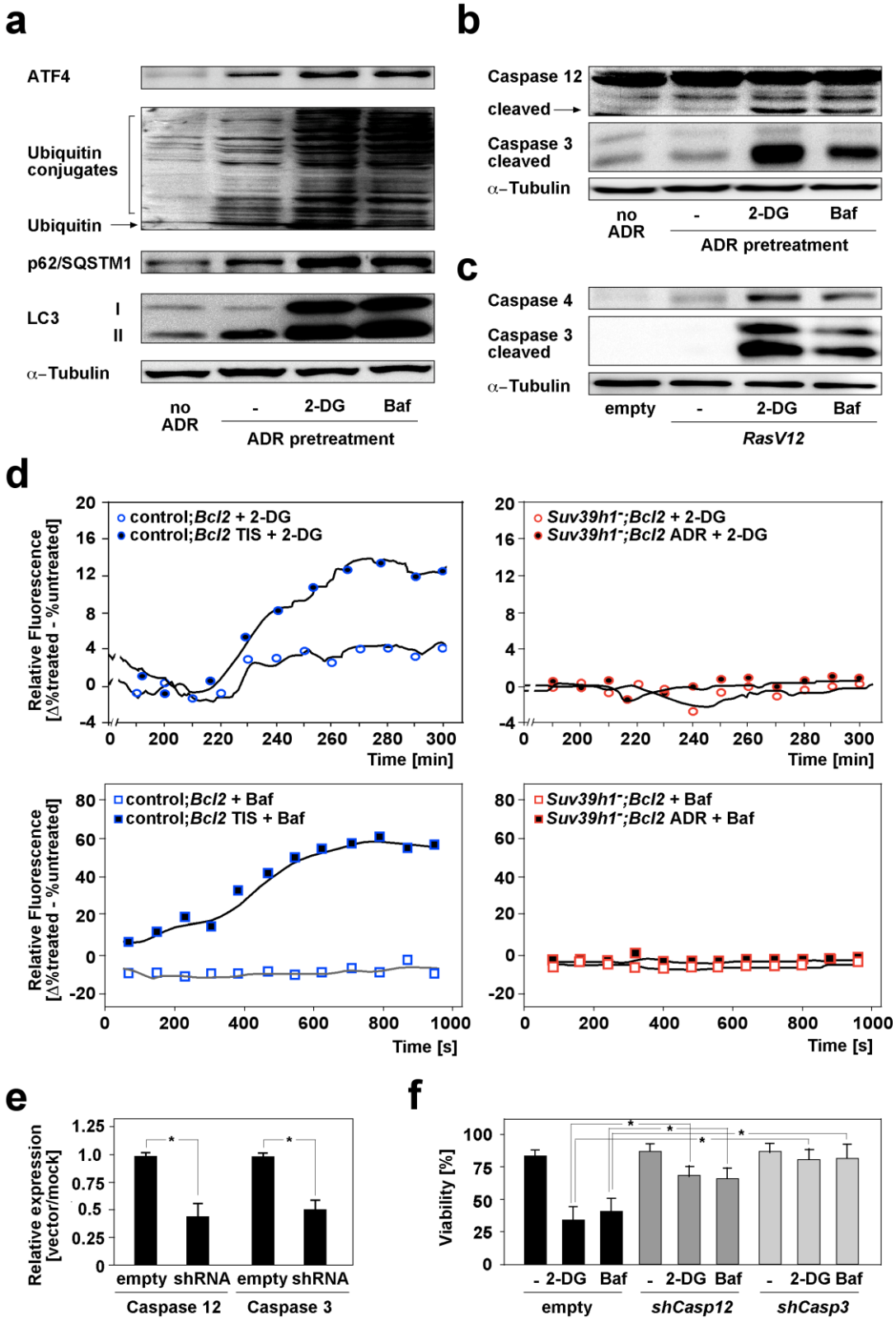

Figure 19. Mechanism of ER-mediated cell death. a, Immunoblot analyses of ATF4, global protein ubiquitination, p62/SQSTM1, and MAP1-LC3-I to MAP1-LC3-II conversion in control;*Bcl2* LC with no ADR treatment, in TIS LC, and in TIS LC after exposure to 2-deoxyglucose (2-DG) or Bafilomycin A1 (Baf) *in vitro*; representative blot with α-Tubulin as a loading control. Gels were cropped to ease presentation. **b**, Cleavage (activation) of caspase 12 and detection of cleaved caspase 3 by immunoblot analyses of control;*Bcl2* LC as in a;

representative blot with α-Tubulin as a loading control. Gels were cropped to ease presentation; full-length blots are provided in Supplementary Figure 2. **c**, Cleavage (*i.e.* activation) of Caspase 4 (human homolog of Caspase 12) and detection of cleaved Caspase 3 by immunoblot analyses in Tig3 cells that were either untreated, Ras-senescent (OIS) or Ras-senescent followed by exposure to 2-DG or Baf. Representative blot with α-tubulin as a loading control. Gels were cropped to ease presentation; full-length blots are provided in Supplementary Figure 2. **d**, Calcium efflux in TIS *vs.* untreated control;*Bcl2* and ADR-treated *vs.* untreated *Suv39h1*$^{-}$*;Bcl2* LC following incubation with 2-DG or Baf measured as calcium-dependent activation of the fluorescent indicator Fluo-4 AM. Data reflect differences between 2-DG- or Baf-treated and untreated samples at the given time-points. Representative measurements of five independent experiments each. **e**, Knockdown-efficacy of shRNA constructs against *caspase 12* and *caspase 3* in LC measured by RQ-PCR analysis. Results represent means ± s.d. (*n* = 3 each). **f**, Cellular viability of ADR-treated control;*Bcl2* LC infected with short-hairpin RNAs against either *caspase 12* (*shCasp12*) or caspase 3 (*shCasp3*) compared to ADR-treated, empty vector-infected control;*Bcl2* LC. Results represent means ± s.d. (n = 4 each). ***P* < 0.05. Figure adapted from Dörr et al..[103]

This is indicated by additional induction of the UPR marker ATF4 and even higher protein ubiquitination (Figure 19a). This presumably exceeds tolerable endoplasmic reticulum stress levels and triggers an endoplasmic reticulum death signal. Endoplasmic-reticulum-related cell death is characterized by Ca^{2+}-flux-dependent activating cleavage of caspase 12 (or its human homolog caspase 4).[272] This is followed by proteolytic processing of caspase 3, which among other caspases executes apoptosis by degradation of nuclear and cytoskeletal proteins and DNA fragmentation as shown for TIS cells and Ras-senescent Tig3 fibroblasts respectively after energy depletion by 2-DG or direct inhibition of autophagy by Bafilomycin A1 (Figure 19b, c).[273] The inibitor treatments were also sufficient to selectively trigger calcium efflux from the ER (Figure 19d) in TIS cells, which supports the model of a caspase-12-initiated and caspase-3-executed cell death. Furthermore, stable knockdown of either *caspase 12* or *caspase 3* by shRNA (*shCasp3* and *shCasp12* respectively) in TIS cells blocked apoptosis in response to treatment with either 2-DG or Bafilomycin A1 (Figure 19e, f).

TIS-specific vulnarabilities *in vivo*

To test whether such a liability may be therapeutically exploitable *in vivo*, CTX-senescent control;*Bcl2* lymphomas were exposed to either 2DG or Bafilomycin A1 *in vivo*. As demonstrated in Figure 20 this resulted – despite the protection from CTX-

induced cell death due to Bcl2 overexpression – in rapid apoptotic tumor regression as measured by color-coded whole-body fluorescence imaging to visualize green fluorescent protein (GFP)-tagged tumor burden and TdT-mediated dUTP nick end labelling (TUNEL) staining of lymph node sections *in situ* (Figure 20a). When control;*Bcl2* lymphoma-bearing mice were monitored for long-term outcome after CTX, they achieved a significantly extended overall survival when subsequently exposed to Bafilomycin A1 treatment (Figure 20b). Importantly, no Bafilomycin- A1-dependent improvement of the long-term outcome was detectable in cohorts of *Suv39h1*$^{-}$*;Bcl2* lymphoma-bearing mice treated with CTX and Bafilomycin A1 compared to mice treated with CTX only (Figure 20c).

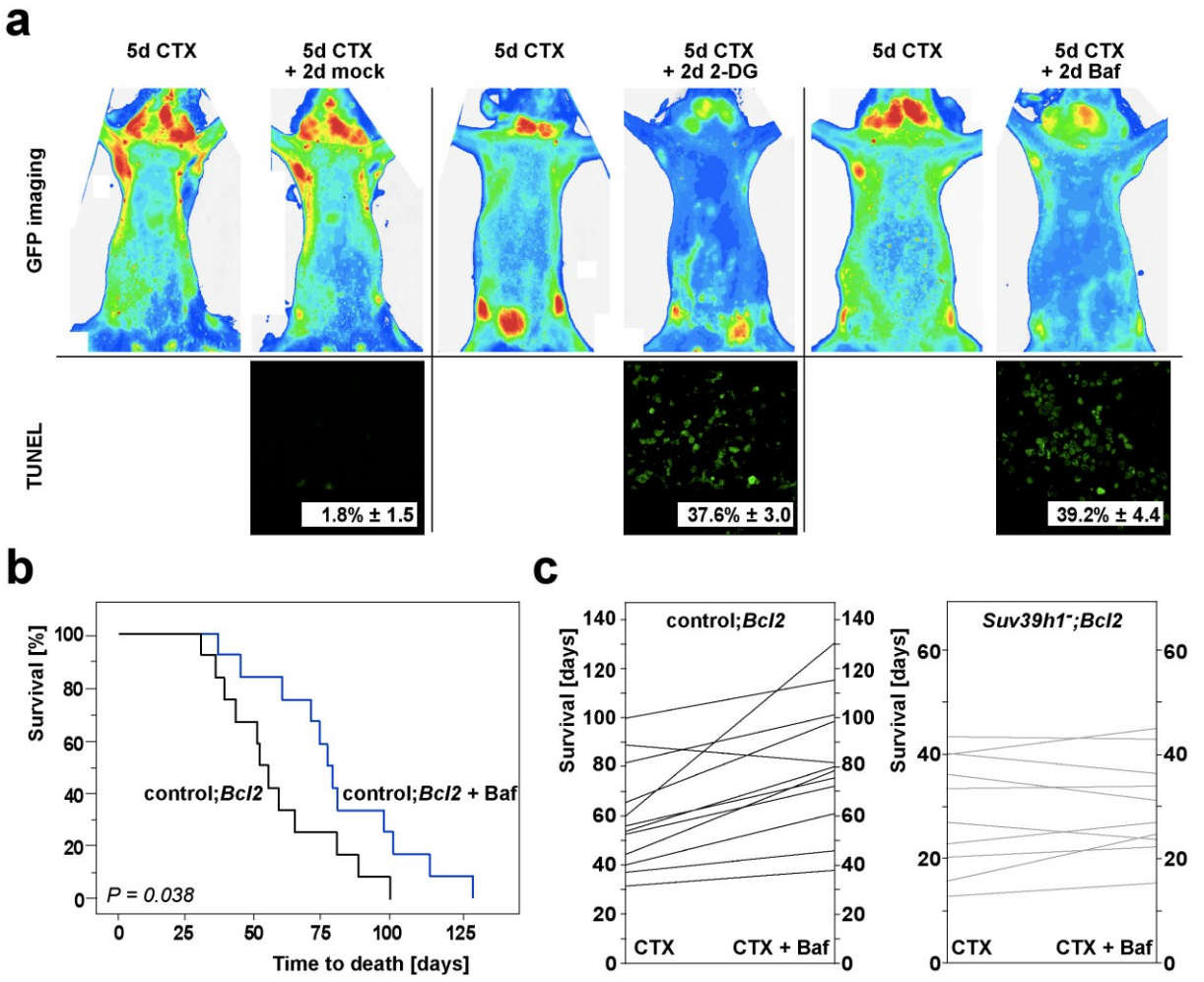

Figure 20. Synthetic lethal targeting of TIS *in vivo*. **a**, Color-coded whole-body fluorescence imaging to visualize green fluorescent protein (GFP)-tagged tumor burden in time-courses of three representative mice harbouring CTX-senescent control;*Bcl2* lymphomas at day 5 (see Figure 2a), and two days later, after the administration of 2-DG (n = 3 mice), Bafilomycin A1 (n = 5 mice) or mock treatment (n = 4 mice) starting from day five post CTX (red, highest intensities; blue, lowest intensities). TdT-mediated dUTP nick end labeling

(TUNEL) staining of lymph node sections *in situ* to visualize apoptosis at day 7. Numbers represent means ± s.d. (n = 3). **b**, Overall survival plotted in Kaplan-Meier format of control;*Bcl2* lymphoma-bearing mice randomly assigned to sequential exposure to Bafilomycin A1 (Baf) or mock five days after CTX treatment. **c**, Overall survival of CTX-treated control;*Bcl2* or *Suv39h1*$^{-}$*;Bcl2* lymphoma-bearing mice treated as in b (control;*Bcl2*: *n* = 12 and *Suv39h1*$^{-}$*;Bcl2*: *n* = 10), presented as matched pair analyses (*P* < 0.001 for the control;*Bcl2* comparison; *P* = 0.221 for the *Suv39h1*$^{-}$*;Bcl2* comparison). Figure adapted from Dörr et al..[103]

To confirm our findings across species and tumor entities, human primary acute myeloid leukemia (AML) samples and cancer cell lines from hematological and solid malignancies were screened for their ability to enter TIS and for their susceptibility for metabolic and autophagy inhibitors as shown in Figure 21.

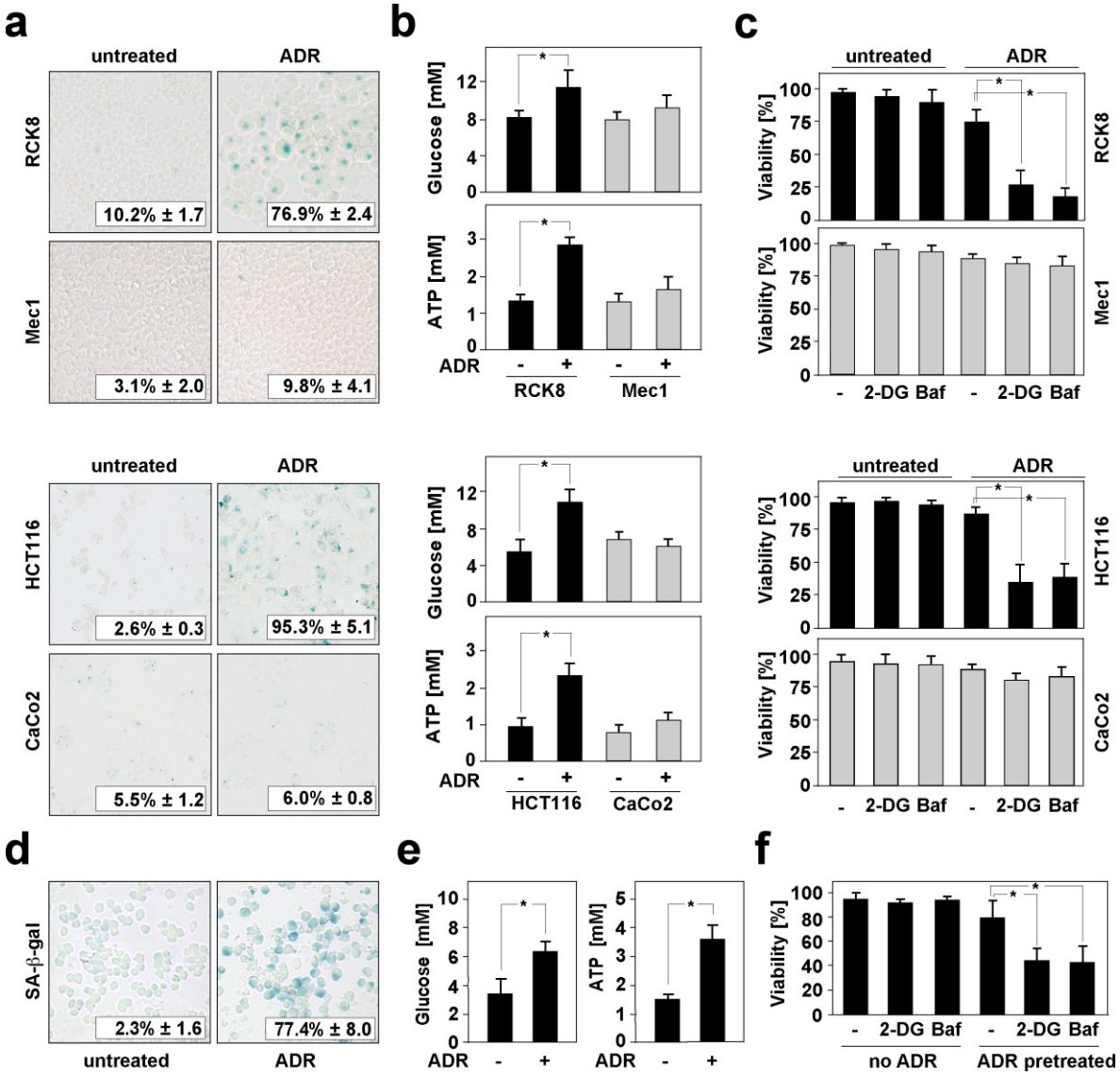

Figure 21. **Synthetic lethal targeting of TIS-related proteotoxicity and hypercatabolism in human cancers. a**, SA-β-gal staining of human B-cell lymphomas (RCK8, Mec1) and colon

carcinomas (HCT116, CaCo2) representing TIS-proficient (RCK8, HCT116) and TIS-resistent (Mec1, CaCo2) cell lines for each entity. **b**, Glucose and ATP levels of ADR-treated *vs.* untreated cells as in a. **c**, Cellular viability by trypan blue dye exclusion of ADR-treated *vs.* untreated cells as in a after exposure to the glycolysis inhibitor 2-DG or the autophagy inhibitor Bafilomycin A1 (Baf) at day 7 *in vitro*. The respective inhibitors were added at day 5 (colon cancer lines) or day 6 (lymphoma lines) after ADR or without any ADR pre-treatment. Note that only senescent cancer cell lines (RCK8 and HCT116) are susceptible to metabolic targeting. Experiments conducted in triplicate, for which the results represent means ± s.d.. **d**, TIS in primary human acute myeloid leukaemia (AML) samples by SA-β-gal staining of ADR treated *vs.* untreated cells *in vitro*. Data represent means ± s.d. (*n* = 5 each). **e**, Intracellular glucose (left) and ATP (right) concentrations in senescent AML cells as in d. **f**, Cellular viability of primary AML samples treated as in d and exposed to inhibitors as in c. Results represent means ± s.d. (*n* = 5 each). ***P* < 0.05. Figure adapted from Dörr et al..[103]

Indeed, only TIS-capable cell lines showed increased cellular glucose and ATP levels, which correlated with selective susceptibility to 2-DG and Bafilomycin A1 treatment (Figure 20a-c). Moreover, primary blast samples from patients diagnosed with acute myeloid leukaemia recapitulated the senescence-conferred hypermetabolic phenotype and the susceptibility to autophagy-blocking or energy-depleting therapies (Figure 20d-f). Hence, an energy-consuming endoplasmic reticulum stress-autophagy cascade confers a critical liability to senescent cancer cells across species and entities.

8. Discussion

TIS and metabolism

The work shows that therapy-induced senescence (TIS) essentially contributes to cancer therapy, and, in particular, that targeted elimination of senescent cells provides an important additional cancer treatment strategy. Since senescent cells rely on enhanced energy production from glucose and fatty acid degradation to manage increased protein synthesis, concomitant proteotoxicity and autophagic protein turnover, they become more sensitive to either inhibition of cellular metabolism, particularly glycolysis, or autophagy. This results in the accumulation of proteotoxic waste, intolerable ER-stress and subsequently caspase-mediated apoptosis. Consequently, pharmacological targeting of these programs following TIS provokes tumor regression and improves treatment outcome in a mouse lymphoma model.

The metabolic reprogramming observed in TIS lymphomas captures features of both enhanced aerobic glycolysis, in which despite oxygen supply glucose is converted into lactate and yields 2 ATP molecules, and mitochondrial respiration, which leads to the complete oxidation of glucose to carbon dioxide and 36 ATP molecules. Aerobic glycolysis was discovered by Otto Warburg, who noticed that even in oxygen-rich conditions cancer cells consume much larger quantities of glucose and produce more lactate than untransformed cells of the same tissue.[208,274] Today, this metabolic change is exploited by [18F]fluoro-deoxyglucose (FDG) positron emission tomography (PET) imaging of tumors, which, when fused with images from computer tomography (PET/CT), provides detailed anatomic and site-specific metabolic information.[275] Thus, FDG-PET imaging has shown to improve the diagnosis and subsequent treatment of many cancers, for example for most lung and gastrointestinal carcinomas, gynecologic cancers, as well as melanoma and most types of lymphoma.[276]

Importantly, positive FDG-PET imaging is widely viewed in the clinic as an indicator of proliferation and therefore tumor progression. However, the interpretation of FDG-PET results seems to depend on the time of the PET analysis.[277] While a persistent,

metabolically active tumor site may indeed reflect an uncontrolled and growing lesion towards the end or after completion of a multi-cycle induction therapy and therefore serves as a predictor for inferior outcome, positive FDG-PET scans obtained early after treatment initiation correlate poorly with treatment resistance.[278,279] For instance, the positive predictive value for tumor progression of a positive early interim FDG-PET (after two or three cycles of therapy) in DLBCL patients is much less robust or even not statistically significant when compared to the negative predictive value (*i.e.* not to encounter tumor progression in the future) of an FDG-negative early interim PET scan.[280,281] The data presented here reflect a scenario of an early PET analysis and unveil that TIS lymphomas exhibit a stronger FDG-PET signal than their untreated counterparts. Therefore, this result comes with three important remarks to current clinical interim FDG-PET interpretation. Firstly, positive FDG-PET scans obtained early during induction therapy may reflect senescent, not actively growing tumor lesions. Secondly, the fact that subsequent elimination of senescent tumor cells is beneficial for treatment outcome, indicates that early FDG avidity, although truly marking senescent cells, might, at least in some cases, account for a potentially detrimental course of the disease. Thirdly, early FDG-PET scans can serve as a tool to select patient cohorts for subsequent anti-senescence therapies, which kill tumor cells after senescence induction by conventional chemotherapy and therefore attenuate or even prevent cancer progression.

Moreover, TIS LC show enhanced glucose metabolism to pyruvate and lactate *in vitro* and *in vivo*. Therefore, it appears as if TIS reinforces the Warburg effect. Whereas Warburg proposed that cancer cells increase glycolysis to compensate for defects in mitochondrial respiration, large comparisons of different tumor entities in more recent years have revealed that while all tumor cells show enhanced rates of glycolysis, the TCA cycle or oxidative phosphorylation in the mitochondria are not generally impaired.[282] Furthermore, aerobic glycolysis has also been observed in almost all nontransformed cells during rapid proliferation, including unicellular organisms.[283] In fact, mitogen stimulation of normal human lymphocytes and mouse lymphocytes leads to enhanced proliferation and increased glucose uptake as well as lactate secretion.[284] Therefore, cancer cells adopt a metabolic phenotype that is shared with

rapidly dividing cells, which suggests that aerobic glycolysis facilitates cell proliferation despite inefficient energy production. A popular theory to accomodate this apparent conundrum claims that aerobic glycolysis supports the anabolic requirements of proliferating tumor cells by diverting glucose carbon from mitochondrial ATP production to the synthesis of biomolecules, i.e. the accumulation of biomass, prior to cell division. In fact, an essential feature of senescent cells is that they grow in size due to the expansion of various cellular organelles, which includes a bigger nucleus or even multiple nuclei, a vacuolated cytoplasma, as well as an enlarged Golgi apparatus and lysosomal compartment.[36,285] However, the kinetics of this phenotype and its functional implications are only partly understood. Commensurate with their enlarged morphology, both total RNA and total protein content are increased.[286] Furthermore, enhanced protein synthesis drives the production of secretory proteins to form the SASP.[198] Since RNA and protein production relies on generation of building blocks, i.e. amino acids and ribonucleotides, from glycolysis, it is conceivable that cells drastically increase glycolysis at least until the full senescent phenotype is established. Importantly, TIS LC present with stably elevated ECAR levels for extended periods of time, which indicates that senescent cells rely also on high glucose turnover to maintain the phenotype.

In addition, TIS LC show an increased flux of glucose into the TCA cycle, the upregulation of PKM1 to fuel the TCA cycle with pyruvate and enhanced AMPK signaling. These findings indicate that the increased glucose utilization of TIS cells also drives the TCA cycle and mitochondrial respiration for efficient energy production. Concomitantly, TIS LC display a constantly elevated OCR. Furthermore, TIS cells increase the breakdown of fatty acids, which is the main source for ATP in energy-demanding tissues such as muscle and heart, to fuel mitochondrial energy production.[287] Therefore, the metabolism of senescent tumor cells aberrantly utilizes both aerobic glycolysis (reminiscent of proliferating tumor cells) and mitochondrial respiration (typical for resting normal cells).

In fact, there is increasing evidence from other cancer entities which link cellular senescence to metabolic reprogramming. $BRAF^{V600E}$-senescent human diploid fibroblasts (HDF) accumulate glucose-derived TCA cycle metabolites and increase

oxidative phosphorylation.[219] In $HRAS^{G12V}$-senescent HDFs the retinoblastoma protein, which as explained in the introduction orchestrates the senescent cell cycle arrest by forming repressive heterochromatin marks around S-phase genes, also activates glycolysis and induces metabolic flux into the TCA cycle and oxidative phosphorylation.[288]

Enzymatically the bimodal activation of aerobic glycolysis and mitochondrial respiration is controlled by the pyruvate dehydrogenase (PDH), which shunts the pyruvate produced from glycolysis into the TCA cycle. Genetic or pharmacologic manipulation of enzymes that modulate PDH activity, such as the negative regulator pyruvate dehydrogenase kinase 1 (PDK1) or the positive regulator pyruvate dehydrogenase phosphatase 2 (PDP2), directly affect metabolic reprogramming and oncogene-induced senescence (OIS): Whereas overexpression of PDK1 impairs oxidative phosphorylation and promotes OIS escape, PDK1 depletion enhances PDH activity, favours oxidative phosphorylation and triggers senescence. Furthermore, overexpression of PDH is sufficient for senescence induction in nontransformed cells.[219] As presented TIS LC also show a decreased expression of PDK1. Furthermore, upregulation of PDK1 abrogates OIS and thereby promotes tumor progression in $BRAF^{V600E}$-$p53^{-/-}$ neonatal melanocytes, whereas xenografts of melanoma cells with PDK1 suppression in nude mice displayed limited growth compared to control melanoma cells.[219]

Interestingly, a similar upregulation of mitochondrial respiration and ATP production was found in a subpopulation of melanoma cells, which show high levels of the histone 3 K4 demethylase JARID1B/KDM5B.[258] Expression of JARID1B is upregulated in benign nevi, which undergo oncogene-induced senescence.[93] Upon the progression to melanoma JARID1B is downregulated in most cells despite a small fraction. These JARID1B high melanoma cells, which can be enriched by chemotherapy, are quiescent and have stem cell-like properties, such as increased colony formation capacity, acitvated Notch signaling and enhanced tumor initiating potential. Due to their increased self-renewal capacity, they are required for melanoma maintenance *in vitro and in vivo*.[289] Furthermore, metabolic treatment of melanoma cells, for example

with inhibitors of the electron transport chain, leads to depletion of JARID1B high cells from the melanoma population.[290] Therefore, quiescent melanoma cells exposed to chemotherapy and TIS lymphoma cells both rely on metabolic reprogramming towards high oxygen consumption and ATP production for their survival.

In addition to alterations in sugar metabolism, senescent cells also display changes in nucleotide and lipid metabolism. In $HRAS^{G12V}$-senescent HDF the levels of all four dNTPs are significantly decreased due to the repression of ribonucleotide reductase subunit M2 (RRM2), which is the rate-limiting protein in dNTP synthesis.[291] However, similar to metabolic reprogramming by modulation of PDH activity, manipulation of RRM2 directly impact on OIS induction and escape: Whereas downregulation of RRM2 and subsequent depletion of dNTPs triggers OIS, its overexpression or supplementation of exogenous nucleosides in OIS HDF overcomes the senescence growth arrest.[292] Furthermore, senescent cells alter their composition of phopholipids in the cell membrane and membranes of organelles.[293] Similar to TIS LC as demonstrated in this thesis, OIS HDF activate the breakdown of fatty acids in mitochondrial β-oxidation.[222] Concomitantly, OIS cells increase their oxygen consumption rate, which drops significantly after either genetic or pharmacological inhibition of β-oxidation. However, abrogation of enhanced fatty metabolism in OIS does not revert senescence, but selectively dampens the SASP.[222]

Whereas the different reports mostly highlight the increased energy demands of senescent tumor cells, the metabolic alterations and their impact on the senescent phenotype seem to vary between OIS and TIS and between different tumor and cell types. In particular, the increased energy production in TIS and OIS primarily protects LC, and $HRas^{G12V}$-infected HDF respectively, from proteotoxic stress and cell death and hence maintains the phenotype. Conversely, modulation of PDH and RRM2 activity in HDF and melanoma cells also plays a mechanistic role in senescence establishment, bypass and escape. Therefore, additional investigations are required to determine (1) whether the metabolic reprogramming – or at least parts of it – may be both cause and consequence of senescence, (2) how the different energetic pathways, i.e. nucleotide, sugar and fatty acid metabolism, are linked to establish and maintain

the senescent phenotype, (3) whether there are central nodes in senescence metabolism, for example pyruvate, and (4) how stimulation or inhibition of these nodes affects senescent cell fate.[294]

TIS and ER stress

Although many questions remain as to why senescent cells boost their ATP production, the presented data suggest that a significant amount of the energy is expended for the SASP – *i.e.* for its production and subsequent degradation of misfolded, potentially oxidized and thereby toxic peptides. Whereas the SASP transcriptome and its relevance in paracrine and autocrine signaling are well investigated, there is very little information about the SASP proteome and its processing from translation to secretion as a source for proteotoxic stress.[295] In TIS it appears that the production of secreted factors is tightly coordinated with other senescence-associated cellular programs, such as the enlargement of the ER and the lysosome as well as activation of autophagy to maintain senescence.[265]

The ER is involved in the processing of the majority of secreted proteins as well as plasma membrane proteins and proteins of cellular organelles and trafficking vesicles.[296] Since about one third of all gene products are destined for secretion and about one third of the secreted proteins are not assembled correctly, protein processing in the ER is pivotal for cellular integrity.[297,298] It includes protein folding, posttranslational modifications, the assembly of multimeric proteins as well as the addition of preformed carbohydrates. These steps are orchestrated and tightly regulated by different classes of enzymes, in particular chaperones, which retain the newly synthesised or misfolded proteins in the ER lumen and hence avoid their release to subsequent steps of the secretory pathway.[299] Alternatively, misfolded proteins are polyubiquitinated and directed towards degradation through the 26S proteasome in a process called ER-associated degradation (ERAD) or through autophagy.[300] If protein homeostasis is disrupted, for example by viral infections, toxic compounds, increase in nascent protein or nutrient deprivation, accumulation of misfolded proteins leads to the activation of the unfolded protein response (UPR). The

UPR attenuates protein synthesis and activates transcription factors that regulate genes encoding for chaperones as well as components of the ERAD system and autophagy to resolve ER stress. The UPR also induces remodeling and expansion of ER membranes, mainly through activation of the transcription factor XBP1, as has been documented for plasma cells prior to antibody secretion. Therefore, the UPR is a pro-survival response which aims at reducing the proteotoxic stress and restoring ER function.[301] Importantly, protein processing in the ER also contributes to metabolic expenditure: Enzymes directly require ATP for protein folding, modification and disassembly. Furthermore, they also need calcium ions and an optimal redox potential, which are both maintained by ATP consuming processes.

TIS LC induce protein synthesis as evidenced by globally enhanced methione incorporation into protein chains. Furthermore, gene expression analysis shows activation of protein maturation and processesing pathways as well as an enhanced UPR in TIS LC. Additionally, senescent cells contain elevated levels of oxidized ER proteins, including chaperones, which reduces their efficacy in protein processing and increases ER stress.[302] Therefore, TIS cells acutely elicit an UPR due to the accumulation of nascent un- or misfolded poplypeptide chains.

At a molecular level, the UPR is orchestrated through at least three ER transmembrane receptors: 1) the pancreatic ER kinase or PKR-like ER kinase (PERK), which activates ATF4, 2) the activating transcription factor-6 (ATF6), which induces XBP-1 transcription, and 3) the inositol-requiring enzyme 1 (IRE1, also known as ERN 1), which directly controls XBP1 splicing and hence its activation. Under low ER stress conditions, the receptors are held inactive in complex with an ER chaperone. Accumulation of unfolded proteins leads to complex disassembly and activation of the three ER stress receptors. When adaptation of cells through the UPR is unsuccessful due to prolonged or unresolved ER stress, this otherwise protective signaling switches to a pro-apoptotic response.[300] Whereas PERK and IRE1 have been implicated in ER-mediated cell death by prolonged activation of ATF4/CHOP and JNK respectively, there is litte evidence for a role of ATF6 in this process.[303]

There are now various examples of ER stress in OIS and TIS as well as replicative senescence in various different cell types, although not all UPR pathways are activated in parallel.[304,305,306] However, no direct connection seems to exist between the senescence trigger, the cell type and the engaged UPR pathway. Furthermore, a role for the UPR in senescence induction has been proposed in $HRAS^{G12V}$-driven melanocytes, in which the fraction of SA-β-gal-positive cells is diminished and the amount of cell death is increased upon genetic inactivation of the UPR machinery.[265] Additionally, compounds that increase ER stress, such as tunicamycin or bortezomib, as well as crosstalk between the UPR and the PI3K/AKT/mTOR pathway induce apoptosis.[307,308,309] Therefore, it appears as if hampering the UPR machinery by genetic, pharmaceutical or metabolic means leads to intolarable stress levels and ER-mediated execution of cell death rather than senescence bypass or escape.

TIS LC show marked signs of prolonged ER stress as evidenced by increased levels of ATF4 and CHOP as well as activation of JNK and XBP1. The UPR response can be augmented by either withdrawal of energy, i.e. inhibition of glycolysis by 2-DG, or blockade of stress release pathways, such as autophagy, by Bafilomycin A1. While mechanistic details on how prolonged ER stress is turned into ER-mediated cell death remain to be investigated, ATF4-driven activation of CHOP as well as IRE1-mediated activation of JNK execute caspase-mediated cell death by altering levels of BCL2-family members, which destabilises mitochondria, and by triggering cytoplasmic calcium signaling.[310,311,312] While Bcl2 protein levels are high in TIS-capable Eμ-myc lymphomas due to the stable retroviral transduction of this moiety and potentially interfere with UPR-mediated mitochondrial membrane permabilization, the results show that increased cytoplasmic calcium concentrations after treatment with 2-DG or Bafilomycin A1 trigger caspase-12- and caspase-3-dependent cell death in TIS.

TIS and protein degradation

Therefore, it appears as if TIS cells rely on autophagy to alleviate ER stress and to clear proteotoxic waste. Numerous reports have described the coexistence of senescence and autophagy in cells, for example in ageing fibroblasts and prematurely

senescent epithelial cells.[313,314] Nevertheless, the crosstalk between the two processes and their potenial interdependency remain poorly defined. In Ras-senescent IMR90 and BJ fibroblasts, autophagy contributes to the induction of OIS, since pharmacologic and genetic approaches that interfere with autophagy at least partially attenuate senescence.[196] However, in this system senescence is not reversed when autophagy is compromised. Similarly, TIS and autophagy in MCF-7 breast tumor cells and HCT-116 colon carcinoma cells appear to be regulated by overlapping signaling pathways and involve the activation of a DDR in response to elevated ROS levels. In this system suppression of autophagy by pharmacological or genetic approaches delays TIS induction, but does not abrogate it.[315] Therefore, a priori inhibition of autophagy delays senescence onset, but autophagy is not required for the establishment of the senescent phenotype. In both systems cell death in response to activation of the senescence trigger, i.e. $HRAS^{G12V}$ or chemotherapy, in the autophagy-compromised backgrounds was not monitored, but seems to play a subordinate role in comparison to senescence bypass. Importantly, however, genetic interference with autophagy before OIS induction also suppresses the establishment of the SASP at the protein level.[196] This would reduce the amount of proteotoxic waste below the threshold of intolerable ER-stress and subsequent execution of cell death. Furthermore, a priori inhibition of autophagy might stimulate the cells to upregulate alternative pathways for the disposal of misfolded proteins, such as their degradation in the proteasome or their secretion, which are not available at short hand if autophagy is acutely inhibited in full-fledged SASP-expressing senescence.

The presented data indicate that autophagolysosomal degradation of proteins in both OIS and TIS is tightly linked to SASP-mediated ER stress. Hence, dampening of the SASP by genetic interference with the NfκB super-repressor IκBαΔN or with a shRNA against IL-6 substantially reduces proteotoxicity. As a result, the UPR is strongly reduced and autophagy is only mildly activated. Although the UPR and autophagy co-occur in response to the SASP, the two processes can also be uncoupled in senescence. In fact, pro-senescent treatmenf of LC with rapamycin, which activates autophagy due to inhibition of mTOR, fails to elicit a SASP and a subsequent UPR. Therefore, only TIS LC, which display a SASP, experience elevelated levels of ER

stress and require autophagolysosomal protein degradation for self-maintenance.

This suggests that in senescent cells, which produce a SASP, autophagy acts as a salvage mechanism that counteracts excessive UPR signaling.[316] The UPR can directly activate autophagy since all three UPR signaling pathways control critical components of the autophagolysosomal machinery. In particular, upon PERK activation, for example in response to treatment with the glycosylation inhibitor tunicamycin, ATF4 and CHOP transcriptionally regulate the majority of *ATG* genes.[317] Furthermore, ATF4 and CHOP target genes, such as *REDD1* and *tribbles-related protein 3 (TRB3)*, inhibit the PI3K/AKT/mTOR pathway at different levels and hence induce autophagy.[318] Additionally, CHOP and ATF4 synergize in the nucleus to trigger expression of the autophagy receptor genes *p62*/*SQSTM1* and *NBR1.*

There are numerous examples that directly link autophagy to ER stress-inducing therapy. For instance, disruption of ER calcium homeostasis by hypericin-mediated photodynamic therapy leads to the aggregation and sequestration of ubiquitinated, unfolded proteins that are degraded by autophagy in a SQSTM1- and NBR1-dependent fashion.[319] Additionally, treatment of glioma cells with cyclosporine A induces ER stress, autophagy (in an IRE1- and PERK-dependent manner) and apoptosis, which increases with the degree of autophagy inhibition.[320] Hence, autophagy or the failure to elicit an UPR seem to protect tumor cells from cell death by ER stress-inducing cancer therapy and may represent a mechanism of treatment resistance. In melanoma cell lines, in which treatment with the BRAF inhibitor PLX4720 triggers a UPR and autophagy, interference with autophagy in addition to PLX4720 treatment sensitizes melanoma cells to cell death.[321] Similarly, induction of apoptosis following treatment with the BRAF inhibitor vemurafenib was associated with the ability of melanoma cells to induce ATF4.[322] However, it remains to be determined whether selective inhibition of the UPR machinery, for example CHOP or ATF4, in senescence critically interferes with the induction of autophagy and whether it activates cellular death programs.

Whereas TIS cells clearly depend on autophagic clearance of proteotoxic waste,

proteasomal protein degradation in Ras-V12-induced senescence has been shown to selectively degrade ERK-phosphorylated proteins.[323] Proteome analysis of this so-called senescence-associated proteasomal degradation (SAPD) showed enforced turnover of proteins linked to growth factor signaling, cell cycle control, cell migration and RNA metabolism.[323] This suggests that proteasomal degradation acts to maintain senescence by inhibiting transformation. Furthermore, the analysis lacked signs of enhanced proteasomal degradation of SASP constituents. Therefore, there seems to be a selective requirement for autophagy in response to SASP-associated proteotoxicity and the activation of a UPR. This is remarkable, because autophagy initally appeared as a back-up system for either insoluble protein aggregates or for excess proteotoxic waste when ubiquitin-mediated proteasomal degradation was overwhelmed.[324,325] However, while the impairment of the proteasome by pharmacological inhibitors leads to an increase in macroautophagy, the inhibition of macroautophagy does not induce proteasome activity.[326,327] In fact, there are now numerous reports that highlight a specific activation of autophagy in response to the UPR, such as in neuroblastoma cells.[328,329] Also, a gradual shift in the degradation pathway for polyubiquitinated proteins occurs from the proteasome pathway to autophagy during replicative senescence in HDFs.[330] Furthermore, autophagy acts as a nodal point in processing protein cargo destined for the extracellular space, because it specifically contributes to both the degradation and the secretion of extracellular proteins, and it is essential for the non-classical secretion of proteins, which do not contain a N-terminal signal peptide.[331] This includes the regulation of pro-inflammatory proteins, for example Il-6, Il-8 and Il1β, as well as hormones, such as the release of precursory forms of insulin from pancreatic β-cells.[198,332] Additionally, autophagy is the major proteolytic pathway following UPR activation in neuronal cells in Alzheimer's disease and defects in autophagy lead to the accumulation of toxic peptides such as amyloid beta in neurons.[333] Therefore, autophagy exerts specific tasks in the disposal of proteotoxic waste, particularly in cells with high secretory capacity.

This selectivity for autophagolysosomal protein degradation in response to an UPR is achieved by the cellular ubiquitination system and by adaptor proteins, such as p62, NBR1 and p97, which target ubiquitinated protein aggregates to either proteasomal or

autophagic degradation.[179] The macroautophagy cargo receptors p62 and NBR1 have a higher affinity for the monoubiquitinated proteins and K63 polyubiquitinated proteins, but can also bind to K48 polyubiquitin chains.[263] Hence, they can act as universal receptors for almost all types of ubiquitinated cargo. In this way, autophagy can maintain the degradation of proteotoxic waste when the proteasome is inhibited. Autophagy receptors often possess an LC3-interacting region, which allows them to deliver their cargo to the autophagolysosome. For instance, p62 links ubiquitinated proteins via its ubiquitin-associated domain to the autophagic protein LC3-II. Thereby, it is itself degraded by autophagy and not in the proteasome. As a consequence, inhibition of macroautophagy by genetic or pharmacological moieties results in the accumulation of p62. In this way it competes with other ubiquitin-binding proteins that deliver their cargo to the proteasome and thereby inhibits proteasomal degradation.[334] In TIS LC there is an accumulation of ubiquitinated proteins and an UPR-mediated upregulation of p62 and the lysosomal V-ATPase. Also, TIS cells display an elevated autophagic flux, since inhibition of autophagy by pharmacological inhibitors leads to a further increase in LC3-II and p62 levels. However, despite globally enhanced protein ubiquitination, the pattern of protein ubiquitination, the distribution of proteotoxic waste between autophagy and the proteasome as well as the role of proteasomal degradation in TIS remain to be determined.

In TIS and OIS cells autophagic turnover of proteotoxic waste requires energy. In Tig3 fibroblasts, Ras-induced senescence only triggers increased oxygen consumption rates in autophagy-competent cells. Also, in TIS LC ATP levels rise in response to an acute inhibition of the ATP consuming V-ATPase. Importantly, upon starvation V-ATPase deficient yeast cells accumulate autophagic bodies and display reduced protein degradation capacity.[335] Similarly, pharmacological inhibition of the V-ATPases or ATP depletion in TIS leads to accumulation of proteotoxic waste and cell death. Therefore, TIS selective cell death upon inhibition of energy production or of autophagy converges at the level of ATP consuming V-ATPases to maintain autolysosomal turnover of proteotoxic waste.

Therefore, the data presented in this thesis suggest that senescence-associated

metabolic reprogramming and autophagy are not merely required for senescence induction, but also for the maintenance of the senescent phenotype. Despite the fact that senescent cells remain growth-arrested and viable for long periods of time, senescence should therefore be viewed as a rather metastable cellular condition, which constantly requires re-inforcement, for example through feedback signals from SASP components, and protection from cell death, for example due to energy crisis or proteotoxicity. Importantly, this underlines the pivotal role of SASP production and turnover for senescence.

TIS and synthetic lethality

The described connection between the SASP, metabolic reprogramming and protein turnover by autophagy provides an opportunity for senescence-selective therapies. The elimination of senescent cells exploited in this work examplifies the principle of contextual synthetic lethality. Although treatment strategies based on classic synthetic lethal interactions provide an important amendment to targeted cancer therapy, they remain pathway-oriented treatment approaches and hence often suffer from the development of treatment resistance.[336] Furthermore, important oncogenes, for example Ras and c-Myc, are difficult to inhibit directly, but may be amenable to synthetic lethal interactions which derive from principles such as oncogene addiction.[232] Despite the enthusiasm for developing synthetic lethality based anticancer therapeutics, few synthetic lethal interactions have succeeded in clinical trials. A possible complication is that synthetic lethality is context dependent.[337] For instance, KRAS mutant lung and pancreatic cancer cell lines can be distinguished by their dependency on KRAS or downstream effector programs for survival. Only KRAS dependent cell lines were susceptible to the depletion of pharmacologically tractable epithelial-mesenchymal transformation (EMT) regulators such as Syk and Ron kinases whose inhibition induces apoptosis.[338]

Similarly, the requirement for high energy production and particularly protein turnover by autophagy are selectively enhanced in TIS cells compared to normal cells. Therefore, the pharmacological interference with these cellular programs provides an

opportunity to specifcally target cancer cells in a sequential treatment approach only following TIS by conventional chemotherapy as illustrated in Figure 22.

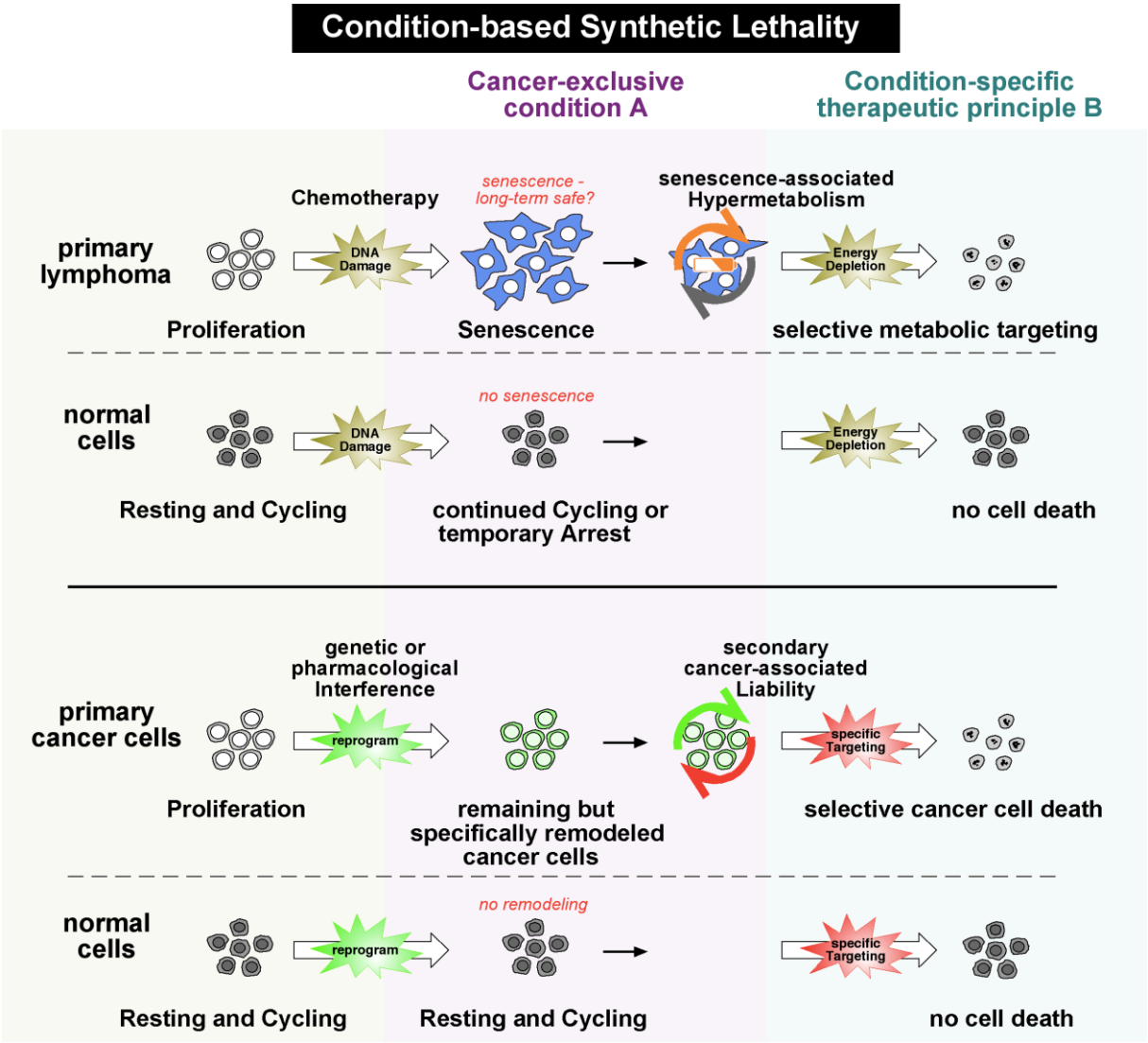

Figure 22. Metabolic targeting of TIS as an example of condition-based synthetic lethality. Schematic illustration of the presented findings and their relevance for cancer therapy. Figure adapted from Dörr et al..[103]

Importantly, TIS provides a therapeutic window for the inhibitors tested in this thesis as TIS cells prove to be particularly sensitive to the interference with energy production and protein turnover. In addition to the genetic heterogeneity of concomitantly activated oncogenes or inactivated tumor suppressor genes and the redundant activation of signaling pathways to maintain cancer cell survival, dynamic interactions between these liabilities, for example during cellular remodelling in response to

chemotherapy, severely complicate approaches that target a particular genetic lesion through synthetic lethality. Therefore, a better understanding of how the cellular context influences synthetic lethal interactions is required to improve target validation and ultimately the selection of the appropriate patient cohort for clinical trials which aim to exploit synthetic lethal treatment principles.

Furthermore, it remains to be tested under which conditions the elimination of senescent cells proves beneficial or detrimental for overall patient survival. This depends on both immediate and potentially late effects of senescence. Importantly, the SASP acutely alters the tumor microenvironment in ways that either promote tumor growth and invasion and therefore reduce survival, or induce spreading of senescence and senescence clearance by the immune system, which both prolong survival.

On the one hand, individual SASP factors from either senescent bystander cells, such as fibroblasts, or senescent tumor cells can induce tumor cell survival and treatment resistance, proliferation and angiogenesis.[339] Additionally, SASP factors alter the tissue architecture by degradation of the extracellular matrix and may thereby facilitate tumor cell migration and metastasis.[171] Lasting detrimental effects of senescence may also include their enhanced self-renewal capacity.[277] Although this seems to be limited to a small fraction of G2-arrested, polyploid cells, this mechanism could increase treatment resistance.[340,341]

On the other hand, SASP factors reinforce senescence in a cell autonomous and autocrine fashion and induce paracrine senescence in proliferating tumor cells.[28,153,156] In this way TIS may elicit a continuous spreading of senescence and hence enforce a permanent tumor growth control. Furthermore, the SASP attracts both the innate and adaptive immune system, particularly macrophages and CD4 T cells, which act in concert to eliminate senescent tumor cells.[342] Additionally, senescent cells promote T cell activation by cellular interactions via costimulatory surface molecules. Upon stimulation by senescent cells the immune system may also be targeted to pre-cancerous lesions or proliferating tumor cells in the vicinity and thereby create a long-lasting anti-tumor immune response.

Therefore, it is likely that the effect of senescence on overall survival will depend on on the propensity of different tumor entities and treatment regimes to favour rather beneficial or detrimental senescence-effector programs. For instance, corticosteroids, which are used as standard components at different stages in the treatment of acute lymphoblastic leukaemia and aggressive lymphomas, suppress the expression of several SASP factors and hence are likely to influence SASP-mediated effects on the tumor microenvironment.[343,344] Similarly, the frequent adiministration of non-steroidal anti-inflammatory drugs, such as ibuprofen, will modulate SASP composition. However, both NSAR and corticosteroids also suppress the immune system and might interfere with the clearance of senescent cells. Of note, the additional inhibition of immune checkpoints might be required to fully launch an anti-senescence immune response following TIS induction. Therefore, the described effects need to be carefully assessed before it will be possible to routinely implement treatment strategies which selectively eliminate or maintain senescent cells or which modulate a defined subset of senescence-effector programs. Nevertheless, the thesis demonstrates that senescence-inducing and senescence-modulating therapies present powerful tools to improve cancer therapy.

9. References

1. Chandler, H. & Peters, G. Stressing the cell cycle in senescence and aging. *Curr. Opin. Cell Biol.* **25,** 765–771 (2013).
2. Baker, D. J. *et al.* Clearance of p16Ink4a-positive senescent cells delays ageing-associated disorders. *Nature* **479,** 232–236 (2011).
3. Young, A. R. J. & Narita, M. SASP reflects senescence. *EMBO Rep.* **10,** 228–230 (2009).
4. Campisi, J. Aging, cellular senescence, and cancer. *Annu. Rev. Physiol.* **75,** 685–705 (2013).
5. Muñoz-Espín, D. & Serrano, M. Cellular senescence: from physiology to pathology. *Nat. Rev. Mol. Cell Biol.* **15,** 482–496 (2014).
6. Baumann, K. Cellular senescence: Senescence and reprogramming go hand-in-hand. *Nat. Rev. Mol. Cell Biol.* **18,** 4 (2016).
7. Banito, A. & Lowe, S. W. A new development in senescence. *Cell* **155,** 977–978 (2013).
8. Muñoz-Espín, D. *et al.* Programmed cell senescence during mammalian embryonic development. *Cell* **155,** 1104–1118 (2013).
9. Storer, M. *et al.* Senescence is a developmental mechanism that contributes to embryonic growth and patterning. *Cell* **155,** 1119–1130 (2013).
10. Balogh, J. *et al.* Hepatocellular carcinoma: a review. *J. Hepatocell. Carcinoma* **3,** 41–53 (2016).
11. Lujambio, A. *et al.* Non-cell-autonomous tumor suppression by p53. *Cell* **153,** 449–460 (2013).
12. Childs, B. G., Durik, M., Baker, D. J. & van Deursen, J. M. Cellular senescence in aging and age-related disease: from mechanisms to therapy. *Nat. Med.* **21,** 1424–1435 (2015).
13. Minamino, T. *et al.* A crucial role for adipose tissue p53 in the regulation of insulin resistance. *Nat. Med.* **15,** 1082–1087 (2009).
14. Tavana, O. & Zhu, C. Too many breaks (brakes): pancreatic β-cell senescence leads to diabetes. *Cell Cycle Georget. Tex* **10,** 2471–2484 (2011).
15. Baker, D. J. *et al.* Opposing roles for p16Ink4a and p19Arf in senescence and ageing caused by BubR1 insufficiency. *Nat. Cell Biol.* **10,** 825–836 (2008).
16. Baker, D. J. *et al.* BubR1 insufficiency causes early onset of aging-associated phenotypes and infertility in mice. *Nat. Genet.* **36,** 744–749 (2004).
17. Pérez-Mancera, P. A., Young, A. R. J. & Narita, M. Inside and out: the activities of senescence in cancer. *Nat. Rev. Cancer* **14,** 547–558 (2014).
18. Schmitt, C. A. Senescence, apoptosis and therapy--cutting the lifelines of cancer. *Nat. Rev. Cancer* **3,** 286–295 (2003).
19. Nardella, C., Clohessy, J. G., Alimonti, A. & Pandolfi, P. P. Pro-senescence therapy for cancer treatment. *Nat. Rev. Cancer* **11,** 503–511 (2011).
20. Serrano, M., Lin, A. W., McCurrach, M. E., Beach, D. & Lowe, S. W. Oncogenic ras provokes premature cell senescence associated with accumulation of p53 and p16INK4a. *Cell* **88,** 593–602 (1997).
21. Bansal, R. & Nikiforov, M. A. Pathways of oncogene-induced senescence in human melanocytic cells. *Cell Cycle* **9,** 2782–2788 (2010).
22. Collado, M. & Serrano, M. Senescence in tumours: evidence from mice and

humans. *Nat. Rev. Cancer* **10,** 51–57 (2010).
23. te Poele, R. H., Okorokov, A. L., Jardine, L., Cummings, J. & Joel, S. P. DNA damage is able to induce senescence in tumor cells in vitro and in vivo. *Cancer Res.* **62,** 1876–1883 (2002).
24. Xue, W. *et al.* Senescence and tumour clearance is triggered by p53 restoration in murine liver carcinomas. *Nature* **445,** 656–660 (2007).
25. Childs, B. G., Baker, D. J., Kirkland, J. L., Campisi, J. & van Deursen, J. M. Senescence and apoptosis: dueling or complementary cell fates? *EMBO Rep.* **15,** 1139–1153 (2014).
26. Schmitt, C. A. Cellular senescence and cancer treatment. *Biochim. Biophys. Acta* **1775,** 5–20 (2007).
27. Brown, J. M. & Wilson, G. Apoptosis genes and resistance to cancer therapy: what does the experimental and clinical data tell us? *Cancer Biol. Ther.* **2,** 477–490 (2003).
28. Acosta, J. C. *et al.* A complex secretory program orchestrated by the inflammasome controls paracrine senescence. *Nat. Cell Biol.* **15,** 978–990 (2013).
29. Tasdemir, N. *et al.* BRD4 Connects Enhancer Remodeling to Senescence Immune Surveillance. *Cancer Discov.* **6,** 612–629 (2016).
30. Coppé, J.-P. *et al.* Senescence-Associated Secretory Phenotypes Reveal Cell-Nonautonomous Functions of Oncogenic RAS and the p53 Tumor Suppressor. *PLoS Biol.* **6,** (2008).
31. Beauséjour, C. M. *et al.* Reversal of human cellular senescence: roles of the p53 and p16 pathways. *EMBO J.* **22,** 4212–4222 (2003).
32. Wang, E. Senescent human fibroblasts resist programmed cell death, and failure to suppress bcl2 is involved. *Cancer Res.* **55,** 2284–2292 (1995).
33. Yeo, E. J., Hwang, Y. C., Kang, C. M., Choy, H. E. & Park, S. C. Reduction of UV-induced cell death in the human senescent fibroblasts. *Mol. Cells* **10,** 415–422 (2000).
34. Zhu, Y. *et al.* Identification of a novel senolytic agent, navitoclax, targeting the Bcl-2 family of anti-apoptotic factors. *Aging Cell* **15,** 428–435 (2016).
35. Acosta, J. C. & Gil, J. Senescence: a new weapon for cancer therapy. *Trends Cell Biol.* **22,** 211–219 (2012).
36. Hayflick, L. THE LIMITED IN VITRO LIFETIME OF HUMAN DIPLOID CELL STRAINS. *Exp. Cell Res.* **37,** 614–636 (1965).
37. van Deursen, J. M. The role of senescent cells in ageing. *Nature* **509,** 439–446 (2014).
38. d'Adda di Fagagna, F. *et al.* A DNA damage checkpoint response in telomere-initiated senescence. *Nature* **426,** 194–198 (2003).
39. Herbig, U., Jobling, W. A., Chen, B. P. C., Chen, D. J. & Sedivy, J. M. Telomere shortening triggers senescence of human cells through a pathway involving ATM, p53, and p21(CIP1), but not p16(INK4a). *Mol. Cell* **14,** 501–513 (2004).
40. Bodnar, A. G. *et al.* Extension of life-span by introduction of telomerase into normal human cells. *Science* **279,** 349–352 (1998).
41. Lanigan, F., Geraghty, J. G. & Bracken, A. P. Transcriptional regulation of cellular senescence. *Oncogene* **30,** 2901–2911 (2011).
42. Kim, W. Y. & Sharpless, N. E. The regulation of INK4/ARF in cancer and aging. *Cell* **127,** 265–275 (2006).

43. Narita, M. *et al.* Rb-mediated heterochromatin formation and silencing of E2F target genes during cellular senescence. *Cell* **113,** 703–716 (2003).
44. Ait-Si-Ali, S. *et al.* A Suv39h-dependent mechanism for silencing S-phase genes in differentiating but not in cycling cells. *EMBO J.* **23,** 605–615 (2004).
45. Wei, W., Hemmer, R. M. & Sedivy, J. M. Role of p14(ARF) in replicative and induced senescence of human fibroblasts. *Mol. Cell. Biol.* **21,** 6748–6757 (2001).
46. Abraham, R. T. Cell cycle checkpoint signaling through the ATM and ATR kinases. *Genes Dev.* **15,** 2177–2196 (2001).
47. Staller, P. *et al.* Repression of p15INK4b expression by Myc through association with Miz-1. *Nat. Cell Biol.* **3,** 392–399 (2001).
48. Passos, J. F. *et al.* Feedback between p21 and reactive oxygen production is necessary for cell senescence. *Mol. Syst. Biol.* **6,** 347 (2010).
49. Collado, M. *et al.* Inhibition of the phosphoinositide 3-kinase pathway induces a senescence-like arrest mediated by p27Kip1. *J. Biol. Chem.* **275,** 21960–21968 (2000).
50. Zhang, R., Chen, W. & Adams, P. D. Molecular dissection of formation of senescence-associated heterochromatin foci. *Mol. Cell. Biol.* **27,** 2343–2358 (2007).
51. Wei, S., Wei, S. & Sedivy, J. M. Expression of catalytically active telomerase does not prevent premature senescence caused by overexpression of oncogenic Ha-Ras in normal human fibroblasts. *Cancer Res.* **59,** 1539–1543 (1999).
52. Sarkisian, C. J. *et al.* Dose-dependent oncogene-induced senescence in vivo and its evasion during mammary tumorigenesis. *Nat. Cell Biol.* **9,** 493–505 (2007).
53. Harper, J. W. & Elledge, S. J. The DNA damage response: ten years after. *Mol. Cell* **28,** 739–745 (2007).
54. d'Adda di Fagagna, F. Living on a break: cellular senescence as a DNA-damage response. *Nat. Rev. Cancer* **8,** 512–522 (2008).
55. Evan, G. I. & d'Adda di Fagagna, F. Cellular senescence: hot or what? *Curr. Opin. Genet. Dev.* **19,** 25–31 (2009).
56. Jackson, J. G. & Pereira-Smith, O. M. Primary and compensatory roles for RB family members at cell cycle gene promoters that are deacetylated and downregulated in doxorubicin-induced senescence of breast cancer cells. *Mol. Cell. Biol.* **26,** 2501–2510 (2006).
57. Chicas, A. *et al.* Dissecting the unique role of the retinoblastoma tumor suppressor during cellular senescence. *Cancer Cell* **17,** 376–387 (2010).
58. Sage, J., Miller, A. L., Pérez-Mancera, P. A., Wysocki, J. M. & Jacks, T. Acute mutation of retinoblastoma gene function is sufficient for cell cycle re-entry. *Nature* **424,** 223–228 (2003).
59. Reimann, M. *et al.* Tumor stroma-derived TGF-beta limits myc-driven lymphomagenesis via Suv39h1-dependent senescence. *Cancer Cell* **17,** 262–272 (2010).
60. Trost, T. M. *et al.* Premature senescence is a primary fail-safe mechanism of ERBB2-driven tumorigenesis in breast carcinoma cells. *Cancer Res.* **65,** 840–849 (2005).
61. Michaloglou, C. *et al.* BRAFE600-associated senescence-like cell cycle arrest

of human naevi. *Nature* **436,** 720–724 (2005).
62. Majumder, P. K. *et al.* A prostatic intraepithelial neoplasia-dependent p27kip1 checkpoint induces senescence, inhibits cell proliferation and cancer progression. *Cancer Cell* **14,** 146–155 (2008).
63. Chen, Z. *et al.* Crucial role of p53-dependent cellular senescence in suppression of Pten-deficient tumorigenesis. *Nature* **436,** 725–730 (2005).
64. Courtois-Cox, S. *et al.* A negative feedback signaling network underlies oncogene-induced senescence. *Cancer Cell* **10,** 459–472 (2006).
65. Gewirtz, D. A., Holt, S. E. & Elmore, L. W. Accelerated senescence: an emerging role in tumor cell response to chemotherapy and radiation. *Biochem. Pharmacol.* **76,** 947–957 (2008).
66. Schmitt, C. A. *et al.* A senescence program controlled by p53 and p16INK4a contributes to the outcome of cancer therapy. *Cell* **109,** 335–346 (2002).
67. Chandrasekaran, A., Idelchik, M. D. P. S. & Melendez, J. A. Redox control of senescence and age-related disease. *Redox Biol.* **11,** 91–102 (2016).
68. Fumagalli, M. *et al.* Telomeric DNA damage is irreparable and causes persistent DNA-damage-response activation. *Nat. Cell Biol.* **14,** 355–365 (2012).
69. Cheng, Q. & Chen, J. Mechanism of p53 stabilization by ATM after DNA damage. *Cell Cycle Georget. Tex* **9,** 472–478 (2010).
70. Zannini, L., Delia, D. & Buscemi, G. CHK2 kinase in the DNA damage response and beyond. *J. Mol. Cell Biol.* **6,** 442–457 (2014).
71. Aird, K. M. *et al.* ATM couples replication stress and metabolic reprogramming during cellular senescence. *Cell Rep.* **11,** 893–901 (2015).
72. Niida, H. *et al.* Cooperative functions of Chk1 and Chk2 reduce tumour susceptibility in vivo. *EMBO J.* **29,** 3558–3570 (2010).
73. Chang, B. D. *et al.* A senescence-like phenotype distinguishes tumor cells that undergo terminal proliferation arrest after exposure to anticancer agents. *Cancer Res.* **59,** 3761–3767 (1999).
74. Zhang, Y. *et al.* DNMT3a plays a role in switches between doxorubicin-induced senescence and apoptosis of colorectal cancer cells. *Int. J. Cancer* **128,** 551–561 (2011).
75. Elmore, L. W. *et al.* Adriamycin-induced senescence in breast tumor cells involves functional p53 and telomere dysfunction. *J. Biol. Chem.* **277,** 35509–35515 (2002).
76. Su, D. *et al.* BMP4-Smad signaling pathway mediates adriamycin-induced premature senescence in lung cancer cells. *J. Biol. Chem.* **284,** 12153–12164 (2009).
77. Varna, M. *et al.* p53 dependent cell-cycle arrest triggered by chemotherapy in xenografted breast tumors. *Int. J. Cancer* **124,** 991–997 (2009).
78. Knappskog, S. *et al.* Concomitant inactivation of the p53- and pRB- functional pathways predicts resistance to DNA damaging drugs in breast cancer in vivo. *Mol. Oncol.* **9,** 1553–1564 (2015).
79. Roberson, R. S., Kussick, S. J., Vallieres, E., Chen, S.-Y. J. & Wu, D. Y. Escape from therapy-induced accelerated cellular senescence in p53-null lung cancer cells and in human lung cancers. *Cancer Res.* **65,** 2795–2803 (2005).
80. Haugstetter, A. M. *et al.* Cellular senescence predicts treatment outcome in metastasised colorectal cancer. *Br. J. Cancer* **103,** 505–509 (2010).
81. Schwarze, S. R., Fu, V. X., Desotelle, J. A., Kenowski, M. L. & Jarrard, D. F.

The identification of senescence-specific genes during the induction of senescence in prostate cancer cells. *Neoplasia N. Y. N* **7,** 816–823 (2005).
82. Ota, H. *et al.* Sirt1 inhibitor, Sirtinol, induces senescence-like growth arrest with attenuated Ras-MAPK signaling in human cancer cells. *Oncogene* **25,** 176–185 (2006).
83. Anders, L. *et al.* A systematic screen for CDK4/6 substrates links FOXM1 phosphorylation to senescence suppression in cancer cells. *Cancer Cell* **20,** 620–634 (2011).
84. Däbritz, J. H. M. *et al.* CD20-Targeting Immunotherapy Promotes Cellular Senescence in B-Cell Lymphoma. *Mol. Cancer Ther.* **15,** 1074–1081 (2016).
85. Bonet, C. *et al.* Aurora B is regulated by the mitogen-activated protein kinase/extracellular signal-regulated kinase (MAPK/ERK) signaling pathway and is a valuable potential target in melanoma cells. *J. Biol. Chem.* **287,** 29887–29898 (2012).
86. Farnebo, M., Bykov, V. J. N. & Wiman, K. G. The p53 tumor suppressor: a master regulator of diverse cellular processes and therapeutic target in cancer. *Biochem. Biophys. Res. Commun.* **396,** 85–89 (2010).
87. Wu, C.-H. *et al.* Cellular senescence is an important mechanism of tumor regression upon c-Myc inactivation. *Proc. Natl. Acad. Sci. U. S. A.* **104,** 13028–13033 (2007).
88. Soucek, L. *et al.* Inhibition of Myc family proteins eradicates KRas-driven lung cancer in mice. *Genes Dev.* **27,** 504–513 (2013).
89. Zuber, J. *et al.* RNAi screen identifies Brd4 as a therapeutic target in acute myeloid leukaemia. *Nature* **478,** 524–528 (2011).
90. Delmore, J. E. *et al.* BET bromodomain inhibition as a therapeutic strategy to target c-Myc. *Cell* **146,** 904–917 (2011).
91. Dawson, M. A. *et al.* Inhibition of BET recruitment to chromatin as an effective treatment for MLL-fusion leukaemia. *Nature* **478,** 529–533 (2011).
92. Collado, M. *et al.* Tumour biology: senescence in premalignant tumours. *Nature* **436,** 642 (2005).
93. Dhomen, N. *et al.* Oncogenic Braf induces melanocyte senescence and melanoma in mice. *Cancer Cell* **15,** 294–303 (2009).
94. Vredeveld, L. C. W. *et al.* Abrogation of BRAFV600E-induced senescence by PI3K pathway activation contributes to melanomagenesis. *Genes Dev.* **26,** 1055–1069 (2012).
95. Chen, X. *et al.* Endogenous expression of Hras(G12V) induces developmental defects and neoplasms with copy number imbalances of the oncogene. *Proc. Natl. Acad. Sci. U. S. A.* **106,** 7979–7984 (2009).
96. Mo, L. *et al.* Hyperactivation of Ha-ras oncogene, but not Ink4a/Arf deficiency, triggers bladder tumorigenesis. *J. Clin. Invest.* **117,** 314–325 (2007).
97. Braig, M. *et al.* Oncogene-induced senescence as an initial barrier in lymphoma development. *Nature* **436,** 660–665 (2005).
98. Hartmann, E. M., Ott, G. & Rosenwald, A. Molecular biology and genetics of lymphomas. *Hematol. Oncol. Clin. North Am.* **22,** 807–823, vii (2008).
99. Shaffer, A. L., Young, R. M. & Staudt, L. M. Pathogenesis of human B cell lymphomas. *Annu. Rev. Immunol.* **30,** 565–610 (2012).
100. Schuetz, J. M. *et al.* BCL2 mutations in diffuse large B-cell lymphoma. *Leukemia* **26,** 1383–1390 (2012).

101. Lim, K.-H., Yang, Y. & Staudt, L. M. Pathogenetic Importance and Therapeutic Implications of NF-κB in Lymphoid Malignancies. *Immunol. Rev.* **246,** 359–378 (2012).
102. Maxwell, S. A. & Mousavi-Fard, S. Non-Hodgkin's B-cell lymphoma: advances in molecular strategies targeting drug resistance. *Exp. Biol. Med. Maywood NJ* **238,** 971–990 (2013).
103. Dörr, J. R. *et al.* Synthetic lethal metabolic targeting of cellular senescence in cancer therapy. *Nature* **501,** 421–425 (2013).
104. Schmitt, C. A., McCurrach, M. E., de Stanchina, E., Wallace-Brodeur, R. R. & Lowe, S. W. INK4a/ARF mutations accelerate lymphomagenesis and promote chemoresistance by disabling p53. *Genes Dev.* **13,** 2670–2677 (1999).
105. Corcoran, L. M., Cory, S. & Adams, J. M. Transposition of the immunoglobulin heavy chain enhancer to the myc oncogene in a murine plasmacytoma. *Cell* **40,** 71–79 (1985).
106. Adams, J. M. *et al.* The c-myc oncogene driven by immunoglobulin enhancers induces lymphoid malignancy in transgenic mice. *Nature* **318,** 533–538 (1985).
107. Schmitt, C. A. *et al.* Dissecting p53 tumor suppressor functions in vivo. *Cancer Cell* **1,** 289–298 (2002).
108. Gorgun, G. *et al.* E(mu)-TCL1 mice represent a model for immunotherapeutic reversal of chronic lymphocytic leukemia-induced T-cell dysfunction. *Proc. Natl. Acad. Sci. U. S. A.* **106,** 6250–6255 (2009).
109. Vaux, D. L., Cory, S. & Adams, J. M. Bcl-2 gene promotes haemopoietic cell survival and cooperates with c-myc to immortalize pre-B cells. *Nature* **335,** 440–442 (1988).
110. van Lohuizen, M. *et al.* Identification of cooperating oncogenes in E mu-myc transgenic mice by provirus tagging. *Cell* **65,** 737–752 (1991).
111. Haupt, Y., Alexander, W. S., Barri, G., Klinken, S. P. & Adams, J. M. Novel zinc finger gene implicated as myc collaborator by retrovirally accelerated lymphomagenesis in E mu-myc transgenic mice. *Cell* **65,** 753–763 (1991).
112. Kelly, P. N., Dakic, A., Adams, J. M., Nutt, S. L. & Strasser, A. Tumor growth need not be driven by rare cancer stem cells. *Science* **317,** 337 (2007).
113. Luger, K., Mäder, A. W., Richmond, R. K., Sargent, D. F. & Richmond, T. J. Crystal structure of the nucleosome core particle at 2.8 A resolution. *Nature* **389,** 251–260 (1997).
114. Kouzarides, T. Chromatin modifications and their function. *Cell* **128,** 693–705 (2007).
115. Bannister, A. J. & Kouzarides, T. Regulation of chromatin by histone modifications. *Cell Res.* **21,** 381–395 (2011).
116. Jenuwein, T. & Allis, C. D. Translating the histone code. *Science* **293,** 1074–1080 (2001).
117. Wilson, V. L. & Jones, P. A. DNA methylation decreases in aging but not in immortal cells. *Science* **220,** 1055–1057 (1983).
118. Santos-Rosa, H. *et al.* Active genes are tri-methylated at K4 of histone H3. *Nature* **419,** 407–411 (2002).
119. Ruthenburg, A. J., Allis, C. D. & Wysocka, J. Methylation of lysine 4 on histone H3: intricacy of writing and reading a single epigenetic mark. *Mol. Cell* **25,** 15–30 (2007).
120. Karachentsev, D., Sarma, K., Reinberg, D. & Steward, R. PR-Set7-dependent

methylation of histone H4 Lys 20 functions in repression of gene expression and is essential for mitosis. *Genes Dev.* **19,** 431–435 (2005).
121. Chicas, A. *et al.* H3K4 demethylation by Jarid1a and Jarid1b contributes to retinoblastoma-mediated gene silencing during cellular senescence. *Proc. Natl. Acad. Sci. U. S. A.* **109,** 8971–8976 (2012).
122. Bhaskara, S. *et al.* Hdac3 is essential for the maintenance of chromatin structure and genome stability. *Cancer Cell* **18,** 436–447 (2010).
123. Rea, S. *et al.* Regulation of chromatin structure by site-specific histone H3 methyltransferases. *Nature* **406,** 593–599 (2000).
124. Li, F. *et al.* Lid2 is required for coordinating H3K4 and H3K9 methylation of heterochromatin and euchromatin. *Cell* **135,** 272–283 (2008).
125. Hublitz, P., Albert, M. & Peters, A. H. F. M. Mechanisms of transcriptional repression by histone lysine methylation. *Int. J. Dev. Biol.* **53,** 335–354 (2009).
126. Greer, E. L. & Shi, Y. Histone methylation: a dynamic mark in health, disease and inheritance. *Nat. Rev. Genet.* **13,** 343–357 (2012).
127. Dou, Y. *et al.* Regulation of MLL1 H3K4 methyltransferase activity by its core components. *Nat. Struct. Mol. Biol.* **13,** 713–719 (2006).
128. Schotta, G. *et al.* A chromatin-wide transition to H4K20 monomethylation impairs genome integrity and programmed DNA rearrangements in the mouse. *Genes Dev.* **22,** 2048–2061 (2008).
129. Pasini, D., Bracken, A. P., Jensen, M. R., Lazzerini Denchi, E. & Helin, K. Suz12 is essential for mouse development and for EZH2 histone methyltransferase activity. *EMBO J.* **23,** 4061–4071 (2004).
130. Ivanova, A. V., Bonaduce, M. J., Ivanov, S. V. & Klar, A. J. The chromo and SET domains of the Clr4 protein are essential for silencing in fission yeast. *Nat. Genet.* **19,** 192–195 (1998).
131. Wustmann, G., Szidonya, J., Taubert, H. & Reuter, G. The genetics of position-effect variegation modifying loci in Drosophila melanogaster. *Mol. Gen. Genet. MGG* **217,** 520–527 (1989).
132. Firestein, R., Cui, X., Huie, P. & Cleary, M. L. Set domain-dependent regulation of transcriptional silencing and growth control by SUV39H1, a mammalian ortholog of Drosophila Su(var)3-9. *Mol. Cell. Biol.* **20,** 4900–4909 (2000).
133. Peters, A. H. *et al.* Loss of the Suv39h histone methyltransferases impairs mammalian heterochromatin and genome stability. *Cell* **107,** 323–337 (2001).
134. Braig, M. & Schmitt, C. A. Oncogene-induced senescence: putting the brakes on tumor development. *Cancer Res.* **66,** 2881–2884 (2006).
135. Petti, E. *et al.* Altered telomere homeostasis and resistance to skin carcinogenesis in Suv39h1 transgenic mice. *Cell Cycle Georget. Tex* **14,** 1438–1446 (2015).
136. Steele-Perkins, G. *et al.* Tumor formation and inactivation of RIZ1, an Rb-binding member of a nuclear protein-methyltransferase superfamily. *Genes Dev.* **15,** 2250–2262 (2001).
137. Wee, S. *et al.* Targeting epigenetic regulators for cancer therapy. *Ann. N. Y. Acad. Sci.* **1309,** 30–36 (2014).
138. Nielsen, S. J. *et al.* Rb targets histone H3 methylation and HP1 to promoters. *Nature* **412,** 561–565 (2001).
139. DiMauro, T. & David, G. Chromatin modifications: The driving force of senescence and aging? *Aging* **1,** 182–190 (2009).

140. Ye, X. *et al.* Definition of pRB- and p53-dependent and -independent steps in HIRA/ASF1a-mediated formation of senescence-associated heterochromatin foci. *Mol. Cell. Biol.* **27,** 2452–2465 (2007).
141. Sdek, P. *et al.* Rb and p130 control cell cycle gene silencing to maintain the postmitotic phenotype in cardiac myocytes. *J. Cell Biol.* **194,** 407–423 (2011).
142. Chandra, T. & Narita, M. High-order chromatin structure and the epigenome in SAHFs. *Nucleus* **4,** 23–28 (2013).
143. Zhang, R., Chen, W. & Adams, P. D. Molecular dissection of formation of senescence-associated heterochromatin foci. *Mol. Cell. Biol.* **27,** 2343–2358 (2007).
144. Funayama, R., Saito, M., Tanobe, H. & Ishikawa, F. Loss of linker histone H1 in cellular senescence. *J. Cell Biol.* **175,** 869–880 (2006).
145. Narita, M. *et al.* A novel role for high-mobility group a proteins in cellular senescence and heterochromatin formation. *Cell* **126,** 503–514 (2006).
146. Chandra, T. *et al.* Independence of Repressive Histone Marks and Chromatin Compaction during Senescent Heterochromatic Layer Formation. *Mol. Cell* **47,** 203–214 (2012).
147. Kosar, M. *et al.* Senescence-associated heterochromatin foci are dispensable for cellular senescence, occur in a cell type- and insult-dependent manner and follow expression of p16(ink4a). *Cell Cycle Georget. Tex* **10,** 457–468 (2011).
148. Aird, K. M. & Zhang, R. Detection of senescence-associated heterochromatin foci (SAHF). *Methods Mol. Biol. Clifton NJ* **965,** 185–196 (2013).
149. Kennedy, A. L. *et al.* Senescent mouse cells fail to overtly regulate the HIRA histone chaperone and do not form robust Senescence Associated Heterochromatin Foci. *Cell Div.* **5,** 16 (2010).
150. Chen, Q. M. Replicative senescence and oxidant-induced premature senescence. Beyond the control of cell cycle checkpoints. *Ann. N. Y. Acad. Sci.* **908,** 111–125 (2000).
151. Salama, R., Sadaie, M., Hoare, M. & Narita, M. Cellular senescence and its effector programs. *Genes Dev.* **28,** 99–114 (2014).
152. Dimri, G. P. *et al.* A biomarker that identifies senescent human cells in culture and in aging skin in vivo. *Proc. Natl. Acad. Sci. U. S. A.* **92,** 9363–9367 (1995).
153. Kuilman, T. *et al.* Oncogene-induced senescence relayed by an interleukin-dependent inflammatory network. *Cell* **133,** 1019–1031 (2008).
154. Purcell, M., Kruger, A. & Tainsky, M. A. Gene expression profiling of replicative and induced senescence. *Cell Cycle Georget. Tex* **13,** 3927–3937 (2014).
155. Mason, D. X., Jackson, T. J. & Lin, A. W. Molecular signature of oncogenic ras-induced senescence. *Oncogene* **23,** 9238–9246 (2004).
156. Kuilman, T. & Peeper, D. S. Senescence-messaging secretome: SMS-ing cellular stress. *Nat. Rev. Cancer* **9,** 81–94 (2009).
157. Fumagalli, M. & d'Adda di Fagagna, F. SASPense and DDRama in cancer and ageing. *Nat. Cell Biol.* **11,** 921–923 (2009).
158. Coppé, J.-P. *et al.* Tumor suppressor and aging biomarker p16(INK4a) induces cellular senescence without the associated inflammatory secretory phenotype. *J. Biol. Chem.* **286,** 36396–36403 (2011).
159. Freund, A., Patil, C. K. & Campisi, J. p38MAPK is a novel DNA damage response-independent regulator of the senescence-associated secretory phenotype. *EMBO J.* **30,** 1536–1548 (2011).

160. Rodier, F. *et al.* Persistent DNA damage signalling triggers senescence-associated inflammatory cytokine secretion. *Nat. Cell Biol.* **11,** 973–979 (2009).
161. Hayden, M. S. & Ghosh, S. Signaling to NF-kappaB. *Genes Dev.* **18,** 2195–2224 (2004).
162. Panwalkar, A., Verstovsek, S. & Giles, F. Nuclear factor-kappaB modulation as a therapeutic approach in hematologic malignancies. *Cancer* **100,** 1578–1589 (2004).
163. Rothwarf, D. M., Zandi, E., Natoli, G. & Karin, M. IKK-gamma is an essential regulatory subunit of the IkappaB kinase complex. *Nature* **395,** 297–300 (1998).
164. Krappmann, D., Wulczyn, F. G. & Scheidereit, C. Different mechanisms control signal-induced degradation and basal turnover of the NF-kappaB inhibitor IkappaB alpha in vivo. *EMBO J.* **15,** 6716–6726 (1996).
165. Chien, Y. *et al.* Control of the senescence-associated secretory phenotype by NF-κB promotes senescence and enhances chemosensitivity. *Genes Dev.* **25,** 2125–2136 (2011).
166. Jing, H. *et al.* Opposing roles of NF-κB in anti-cancer treatment outcome unveiled by cross-species investigations. *Genes Dev.* **25,** 2137–2146 (2011).
167. Acosta, J. C. *et al.* Chemokine signaling via the CXCR2 receptor reinforces senescence. *Cell* **133,** 1006–1018 (2008).
168. Rodier, F. & Campisi, J. Four faces of cellular senescence. *J. Cell Biol.* **192,** 547–556 (2011).
169. Wajapeyee, N., Serra, R. W., Zhu, X., Mahalingam, M. & Green, M. R. Oncogenic BRAF induces senescence and apoptosis through pathways mediated by the secreted protein IGFBP7. *Cell* **132,** 363–374 (2008).
170. Kortlever, R. M., Higgins, P. J. & Bernards, R. Plasminogen activator inhibitor-1 is a critical downstream target of p53 in the induction of replicative senescence. *Nat. Cell Biol.* **8,** 877–884 (2006).
171. Laberge, R.-M., Awad, P., Campisi, J. & Desprez, P.-Y. Epithelial-mesenchymal transition induced by senescent fibroblasts. *Cancer Microenviron. Off. J. Int. Cancer Microenviron. Soc.* **5,** 39–44 (2012).
172. Parrinello, S., Coppe, J.-P., Krtolica, A. & Campisi, J. Stromal-epithelial interactions in aging and cancer: senescent fibroblasts alter epithelial cell differentiation. *J. Cell Sci.* **118,** 485–496 (2005).
173. Liu, D. & Hornsby, P. J. Senescent human fibroblasts increase the early growth of xenograft tumors via matrix metalloproteinase secretion. *Cancer Res.* **67,** 3117–3126 (2007).
174. Coppé, J.-P., Kauser, K., Campisi, J. & Beauséjour, C. M. Secretion of vascular endothelial growth factor by primary human fibroblasts at senescence. *J. Biol. Chem.* **281,** 29568–29574 (2006).
175. Devenish, R. J. & Klionsky, D. J. Autophagy: mechanism and physiological relevance 'brewed' from yeast studies. *Front. Biosci. Sch. Ed.* **4,** 1354–1363 (2012).
176. Settembre, C., Fraldi, A., Medina, D. L. & Ballabio, A. Signals from the lysosome: a control centre for cellular clearance and energy metabolism. *Nat. Rev. Mol. Cell Biol.* **14,** 283–296 (2013).
177. Todde, V., Veenhuis, M. & van der Klei, I. J. Autophagy: principles and significance in health and disease. *Biochim. Biophys. Acta* **1792,** 3–13 (2009).
178. Mizushima, N. & Levine, B. Autophagy in mammalian development and

differentiation. *Nat. Cell Biol.* **12,** 823–830 (2010).
179. Tyedmers, J., Mogk, A. & Bukau, B. Cellular strategies for controlling protein aggregation. *Nat. Rev. Mol. Cell Biol.* **11,** 777–788 (2010).
180. Stanley, R. E., Ragusa, M. J. & Hurley, J. H. The beginning of the end: how scaffolds nucleate autophagosome biogenesis. *Trends Cell Biol.* **24,** 73–81 (2014).
181. Furuya, N., Yu, J., Byfield, M., Pattingre, S. & Levine, B. The evolutionarily conserved domain of Beclin 1 is required for Vps34 binding, autophagy and tumor suppressor function. *Autophagy* **1,** 46–52 (2005).
182. Wu, Y.-T. *et al.* Dual role of 3-methyladenine in modulation of autophagy via different temporal patterns of inhibition on class I and III phosphoinositide 3-kinase. *J. Biol. Chem.* **285,** 10850–10861 (2010).
183. Ichimura, Y. *et al.* A ubiquitin-like system mediates protein lipidation. *Nature* **408,** 488–492 (2000).
184. Barth, S., Glick, D. & Macleod, K. F. Autophagy: assays and artifacts. *J. Pathol.* **221,** 117–124 (2010).
185. Benbrook, D. M. & Long, A. Integration of autophagy, proteasomal degradation, unfolded protein response and apoptosis. *Exp. Oncol.* **34,** 286–297 (2012).
186. Beyenbach, K. W. & Wieczorek, H. The V-type H+ ATPase: molecular structure and function, physiological roles and regulation. *J. Exp. Biol.* **209,** 577–589 (2006).
187. Mauvezin, C., Nagy, P., Juhász, G. & Neufeld, T. P. Autophagosome-lysosome fusion is independent of V-ATPase-mediated acidification. *Nat. Commun.* **6,** 7007 (2015).
188. Ruggiano, A., Foresti, O. & Carvalho, P. Quality control: ER-associated degradation: protein quality control and beyond. *J. Cell Biol.* **204,** 869–879 (2014).
189. Shaid, S., Brandts, C. H., Serve, H. & Dikic, I. Ubiquitination and selective autophagy. *Cell Death Differ.* **20,** 21–30 (2013).
190. Husnjak, K. & Dikic, I. Ubiquitin-binding proteins: decoders of ubiquitin-mediated cellular functions. *Annu. Rev. Biochem.* **81,** 291–322 (2012).
191. Chan, E. Y. mTORC1 phosphorylates the ULK1-mAtg13-FIP200 autophagy regulatory complex. *Sci. Signal.* **2,** pe51 (2009).
192. Inoki, K., Kim, J. & Guan, K.-L. AMPK and mTOR in cellular energy homeostasis and drug targets. *Annu. Rev. Pharmacol. Toxicol.* **52,** 381–400 (2012).
193. Mizushima, N. & Klionsky, D. J. Protein Turnover Via Autophagy: Implications for Metabolism. *Annu. Rev. Nutr.* **27,** 19–40 (2007).
194. Mathew, R. *et al.* Functional role of autophagy-mediated proteome remodeling in cell survival signaling and innate immunity. *Mol. Cell* **55,** 916–930 (2014).
195. Capparelli, C. *et al.* CDK inhibitors (p16/p19/p21) induce senescence and autophagy in cancer-associated fibroblasts, 'fueling' tumor growth via paracrine interactions, without an increase in neo-angiogenesis. *Cell Cycle Georget. Tex* **11,** 3599–3610 (2012).
196. Young, A. R. J. *et al.* Autophagy mediates the mitotic senescence transition. *Genes Dev.* **23,** 798–803 (2009).
197. Dulic, V. Senescence regulation by mTOR. *Methods Mol. Biol. Clifton NJ* **965,** 15–35 (2013).

198. Narita, M. *et al.* Spatial Coupling of mTOR and Autophagy Augments Secretory Phenotypes. *Science* **332,** 966–970 (2011).
199. Nam, H. Y., Han, M. W., Chang, H. W., Kim, S. Y. & Kim, S. W. Prolonged autophagy by MTOR inhibitor leads radioresistant cancer cells into senescence. *Autophagy* **9,** 1631–1632 (2013).
200. Herranz, N. *et al.* mTOR regulates MAPKAPK2 translation to control the senescence-associated secretory phenotype. *Nat. Cell Biol.* **17,** 1205–1217 (2015).
201. Lunt, S. Y. & Vander Heiden, M. G. Aerobic Glycolysis: Meeting the Metabolic Requirements of Cell Proliferation. *Annu. Rev. Cell Dev. Biol.* **27,** 441–464 (2011).
202. DeBerardinis, R. J. & Cheng, T. Q's next: the diverse functions of glutamine in metabolism, cell biology and cancer. *Oncogene* **29,** 313–324 (2010).
203. DeBerardinis, R. J. *et al.* Beyond aerobic glycolysis: transformed cells can engage in glutamine metabolism that exceeds the requirement for protein and nucleotide synthesis. *Proc. Natl. Acad. Sci. U. S. A.* **104,** 19345–19350 (2007).
204. Gowans, G. J., Hawley, S. A., Ross, F. A. & Hardie, D. G. AMP is a true physiological regulator of AMP-activated protein kinase by both allosteric activation and enhancing net phosphorylation. *Cell Metab.* **18,** 556–566 (2013).
205. Hardie, D. G., Ross, F. A. & Hawley, S. A. AMPK: a nutrient and energy sensor that maintains energy homeostasis. *Nat. Rev. Mol. Cell Biol.* **13,** 251–262 (2012).
206. Auciello, F. R., Ross, F. A., Ikematsu, N. & Hardie, D. G. Oxidative stress activates AMPK in cultured cells primarily by increasing cellular AMP and/or ADP. *FEBS Lett.* **588,** 3361–3366 (2014).
207. Hanahan, D. & Weinberg, R. A. Hallmarks of cancer: the next generation. *Cell* **144,** 646–674 (2011).
208. Warburg, O., Wind, F. & Negelein, E. THE METABOLISM OF TUMORS IN THE BODY. *J. Gen. Physiol.* **8,** 519–530 (1927).
209. Ward, P. S. & Thompson, C. B. Metabolic reprogramming: a cancer hallmark even warburg did not anticipate. *Cancer Cell* **21,** 297–308 (2012).
210. Faubert, B. *et al.* AMPK is a negative regulator of the Warburg effect and suppresses tumor growth in vivo. *Cell Metab.* **17,** 113–124 (2013).
211. Nogueira, V. *et al.* Akt determines replicative senescence and oxidative or oncogenic premature senescence and sensitizes cells to oxidative apoptosis. *Cancer Cell* **14,** 458–470 (2008).
212. Galluzzi, L., Kepp, O., Heiden, M. G. V. & Kroemer, G. Metabolic targets for cancer therapy. *Nat. Rev. Drug Discov.* **12,** 829–846 (2013).
213. Phan, L. M., Yeung, S.-C. J. & Lee, M.-H. Cancer metabolic reprogramming: importance, main features, and potentials for precise targeted anti-cancer therapies. *Cancer Biol. Med.* **11,** 1–19 (2014).
214. Ho, D. H., Whitecar, J. P., Luce, J. K. & Frei, E. L-asparagine requirement and the effect of L-asparaginase on the normal and leukemic human bone marrow. *Cancer Res.* **30,** 466–472 (1970).
215. Bost, F., Sahra, I. B., Le Marchand-Brustel, Y. & Tanti, J.-F. Metformin and cancer therapy. *Curr. Opin. Oncol.* **24,** 103–108 (2012).
216. Papandreou, I., Goliasova, T. & Denko, N. C. Anticancer drugs that target metabolism: Is dichloroacetate the new paradigm? *Int. J. Cancer* **128,** 1001–

1008 (2011).
217. Shen, H., Hau, E., Joshi, S., Dilda, P. J. & McDonald, K. L. Sensitization of Glioblastoma Cells to Irradiation by Modulating the Glucose Metabolism. *Mol. Cancer Ther.* **14,** 1794–1804 (2015).
218. Zhang, D. *et al.* 2-Deoxy-D-glucose targeting of glucose metabolism in cancer cells as a potential therapy. *Cancer Lett.* **355,** 176–183 (2014).
219. Kaplon, J. *et al.* A key role for mitochondrial gatekeeper pyruvate dehydrogenase in oncogene-induced senescence. *Nature* **498,** 109–112 (2013).
220. Boroughs, L. K. & DeBerardinis, R. J. Metabolic pathways promoting cancer cell survival and growth. *Nat. Cell Biol.* **17,** 351–359 (2015).
221. Jiang, P., Du, W., Mancuso, A., Wellen, K. E. & Yang, X. Reciprocal regulation of p53 and malic enzymes modulates metabolism and senescence. *Nature* **493,** 689–693 (2013).
222. Quijano, C. *et al.* Oncogene-induced senescence results in marked metabolic and bioenergetic alterations. *Cell Cycle Georget. Tex* **11,** 1383–1392 (2012).
223. Hutter, E. *et al.* Senescence-associated changes in respiration and oxidative phosphorylation in primary human fibroblasts. *Biochem. J.* **380,** 919–928 (2004).
224. Passos, J. F., Saretzki, G. & von Zglinicki, T. DNA damage in telomeres and mitochondria during cellular senescence: is there a connection? *Nucleic Acids Res.* **35,** 7505–7513 (2007).
225. Mookerjee, S. A., Divakaruni, A. S., Jastroch, M. & Brand, M. D. Mitochondrial uncoupling and lifespan. *Mech. Ageing Dev.* **131,** 463–472 (2010).
226. Moiseeva, O., Bourdeau, V., Roux, A., Deschênes-Simard, X. & Ferbeyre, G. Mitochondrial dysfunction contributes to oncogene-induced senescence. *Mol. Cell. Biol.* **29,** 4495–4507 (2009).
227. Dalle Pezze, P. *et al.* Dynamic modelling of pathways to cellular senescence reveals strategies for targeted interventions. *PLoS Comput. Biol.* **10,** e1003728 (2014).
228. Lucchesi, J. C. Synthetic lethality and semi-lethality among functionally related mutants of Drosophila melanfgaster. *Genetics* **59,** 37–44 (1968).
229. Tong, A. H. Y. *et al.* Global mapping of the yeast genetic interaction network. *Science* **303,** 808–813 (2004).
230. Luo, J. *et al.* A genome-wide RNAi screen identifies multiple synthetic lethal interactions with the Ras oncogene. *Cell* **137,** 835–848 (2009).
231. Kaelin, W. G. The concept of synthetic lethality in the context of anticancer therapy. *Nat. Rev. Cancer* **5,** 689–698 (2005).
232. Fece de la Cruz, F., Gapp, B. V. & Nijman, S. M. B. Synthetic lethal vulnerabilities of cancer. *Annu. Rev. Pharmacol. Toxicol.* **55,** 513–531 (2015).
233. Bryant, H. E. *et al.* Specific killing of BRCA2-deficient tumours with inhibitors of poly(ADP-ribose) polymerase. *Nature* **434,** 913–917 (2005).
234. Farmer, H. *et al.* Targeting the DNA repair defect in BRCA mutant cells as a therapeutic strategy. *Nature* **434,** 917–921 (2005).
235. O'Shaughnessy, J. *et al.* Iniparib plus chemotherapy in metastatic triple-negative breast cancer. *N. Engl. J. Med.* **364,** 205–214 (2011).
236. Kolch, W., Halasz, M., Granovskaya, M. & Kholodenko, B. N. The dynamic control of signal transduction networks in cancer cells. *Nat. Rev. Cancer* **15,** 515–527 (2015).
237. Bieging, K. T., Mello, S. S. & Attardi, L. D. Unravelling mechanisms of p53-

mediated tumour suppression. *Nat. Rev. Cancer* **14,** 359–370 (2014).
238. Mello, S. S. & Attardi, L. D. Not all p53 gain-of-function mutants are created equal. *Cell Death Differ.* **20,** 855–857 (2013).
239. Timofeev, O. *et al.* p53 DNA binding cooperativity is essential for apoptosis and tumor suppression in vivo. *Cell Rep.* **3,** 1512–1525 (2013).
240. Shields, A. F. *et al.* Imaging proliferation in vivo with [F-18]FLT and positron emission tomography. *Nat. Med.* **4,** 1334–1336 (1998).
241. Marciniak, S. J. *et al.* CHOP induces death by promoting protein synthesis and oxidation in the stressed endoplasmic reticulum. *Genes Dev.* **18,** 3066–3077 (2004).
242. Walenta, S. *et al.* High lactate levels predict likelihood of metastases, tumor recurrence, and restricted patient survival in human cervical cancers. *Cancer Res.* **60,** 916–921 (2000).
243. Kempa, S. *et al.* An automated GCxGC-TOF-MS protocol for batch-wise extraction and alignment of mass isotopomer matrixes from differential 13C-labelling experiments: a case study for photoautotrophic-mixotrophic grown Chlamydomonas reinhardtii cells. *J. Basic Microbiol.* **49,** 82–91 (2009).
244. Giavalisco, P. *et al.* High-resolution direct infusion-based mass spectrometry in combination with whole 13C metabolome isotope labeling allows unambiguous assignment of chemical sum formulas. *Anal. Chem.* **80,** 9417–9425 (2008).
245. Lisec, J., Schauer, N., Kopka, J., Willmitzer, L. & Fernie, A. R. Gas chromatography mass spectrometry-based metabolite profiling in plants. *Nat. Protoc.* **1,** 387–396 (2006).
246. Cuadros-Inostroza, A. *et al.* TargetSearch--a Bioconductor package for the efficient preprocessing of GC-MS metabolite profiling data. *BMC Bioinformatics* **10,** 428 (2009).
247. Lisec, J. *et al.* Corn hybrids display lower metabolite variability and complex metabolite inheritance patterns. *Plant J. Cell Mol. Biol.* **68,** 326–336 (2011).
248. Stacklies, W., Redestig, H., Scholz, M., Walther, D. & Selbig, J. pcaMethods--a bioconductor package providing PCA methods for incomplete data. *Bioinforma. Oxf. Engl.* **23,** 1164–1167 (2007).
249. Bode, C. & Gräler, M. H. Quantification of sphingosine-1-phosphate and related sphingolipids by liquid chromatography coupled to tandem mass spectrometry. *Methods Mol. Biol. Clifton NJ* **874,** 33–44 (2012).
250. Castro, F. *et al.* High-throughput SNP-based authentication of human cell lines. *Int. J. Cancer J. Int. Cancer* **132,** 308–314 (2013).
251. Berns, K. *et al.* A large-scale RNAi screen in human cells identifies new components of the p53 pathway. *Nature* **428,** 431–437 (2004).
252. Greer, E. L. *et al.* The energy sensor AMP-activated protein kinase directly regulates the mammalian FOXO3 transcription factor. *J. Biol. Chem.* **282,** 30107–30119 (2007).
253. Matoba, S. *et al.* p53 regulates mitochondrial respiration. *Science* **312,** 1650–1653 (2006).
254. Jones, R. G. *et al.* AMP-activated protein kinase induces a p53-dependent metabolic checkpoint. *Mol. Cell* **18,** 283–293 (2005).
255. Christofk, H. R. *et al.* The M2 splice isoform of pyruvate kinase is important for cancer metabolism and tumour growth. *Nature* **452,** 230–233 (2008).
256. Zhang, S., Hulver, M. W., McMillan, R. P., Cline, M. A. & Gilbert, E. R. The

pivotal role of pyruvate dehydrogenase kinases in metabolic flexibility. *Nutr. Metab.* **11,** 10 (2014).
257. Israelsen, W. J. *et al.* PKM2 isoform-specific deletion reveals a differential requirement for pyruvate kinase in tumor cells. *Cell* **155,** (2013).
258. Wolf, D. A. Is Reliance on Mitochondrial Respiration a 'Chink in the Armor' of Therapy-Resistant Cancer? *Cancer Cell* **26,** 788–795 (2014).
259. Goldberg, A. L. Protein degradation and protection against misfolded or damaged proteins. *Nature* **426,** 895–899 (2003).
260. Peth, A., Nathan, J. A. & Goldberg, A. L. The ATP Costs and Time Required to Degrade Ubiquitinated Proteins by the 26 S Proteasome. *J. Biol. Chem.* **288,** 29215–29222 (2013).
261. White, E. & Lowe, S. W. Eating to exit: autophagy-enabled senescence revealed. *Genes Dev.* **23,** 784–787 (2009).
262. Kroemer, G., Mariño, G. & Levine, B. Autophagy and the integrated stress response. *Mol. Cell* **40,** 280–293 (2010).
263. Lippai, M. & Lőw, P. The role of the selective adaptor p62 and ubiquitin-like proteins in autophagy. *BioMed Res. Int.* **2014,** 832704 (2014).
264. Wang, D. & Baldwin, A. S. Activation of nuclear factor-kappaB-dependent transcription by tumor necrosis factor-alpha is mediated through phosphorylation of RelA/p65 on serine 529. *J. Biol. Chem.* **273,** 29411–29416 (1998).
265. Denoyelle, C. *et al.* Anti-oncogenic role of the endoplasmic reticulum differentially activated by mutations in the MAPK pathway. *Nat. Cell Biol.* **8,** 1053–1063 (2006).
266. Mijaljica, D., Prescott, M. & Devenish, R. J. V-ATPase engagement in autophagic processes. *Autophagy* **7,** 666–668 (2011).
267. Wall, M. *et al.* The mTORC1 inhibitor everolimus prevents and treats Eμ-Myc lymphoma by restoring oncogene-induced senescence. *Cancer Discov.* **3,** 82–95 (2013).
268. Ravikumar, B. *et al.* Inhibition of mTOR induces autophagy and reduces toxicity of polyglutamine expansions in fly and mouse models of Huntington disease. *Nat. Genet.* **36,** 585–595 (2004).
269. Mizushima, N. *et al.* A protein conjugation system essential for autophagy. *Nature* **395,** 395–398 (1998).
270. Noda, T. & Ohsumi, Y. Tor, a phosphatidylinositol kinase homologue, controls autophagy in yeast. *J. Biol. Chem.* **273,** 3963–3966 (1998).
271. Pankiv, S. *et al.* p62/SQSTM1 binds directly to Atg8/LC3 to facilitate degradation of ubiquitinated protein aggregates by autophagy. *J. Biol. Chem.* **282,** 24131–24145 (2007).
272. Nakagawa, T. *et al.* Caspase-12 mediates endoplasmic-reticulum-specific apoptosis and cytotoxicity by amyloid-beta. *Nature* **403,** 98–103 (2000).
273. Elmore, S. Apoptosis: A Review of Programmed Cell Death. *Toxicol. Pathol.* **35,** 495–516 (2007).
274. Warburg, O. On respiratory impairment in cancer cells. *Science* **124,** 269–270 (1956).
275. Rohren, E. M., Turkington, T. G. & Coleman, R. E. Clinical applications of PET in oncology. *Radiology* **231,** 305–332 (2004).
276. Zhu, A., Lee, D. & Shim, H. Metabolic PET Imaging in Cancer Detection and

Therapy Response. *Semin. Oncol.* **38,** 55–69 (2011).
277. Hutchings, M. & Barrington, S. F. PET/CT for therapy response assessment in lymphoma. *J. Nucl. Med. Off. Publ. Soc. Nucl. Med.* **50 Suppl 1,** 21S–30S (2009).
278. Barrington, S. F. *et al.* Role of imaging in the staging and response assessment of lymphoma: consensus of the International Conference on Malignant Lymphomas Imaging Working Group. *J. Clin. Oncol. Off. J. Am. Soc. Clin. Oncol.* **32,** 3048–3058 (2014).
279. Yoo, C. *et al.* Limited role of interim PET/CT in patients with diffuse large B-cell lymphoma treated with R-CHOP. *Ann. Hematol.* **90,** 797–802 (2011).
280. Cashen, A. F. *et al.* 18F-FDG PET/CT for Early Response Assessment in Diffuse Large B-Cell Lymphoma: Poor Predictive Value of International Harmonization Project Interpretation. *J. Nucl. Med. Off. Publ. Soc. Nucl. Med.* **52,** 386–392 (2011).
281. Pregno, P. *et al.* Interim 18-FDG-PET/CT failed to predict the outcome in diffuse large B-cell lymphoma patients treated at the diagnosis with rituximab-CHOP. *Blood* **119,** 2066–2073 (2012).
282. Jose, C., Bellance, N. & Rossignol, R. Choosing between glycolysis and oxidative phosphorylation: a tumor's dilemma? *Biochim. Biophys. Acta* **1807,** 552–561 (2011).
283. Schuster, S., Boley, D., Möller, P., Stark, H. & Kaleta, C. Mathematical models for explaining the Warburg effect: a review focussed on ATP and biomass production. *Biochem. Soc. Trans.* **43,** 1187–1194 (2015).
284. Stark, H., Fichtner, M., König, R., Lorkowski, S. & Schuster, S. Causes of upregulation of glycolysis in lymphocytes upon stimulation. A comparison with other cell types. *Biochimie* **118,** 185–194 (2015).
285. Becker, T. & Haferkamp, S. in *Senescence and Senescence-Related Disorders* (ed. Zhiwei, W.) (InTech, 2013).
286. De Cecco, M., Jeyapalan, J., Zhao, X., Tamamori-Adachi, M. & Sedivy, J. M. Nuclear protein accumulation in cellular senescence and organismal aging revealed with a novel single-cell resolution fluorescence microscopy assay. *Aging* **3,** 955–967 (2011).
287. Carracedo, A., Cantley, L. C. & Pandolfi, P. P. Cancer metabolism: fatty acid oxidation in the limelight. *Nat. Rev. Cancer* **13,** 227–232 (2013).
288. Takebayashi, S. *et al.* Retinoblastoma protein promotes oxidative phosphorylation through upregulation of glycolytic genes in oncogene-induced senescent cells. *Aging Cell* n/a-n/a (2015). doi:10.1111/acel.12351
289. Roesch, A. *et al.* A temporarily distinct subpopulation of slow-cycling melanoma cells is required for continuous tumor growth. *Cell* **141,** 583–594 (2010).
290. Roesch, A. *et al.* Overcoming Intrinsic Multidrug Resistance in Melanoma by Blocking the Mitochondrial Respiratory Chain of Slow-Cycling JARID1Bhigh Cells. *Cancer Cell* **23,** 811–825 (2013).
291. Aird, K. M. *et al.* Suppression of nucleotide metabolism underlies the establishment and maintenance of oncogene-induced senescence. *Cell Rep.* **3,** 1252–1265 (2013).
292. Aird, K. M. & Zhang, R. Metabolic alterations accompanying oncogene-induced senescence. *Mol. Cell. Oncol.* **1,** e963481 (2014).
293. Gey, C. & Seeger, K. Metabolic changes during cellular senescence

investigated by proton NMR-spectroscopy. *Mech. Ageing Dev.* **134,** 130–138 (2013).
294. Olenchock, B. A. & Vander Heiden, M. G. Pyruvate as a Pivot Point for Oncogene-Induced Senescence. *Cell* **153,** 1429–1430 (2013).
295. Coppé, J.-P. *et al.* Senescence-associated secretory phenotypes reveal cell-nonautonomous functions of oncogenic RAS and the p53 tumor suppressor. *PLoS Biol.* **6,** 2853–2868 (2008).
296. McCaffrey, K. & Braakman, I. Protein quality control at the endoplasmic reticulum. *Essays Biochem.* **60,** 227–235 (2016).
297. Pluquet, O., Pourtier, A. & Abbadie, C. The unfolded protein response and cellular senescence. A review in the theme: cellular mechanisms of endoplasmic reticulum stress signaling in health and disease. *Am. J. Physiol. Cell Physiol.* **308,** C415-425 (2015).
298. Brown, M. K. & Naidoo, N. The endoplasmic reticulum stress response in aging and age-related diseases. *Front. Physiol.* **3,** (2012).
299. Helenius, A. & Aebi, M. Intracellular functions of N-linked glycans. *Science* **291,** 2364–2369 (2001).
300. Gorman, A. M., Healy, S. J. M., Jäger, R. & Samali, A. Stress management at the ER: Regulators of ER stress-induced apoptosis. *Pharmacol. Ther.* **134,** 306–316 (2012).
301. Schröder, M. & Kaufman, R. J. The mammalian unfolded protein response. *Annu. Rev. Biochem.* **74,** 739–789 (2005).
302. Baraibar, M. A. & Friguet, B. Oxidative proteome modifications target specific cellular pathways during oxidative stress, cellular senescence and aging. *Exp. Gerontol.* **48,** 620–625 (2013).
303. Wang, M. & Kaufman, R. J. The impact of the endoplasmic reticulum protein-folding environment on cancer development. *Nat. Rev. Cancer* **14,** 581–597 (2014).
304. Matos, L., Gouveia, A. M. & Almeida, H. ER Stress Response in Human Cellular Models of Senescence. *J. Gerontol. A. Biol. Sci. Med. Sci.* **70,** 924–935 (2015).
305. Zhu, B. *et al.* The nuclear receptor peroxisome proliferator-activated receptor-β/δ (PPARβ/δ) promotes oncogene-induced cellular senescence through repression of endoplasmic reticulum stress. *J. Biol. Chem.* **289,** 20102–20119 (2014).
306. Panganiban, R. A. M., Mungunsukh, O. & Day, R. M. X-irradiation induces ER stress, apoptosis, and senescence in pulmonary artery endothelial cells. *Int. J. Radiat. Biol.* **89,** 656–667 (2013).
307. Obeng, E. A. *et al.* Proteasome inhibitors induce a terminal unfolded protein response in multiple myeloma cells. *Blood* **107,** 4907–4916 (2006).
308. Oda, T., Kosuge, Y., Arakawa, M., Ishige, K. & Ito, Y. Distinct mechanism of cell death is responsible for tunicamycin-induced ER stress in SK-N-SH and SH-SY5Y cells. *Neurosci. Res.* **60,** 29–39 (2008).
309. Appenzeller-Herzog, C. & Hall, M. N. Bidirectional crosstalk between endoplasmic reticulum stress and mTOR signaling. *Trends Cell Biol.* **22,** 274–282 (2012).
310. Puthalakath, H. *et al.* ER stress triggers apoptosis by activating BH3-only protein Bim. *Cell* **129,** 1337–1349 (2007).

311. Timmins, J. M. *et al.* Calcium/calmodulin-dependent protein kinase II links ER stress with Fas and mitochondrial apoptosis pathways. *J. Clin. Invest.* **119,** 2925–2941 (2009).
312. Nakagawa, T. & Yuan, J. Cross-talk between two cysteine protease families. Activation of caspase-12 by calpain in apoptosis. *J. Cell Biol.* **150,** 887–894 (2000).
313. Gerland, L.-M. *et al.* Association of increased autophagic inclusions labeled for beta-galactosidase with fibroblastic aging. *Exp. Gerontol.* **38,** 887–895 (2003).
314. Patschan, S. *et al.* Lipid mediators of autophagy in stress-induced premature senescence of endothelial cells. *Am. J. Physiol. Heart Circ. Physiol.* **294,** H1119-1129 (2008).
315. Goehe, R. W. *et al.* The autophagy-senescence connection in chemotherapy: must tumor cells (self) eat before they sleep? *J. Pharmacol. Exp. Ther.* **343,** 763–778 (2012).
316. Sano, R. & Reed, J. C. ER stress-induced cell death mechanisms. *Biochim. Biophys. Acta BBA - Mol. Cell Res.* **1833,** 3460–3470 (2013).
317. B'chir, W. *et al.* The eIF2α/ATF4 pathway is essential for stress-induced autophagy gene expression. *Nucleic Acids Res.* **41,** 7683–7699 (2013).
318. Deegan, S., Saveljeva, S., Gorman, A. M. & Samali, A. Stress-induced self-cannibalism: on the regulation of autophagy by endoplasmic reticulum stress. *Cell. Mol. Life Sci. CMLS* **70,** 2425–2441 (2013).
319. Rubio, N. *et al.* p38(MAPK)-regulated induction of p62 and NBR1 after photodynamic therapy promotes autophagic clearance of ubiquitin aggregates and reduces reactive oxygen species levels by supporting Nrf2-antioxidant signaling. *Free Radic. Biol. Med.* **67,** 292–303 (2014).
320. Ciechomska, I. A., Gabrusiewicz, K., Szczepankiewicz, A. A. & Kaminska, B. Endoplasmic reticulum stress triggers autophagy in malignant glioma cells undergoing cyclosporine a-induced cell death. *Oncogene* **32,** 1518–1529 (2013).
321. Ma, X.-H. *et al.* Targeting ER stress-induced autophagy overcomes BRAF inhibitor resistance in melanoma. *J. Clin. Invest.* **124,** 1406–1417 (2014).
322. Beck, D. *et al.* Vemurafenib potently induces endoplasmic reticulum stress-mediated apoptosis in BRAFV600E melanoma cells. *Sci. Signal.* **6,** ra7 (2013).
323. Deschênes-Simard, X. *et al.* Tumor suppressor activity of the ERK/MAPK pathway by promoting selective protein degradation. *Genes Dev.* **27,** 900–915 (2013).
324. Senft, D. & Ronai, Z. A. UPR, autophagy, and mitochondria crosstalk underlies the ER stress response. *Trends Biochem. Sci.* **40,** 141–148 (2015).
325. Houck, S. A. *et al.* Quality control autophagy degrades soluble ERAD-resistant conformers of the misfolded membrane protein GnRHR. *Mol. Cell* **54,** 166–179 (2014).
326. Du, Y. *et al.* An insight into the mechanistic role of p53-mediated autophagy induction in response to proteasomal inhibition-induced neurotoxicity. *Autophagy* **5,** 663–675 (2009).
327. Pandey, U. B. *et al.* HDAC6 rescues neurodegeneration and provides an essential link between autophagy and the UPS. *Nature* **447,** 859–863 (2007).
328. Rashid, H.-O., Yadav, R. K., Kim, H.-R. & Chae, H.-J. ER stress: Autophagy induction, inhibition, and selection. *Autophagy* **0,** 00–00 (2015).
329. Sailaja, G. S. *et al.* The secreted protein acidic and rich in cysteine (SPARC)

induces endoplasmic reticulum stress leading to autophagy-mediated apoptosis in neuroblastoma. *Int. J. Oncol.* **42,** 188–196 (2013).
330. Gamerdinger, M. *et al.* Protein quality control during aging involves recruitment of the macroautophagy pathway by BAG3. *EMBO J.* **28,** 889–901 (2009).
331. Kraya, A. A. *et al.* Identification of secreted proteins that reflect autophagy dynamics within tumor cells. *Autophagy* **11,** 60–74 (2014).
332. Dupont, N. *et al.* Autophagy-based unconventional secretory pathway for extracellular delivery of IL-1β. *EMBO J.* **30,** 4701–4711 (2011).
333. Nijholt, D. a. T. *et al.* Endoplasmic reticulum stress activates autophagy but not the proteasome in neuronal cells: implications for Alzheimer's disease. *Cell Death Differ.* **18,** 1071–1081 (2011).
334. Korolchuk, V. I., Mansilla, A., Menzies, F. M. & Rubinsztein, D. C. Autophagy inhibition compromises degradation of ubiquitin-proteasome pathway substrates. *Mol. Cell* **33,** 517–527 (2009).
335. Nakamura, N., Matsuura, A., Wada, Y. & Ohsumi, Y. Acidification of vacuoles is required for autophagic degradation in the yeast, Saccharomyces cerevisiae. *J. Biochem. (Tokyo)* **121,** 338–344 (1997).
336. Kaelin, W. G. The concept of synthetic lethality in the context of anticancer therapy. *Nat. Rev. Cancer* **5,** 689–698 (2005).
337. McLornan, D. P., List, A. & Mufti, G. J. Applying Synthetic Lethality for the Selective Targeting of Cancer. *N. Engl. J. Med.* **371,** 1725–1735 (2014).
338. Singh, A. *et al.* A gene expression signature associated with 'K-Ras addiction' reveals regulators of EMT and tumor cell survival. *Cancer Cell* **15,** 489–500 (2009).
339. Pazolli, E. *et al.* Senescent stromal-derived osteopontin promotes preneoplastic cell growth. *Cancer Res.* **69,** 1230–1239 (2009).
340. Jackson, T. R. *et al.* DNA damage causes TP53-dependent coupling of self-renewal and senescence pathways in embryonal carcinoma cells. *Cell Cycle* **12,** 430–441 (2013).
341. Erenpreisa, J. & Cragg, M. S. Three steps to the immortality of cancer cells: senescence, polyploidy and self-renewal. *Cancer Cell Int.* **13,** 92 (2013).
342. Kang, T.-W. *et al.* Senescence surveillance of pre-malignant hepatocytes limits liver cancer development. *Nature* **479,** 547–551 (2011).
343. Schlossmacher, G., Stevens, A. & White, A. Glucocorticoid receptor-mediated apoptosis: mechanisms of resistance in cancer cells. *J. Endocrinol.* **211,** 17–25 (2011).
344. Laberge, R.-M. *et al.* Glucocorticoids suppress selected components of the senescence-associated secretory phenotype. *Aging Cell* **11,** 569–578 (2012).

10. Appendix

Supplementary Figure 1. Lageso Score Sheet

Für die Dokumentation der im Rahmen der regelmäßigen Tier-Visiten erhobenen klinischen Symptome und Untersuchungsergebnisse und als allgemeine Entscheidungsgrundlage wurde folgendes Score Sheet, welches zudem durch weitere Kriterien, die spezifisch für das Eμ-*myc* Tumormodell zutreffen, ergänzt wurde, für *alle* am Versuchsvorhaben beteiligten KollegInnen (wissenschaftliche MitarbeiterInnen, Pflegepersonal, Tierschutzbeauftragte) entwickelt:

	Anweisungen
A	Bei nur einem Symptom der Kategorie A: das Tier täglich (ggf. auch mehrmals) beobachten. Spätestens bei Kombination von **zwei oder mehr Symptomen der Kategorie A** muss dem Projektleiter vorgestellt werden.
B	Bei einem Symptom der Kategorie B: das Tier muss dem Projektleiter vorgestellt werden. Bei Kombination eines B mit Torkeln, Schmerz, Blässe oder Blut ist das Tier unverzüglich schmerzlos (Isofluran) zu töten (siehe C)! Bei anderen Kombinationen verschiedener Symptome der Kategorie B ist das Tier hingegen zunächst unverzüglich dem Projektleiter vorzustellen.
C	**Unverzüglich schmerzlos töten (Isofluran)!** (Angaben zu technischer Umsetzung, Zeitablauf sowie ausführenden bzw. diesbezüglich bevollmächtigten Personen finden sich im Antrag bzw. sind in der Tierexperimentellen Einrichtung der Charité, Campus Virchow-Klinikum, hinterlegt).

Achten Sie auf folgende SYMPTOME und handeln Sie nach den ANWEISUNGEN:	
SYMPTOME	ANWEISUNGEN
1. Beim täglichen Blick in den Käfig	
Tier isoliert sich	A
Struppiges Fell, ungepflegtes Fell, Augenränder, Piloerektion	A
Aufgetriebener Leib	A
Geringfügig verstärkte Atmung	A
Urin u./o. Kot abweichend in Menge, Farbe und Konsistenz (einzeln oder kombiniert)	A

Anhaltende Obstipation	A
Schmerz (Gesichtsausdruck, Haltung gekrümmt oder Leib aufgezogen)	B
Eingesunkene, trübe Augen	B
Blässe (Augen, Ohren, Haut)	B
Blut an Körperöffnungen, blutiger Kot	B
Deutlich verstärkte Atmung / Keuchen	B
Durchfall, wenn schwächend oder Andauernd	B
Kurzzeitige Krampfanfälle, Torkeln, vorübergehende Apathie	B
Kopfschiefhaltung	B
Parese(n)	B
Paralysen, spätestens sobald die Gefahr besteht, dass die Tiere aus eigener Kraft Wasser und Futter nicht mehr erreichen	C
Nackensteifigkeit in Kombination mit Hyperkyphosierung/ Rundrückenausbildung	C
Repetitive, schraubende Kopfbewegungen	C
2. Beim Umsetzen	
Verletzungen, Hautveränderungen	A
Tier vermeidet Bewegungen	A
Teilnahmslosigkeit	A
Ruhelosigkeit	A
Stereotype Bewegungen im Kreis (circling)	A
Lokale Infektion(en)	B
Bauch hart oder gespannt	B
Hautfalten bleiben stehen, Dehydratation	B
Ödembildung	B
Automutilation (z.B. Annagen von Zehen)	B
Lautäußerungen beim Ergreifen	B
Ulzerierende Tumore	C
Moribund	C

3. Beim Wiegen	
Deutliche Gewichtszunahme ohne palpierbare Lymphadenopathie (z.B. aufgrund einer internen, d.h. nicht peripher palpierbaren Tumorlast oder Aszites)	B
Fortschreitende Gewichtsabnahme (bis 10 % verglichen mit gesunden Tieren des gleichen Stamms und Alters)	B
Unklare Einschätzbarkeit des Wiegeergebnisses (gemeinsames Vorliegen von Tumorlast, Aszites und möglicher beginnender Kachexie, selten) bzw. >10% Gewichtsverlust	B

Supplementary Figure 2. Full-lengh immunoblots. Uncropped images of the blots probed for the indicated proteins as presented in Figures 11, 14 and 19.

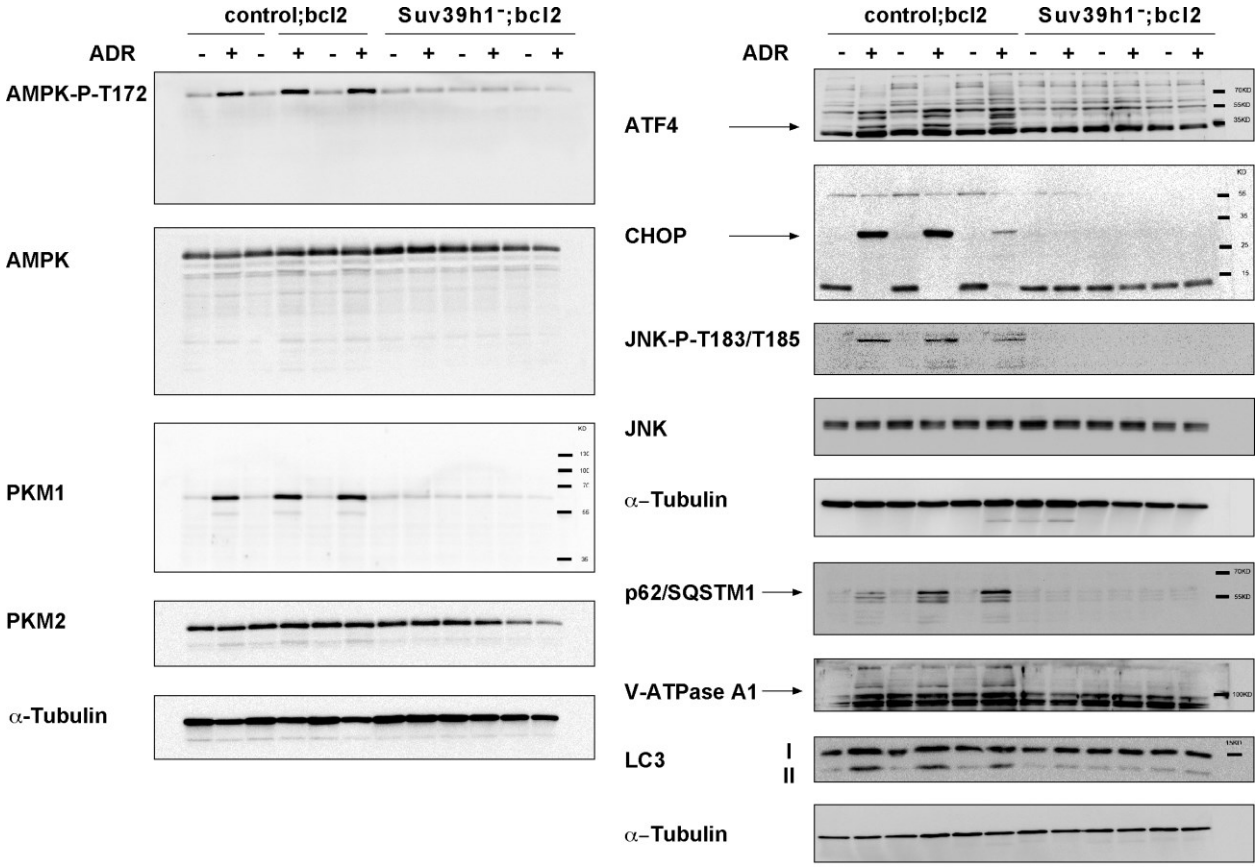

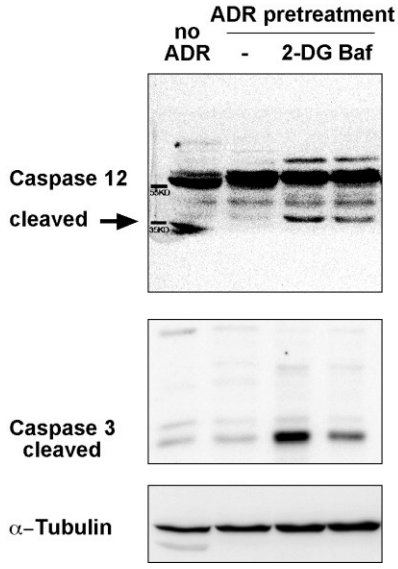

11. Acknowledgements

Ich bedanke mich bei Prof. Clemens Schmitt für die Möglichkeit, meine Doktorarbeit in seinem Labor durchzuführen und für die Förderung meiner Ausbildung zum MD/PhD. Besonders dankbar bin ich für seine Supervision bei der 2013 erfolgten Publikation der Ergebnisse in der Fachzeitschrift Nature sowie für die kontinuierliche finanzielle Unterstützung bei der Fertigstellung der Doktorarbeit auch während meines Medizinstudiums.

Weiterhin bedanke ich mich bei Prof. Thomas Sommer und Prof. Simone Fulda für die unkomplizierte Übernahme der Promotionsgutachten sowie bei Prof. Andreas Herrmann und Prof. Achim Leutz für die Bereitschaft, mein Promotionsverfahren als Mitglieder der Prüfungskommission zu unterstützen.

Mein besonderer Dank gilt dem Boehringer Ingelheim Fonds für die finanzielle und intellektuelle Unterstützung im Rahmen des PhD Fellowship Programms. Ich habe vor allem von den Sommerseminaren sehr profitiert und den Austausch mit anderen Stipendiaten und Mitarbeitern des Boehringer Ingelheim Fonds sehr genossen.

Bei den Mitgliedern des Labors und allen Kollaborationspartnern bedanke ich mich ausdrücklich für die Hilfe bei der Durchführung der Experimente im Rahmen der Nature Publikation 2013. Mein besonderer Dank gilt Yong Yu und Maja Milanovic für die umfangreiche Unterstützung bei Western Blots und Genexpressionsanalysen sowie Nadine Burbach, Katharina Schleicher und Julia Dräger für ihre Hilfe bei der Maus- und Zellkulturarbeit.

Mein größter Dank gilt meinen Eltern und Anne für ihre Liebe und den fortwährenden Zuspruch in allen Projekt- und Lebenslagen. Ich bin ihnen für die bedingunglose Unterstützung meiner langjährigen wissenschaftlichen und medizinischen Ausbildung über alle Maßen dankbar.

12. Statement

Hiermit erkläre ich, dass ich die vorliegende Arbeit selbstständig und nur unter Verwendung der angegebenen Hilfsmittel angefertigt habe. Diese Arbeit wurde nicht in gleicher oder ähnlicher Form einer anderen Prüfungsbehörde vorgelegt. Die Promotionsordnung der Lebenswissenschaftlichen Fakultät der Humboldt-Universität zu Berlin vom 27.06.2012 habe ich gelesen und akzeptiert.

Datum und Unterschrift